6 Discrete cell modeling[1]

With P. Macklin and M.E. Edgerton

In this chapter, we: introduce discrete cancer cell modeling; assess the strengths and weaknesses of available discrete cell modeling approaches; sample the major discrete cell modeling approaches employed in current computational cancer modeling; and introduce a discrete, agent-based cell modeling framework currently being developed by the authors and collaborators that will be used to implement a next-generation, multiscale cancer modeling framework as detailed in Chapter 7.

6.1 A brief review of discrete modeling in cancer biology

Thus far, we have discussed continuum modeling efforts that model cancer at the *tissue* scale and average out the effects of individual cells. We now turn our attention to *discrete* models that address the behavior of one or more individual cells as they interact with one another and the microenvironment.

Discrete modeling has enjoyed a long history in applied mathematics and biology, dating as far back as the 1940s when John von Neumann applied lattice crystal models to study the necessary rulesets for self-replicating robots [677]. Perhaps the most famous early example of discrete biological modeling is John Conway's 1970 "game of life," a 2-D rectangular lattice of "cells" that changed colors according to rules based upon the colors of the neighboring cells [261]. Even simple rules can lead to complex emergent behavior, and Conway's model was later shown to be Turing complete [598]. Today, discrete cell modeling has advanced to study a broad swath of cancer biology, spanning carcinogenesis, tumor growth, invasion, and angiogenesis.

Discrete, or individual-based, models are generally divided into two categories: lattice-based (including cellular automata) and lattice-free (agent-based). Both aproaches track and update individual cells according to a set of biophysical rules. Typically these models involve a composite[2] discrete-continuum approach

[1] The agent model presented in this chapter is an extension of the work by Macklin et al. (2009) [435], and an advance copy of the work to be submitted by Macklin et al. in [436].

[2] Many refer to these as hybrid models, but we reserve the term for models that simultaneously combine discrete and continuum representations for cells.

in the sense that microenvironmental variables (glucose, oxygen, extracellular matrix, growth factors, etc.) are described using continuum fields while the cells are discrete. See the reviews by Aber et al. [11], Moreira and Deutsch [478], Drasdo [183], Araujo and McElwain [36], Quaranta et al. [556, 555], Hatzikirou et al. [309], Nagy [493], Abbott et al. [2], Byrne et al. [98], Fasano et al. [210], Galle et al. [253], Drasdo and Höhme [187], Thorne et al. [659], Anderson et al. [29], Deisboeck et al. [170], Anderson and Quaranta [30], and Zhang et al. [723]. We now review these two main approaches and give some key examples from the literature. Further review can be found in [427].

6.1.1 Lattice-based models

In lattice-based modeling, the cells are confined to a regular 2-D or 3-D lattice. Each computational mesh point is updated in time according to deterministic or stochastic rules derived from physical conservation laws and biological constraints. Some models use a high-resolution mesh to discretize the cells and the surrounding microenvironment with subcellular resolution, allowing a description of the cells' finite sizes, morphologies, and biomechanical interactions. Cellular automata (CA) models, which describe each cell with a single computational mesh point, can be viewed as a special case of the approach.

The simple spatial arrangement of lattice-based models is relatively easy to implement, rendering them broadly accessible beyond the traditional scientific computing comunities with less need for advanced computational expertise. The regular structure imposed by the computational mesh also eliminates the need for elaborate interaction testing between the discrete cells. This is particularly true for CA models on rectangular meshes, where cell-cell interaction is based upon the immediate neighboring mesh points. It is also straightforward to directly couple lattice-based methods to the microenvironment by assigning continuum variables to every mesh point (in the case of CA methods) or a coarsened submesh (in the more general case).

The uniform spacing of lattice-based methods can be a weakness. While computationally efficient, low-resolution lattices (CA methods) can impose artificial constraints on the arrangement, orientation, and interaction of the cells, which can sometimes be observed as square or diamond-like artifacts. Such low-resolution lattice-based models cannot capture non-lattice cell patternings often found in both normal tissue (e.g., hepatic lobules) and cancer (e.g., cribriform ductal carcinoma in situ, or DCIS). Because the cells only have several possible orientations, these models can only crudely treat cell polarization; cell mechanics can only be modeled with great difficulty. Hence, low-resolution models are poorly-suited to the rigorous exploration of the balance of cell-cell adhesion, cell-BM adhesion, and cell mechanics (e.g., deformability). High-resolution (subcellular) meshes can better approximate cell mechanics, but are much more computationally expensive, hence impeding their ability to describe large systems of cells and microenvironment.

6.1.2 Lattice-free models

Lattice-free models, frequently referred to as agent-based models, do not restrict the cells' positions and orientations in space. This allows a more complex and accurate coupling between the cells and their microenvironment, and imposes fewer artifical constraints on the behavior of multicellular systems. The cells are treated as distinct objects or agents and are allowed to move, divide, and die individually according to biophysically-based rules. For example, many models apply free-body force diagrams to the individual cells, allowing a mechanistic description of cell-cell and cell-ECM interactions. The level of detail in the cell size, volume, and morphology can vary from simple (e.g., infinitesimal points in 3-D space, such as in [1, 59, 427, 229]) to complex (e.g., evolving deformable spheres that develop cusps during mitosis, as in [188]). The agent interpretation of the cells makes modern object-oriented programming languages (e.g., C++ and Java) ideal for implementing these models.

Agent-based models are ideal for situations of freely-wandering and nonuniformly arranged cells, such as angiogenesis, carcinogenesis, immune system attacks on tumor cells, and metastasis. The level of detail of the agents can be tailored to the simulation. Each cell agent can be assigned individual protein and surface receptor signaling networks, a model of cell cycle progression, and genotypic and phenotypic characteristics; this makes agent-based modeling a powerful tool in multiscale frameworks. (Some agent-based models are restricted to motion on a regular lattice to save on computational cost. See [721, 722] for some examples.) The flexibility in detail, at times even down to the biochemical level, can make agent-based models easier to calibrate to biological data.

This flexibility comes at a price, however. Because each individual cell can be made almost arbitrarily complex, computational cost can be very high for non-lattice, agent-based models, limiting the approach to smaller systems of cells. The lack of a regular cell arrangement makes cell-cell interaction testing computationally expensive as well. In the worst case where there are n cell agents that may each interact with all n cells and there are no constraints on cell placement, one must test n^2 possible cell-cell interactions for each computational time step. In such a worst case, computational cost increases rapidly as more cells are added to the multicell system, rendering large-scale simulations infeasible.

6.1.3 Comparison with continuum methods

Continuum modeling can be too coarse-scaled to capture the spatial intricacy of tissue microarchitecture when cells are polarized (with visible apex, base, and anisotropic surface receptor distributions), or during individual cell motility. Furthermore, continuum models tend to lump multiple physical properties into one or two phenomenological parameters. For example, the models by [230, 439] lump cell-cell, cell-BM, and cell-ECM adhesion, motility, and ECM rigidity into a single "mobility" parameter, as well as forces on the tumor boundary. While this eases the mathematical analysis of the physical systems, it can be difficult to directly match such lumped parameters to physical measurements. Some key patient-specific measurements occur at the molecular (e.g., immunohistochemistry, or IHC) and cellular scales, i.e., at a finer scale than continuum models.

In contrast, discrete cell models can in some cases be directly matched to such measurements. For example, Zhang, Deisboeck and colleagues have been very successful in tying intracellular signaling models to individual cell phenotype and motility in brain cancer [721]. Their work also made key advances in using molecular and cellular data to inform and calibrate the cell-scale model. Several groups (e.g., [719]) have made considerable advances at linking molecular- and cell-scale models, often with calibration to data at the appropriate scales. This is promising in the context of patient-specific cancer simulation (see Chapter 10) and multiscale modeling , allowing molecular-, cellular-, and tissue-scale data to be matched at their "native" scales; bi-directional data flow subsequently propagates this information to all the scales in the model. See Chapter 7.1, Section 10.4.3, and the Conclusions following Chapter 10 for more on this topic.

Discrete models have some drawbacks when compared with continuum approaches. Because they rely upon the behavior of individual cells to determine emergent system properties, they can be difficult to analyze. In addition, the computational cost of the methods increases rapidly with the number of cells modeled, the lattice resolution (for lattice-based methods), and the complexity of each cell object (for agent models). This can make the models difficult or impossible to apply to large systems, even with parallel programming.

Other difficulties relate to model calibration. Non-local effects (e.g., biomechanics) are often better described by continuum variables, making calibration more feasible at the continuum scale based upon macroscopic measurements. Hybrid modeling (Chapter 7) can address this issue by applying and calibrating discrete and continuum models alongside one another, followed by rigorous information flow between the scales.

Some model parameters, even if clearly related to cell-scale phenomena, may be difficult to measure in controlled experiments, whereas macroscopic measurements based upon the averaged behavior of many cells are simple to measure accurately and match to lumped parameters in continuum models. However, we note that analysis of volume-averaged agent models can sometimes provide further insight on how to motivate and interpret such matching. See Section 6.5 for such an example.

6.1.4 Some discrete modeling examples

We now discuss some discrete modeling examples that sample the range of cell-scale tumor modeling. Our survey is not exhaustive of the immense level of discrete modeling in cancer cell biology; the interested reader is encouraged to examine the reviews listed in Section 6.1, as well as [427].

Composite cellular automata modeling

In an illustrative example of cellular automata modeling, Anderson et al. developed a composite cellular discrete-continuum model of solid tumor growth with microenvironmental interactions [28, 26]. The microenvironmental variables (ECM and MMPs) are continuous concentrations, while tumor cells are discrete cellular automata. Cells move via a biased random walk on a Cartesian lattice; the movement probabilities are generated by discretizing an analogous continuum model of the tumor cell density. The transition probabilities are similar in spirit to the chemotaxis model developed earlier by Othmer and Stevens [512]. The cells respond haptotactically to the ECM density and produce MMPs that degrade the matrix. Cell-cell adhesion was not considered. The model predicts more extensive local tumor invasion in heterogeneous ECM than is predicted by the analogous continuum model.

Building on this work, Anderson et al. extended their model to include cell-cell adhesion by weighing the probability of motion by the number of desired neighbors [26]. Different cell phenotypes are modeled by varying the number of desired neighbors, the proliferation rate, and the nutrient uptake rate. The microenvironment plays an important role in the model: the nutrient supply is assumed to be proportional to the ECM as a model of the pre-existing vasculature, and so matrix degradation disrupts the nutrient supply as well. This model enabled evaluation of how individual cell-cell and cell-ECM interactions may affect the tumor shape. Anderson and co-workers further extended their model to provide a theoretical/experimental framework to quantitatively characterize tumor invasion as a function of microenvironmental selective factors [32]. In the extended model, they considered random mutations among 100 different phenotypes. In agreement with the findings of Cristini and co-workers [151, 725, 147, 231], hypoxia and heterogenous ECM were found to induce invasive fingering in the tumor margins, with selection of the most aggressive phenotypes.

Gerlee and Anderson simplified this model to investigate complex branched cell colony growth patterns arising under nutrient-limited conditions [274]. In agreement with earlier stability analyses (e.g., [151]), the stability of the growth was found to depend on how far the nutrient penetrates into the colony. For low nutrient consumption rates, the penetration distance was large, which stabilized the growth; for high consumption rates the penetration distance was small, leading to unstable branched growth. After incorporating a feed-forward neural network to model the decision-making mechanisms governing the evolution of cell phenotype, Gerlee and Anderson demonstrated how the oxygen concentration may significantly affect the selection pressure, cell population diversity, and tumor morphology [273, 275]. They further extended this model to study the emergence of a glycolytic phenotype [276]. Their results suggest that this phenotype is most likely to arise in hypoxic tissue with dense ECM. The group has further explored these themes recently with Quaranta and Rejniak [555]. Similar discrete modeling work on hypoxia has been pioneered in various collaborations amongst Gatenby, Smallbone, Maini, Gillies, Gavaghan and others (e.g., [264, 629, 265, 268, 630, 627, 628]).

Lattice-gas cellular automata models

Dormann and Deutsch developed a lattice-gas cellular automaton method for simulating the growth and size saturation of avascular multicell tumor spheroids [182, 175]. Unlike traditional cellular automaton methods where at most one cell can be at a single grid point (volume exclusion), lattice-gas models accommodate variable cell densities by allowing multiple cells per mesh point, with separate channels of movement between mesh points. The channels specify direction and velocity magnitude, which may include zero velocity resting states. Lattice-gas models typically require channel-exclusion: only one cell may occupy a channel at any time. Hatzikirou et al. [308] later used this approach to study traveling fronts characterizing glioma cell invasion. Very recently, they performed a mean field analysis of a lattice gas model of moving and proliferating cells to demonstrate that certain macroscopic information (e.g. scaling laws) can be accurately obtained from the microscopic model [308]. Accurate predictions of other macroscopic quantities that sensitively depend on higher-order correlations are more difficult to obtain.

Immersed boundary model

In [563, 564], Rejniak developed a highly detailed lattice-based approach to modeling solid tumor growth. Each individual cell is modeled using the immersed boundary method [534, 533] on a regular computational grid. The cell is represented as the interior of an elastic membrane with the nucleus represented as an interior point. Cell-cell adhesion and cell contractile forces are modeled using linear springs to mimic a discrete set of membrane receptors, adhesion molecules and the effect of the cytoskeleton on cell mechanics. The cytoplasm and interstitial fluid are modeled as viscous, incompressible fluids. The elastic, adhesive, and contractive forces impart singular stresses to the fluids. Cell growth is modeled with an interior volume source; once the cell grows to a threshold volume, contractile forces on opposite sides of the cell create a neck that pinches off to produce two approximately equal-sized daughter drops. Nutrient supply is modeled using continuum reaction-diffusion equations, with uptake localized in the cells. The method can describe individual cell morphology but is computationally expensive, thus restricting simulations to about 100 cells. Rejniak and Dillon recently extended the model to better represent the lipid bilayer cell membrane structure as two closed curves connected by springs [567]; sources and sinks placed in the simulated bilipid membrane modeled water channels.

The immersed boundary cell model has been applied to study preinvasive intraductal tumors, as well as the formation and stability epithelial acini (single-layered spherical shells of polarized cells attached to a BM) [567, 565, 566]; genetic mutations that disrupt cell polarity could lead to abnormal acini and ductal carcinoma. The model has also been used to study the interaction between nutrient availability, metabolism, phenotype, and the growth and morphological stability of avascular tumors [181, 31]. Morphological instabilities are in qualitative agreement with preceding continuum [151, 725, 418, 439] and cellular automata [26, 32, 274, 273] modeling results.

An extended Q-Potts model

A less detailed lattice-based method has been developed using an extended Q-Potts model, which originated in statistical physics to study surface diffusion grain growth in materials science, as in [34]. Graner and Glazier adapted the Q-Potts model to simulate cell sorting through differential cell-cell adhesion [292, 286]. In this approach, now referred to as the GGH (Graner-Glazier-Hogeweg) model, each cell is treated individually and occupies a finite set of grid points within a Cartesian lattice; space is divided into distinct cellular and extracellular regions. Each cell is deformable with a finite volume. Cell-cell adhesion is modeled with an energy functional. A Monte Carlo algorithm is used to update each lattice point and hence change the effective shape and position of a cell. Although the description of the cell shape is less detailed than in the immersed boundary approach described above, finite-size cell effects are incorporated.

Later work incorporated nutrient-dependent proliferation and necrosis in the GGH model to simulate the growth of benign, multicellular avascular tumors to a steady-state [642]; nutrient transport was modeled with a continuum reaction-diffusion equation. The steady state configuration consisted of a central necrotic core, a surrounding band of quiescent cells, and an outermost shell of proliferative cells; parameters were determined by matching the thickness of these regions to experimental measurements. Reference [667] extended the GGH model by incorporating the ECM-MMP dynamics, haptotaxis, and adhesion-controlled proliferation to study tumor invasion. The GGH model has also been extended to account for chemotaxis [594], cell differentiation [321], and cell polarity [718]. Others have modified the GGH model to include a subcellular protein signaling model to tie the cell cycle to growth promoters and inhibitors through continuum reaction-diffusion equations [353]. In that work, parameter values were selected such that model produced avascular tumors that quantitatively replicated experimental measurements of *in vitro* spheroids.

The GGH model has been used to simulate vasculogenesis and tumor angiogenesis [467, 466, 468] in heterogeneous tumor microenvironments [55], as well as the role of the ECM in glioma invasion [578]. Very recently, Poplawski and coworkers used the GGH method to study the morphological evolution of 2-D avascular tumors [541]; the work developed a phase diagram characterizing the tumor morphology and the stability of the tumor/host interface with respect to critical parameters characterizing nutrient limitations and cell-cell adhesion. In particular, they found that morphological stability depends primarily on the diffusional limitation parameter, whereas the morphological details depend on cell-cell adhesion. The results are consistent with previous continuum [151, 147, 418, 439] and discrete [563, 274, 273, 31] modeling results.

Some semi-deformable agent-based models

Drasdo and co-workers developed an agent-based model that incorporates finite cell size to study epithelial cell-fibroblast-fibrocyte aggregates in connective tissue [188]. In their approach, simplified cells are modeled as a roughly spherical space containing a central region. The cells are slightly compressible and are capable of migration, growth and division. An undividing cell is taken to be spherical. As a cell mitoses, it deforms into a dumbbell shape until its volume roughly doubles, and then divides into two daughter cells. Adhesion and repulsion (from limitations on cell deformation and compressibility) among cells are modeled using an interaction energy that describes nearest-neighbor interactions. Mitosis and migration may induce pressure on neighboring cells. The cells respond by changing their mass or orientation to minimize the total interaction energy via a stochastic Metropolis algorithm [470]. Interaction potentials have also been used in agent models by Ramis-Conde and co-workers [560, 561]; in the model, cells move down the gradient of the potential, analogous to minimizing the interaction energy. Others have modeled cells as deformable viscoelastic ellipsoids [522, 163].

Drasdo and Höhme [185] adapted their approach to early-stage avascular tumor spheroids, where growth is not primarily limited by oxygen or nutrient supply, but rather by volume exclusion arising from limited cell compressibility. The biomechanical and kinetic parameters were estimated by comparison with tumor spheroid experiments from [225]. They later extended the model to account for glucose-limited growth, necrosis, and cell lysis, in order to simulate the spatiotemporal growth dynamics of 2-D tumor monolayers and 3-D tumor spheroids with biophysical and kinetic parameters drawn from experimental literature [186]. The results suggested that biomechanical growth inhibition is responsible for the transition from exponential to sub-exponential growth that is observed experimentally for sufficiently large tumors; glucose deprivation was found to primarily determine the size of the necrotic core but not the size of the tumor. Galle et al. extended the model to incorporate the effect of BM contact on cell cycle progress and apoptosis (see Section 2.1.1), and studied epithelial cell growth in monolayers [255]. They found that inactivation of BM-dependent cell cycle progression and apoptosis, or removal of contact-mediated growth inhibition (e.g., see Section 2.1.5) could lead to epithelial tumor growth. In similar monolayer simulations, Drasdo showed how the agent model can be used to determine the rules for a simpler cellular automaton model for use in deriving a continuum model with contact inhibition by coarse-graining, thereby providing a link between different scales and biophysical processes [184]. Byrne and Drasdo performed further analysis of the continuum model [104].

Recent examples of subcellular modeling

Individual cell agents can readily be endowed with subcellular models, making them ideal multiscale modeling platforms. Recently, Ramis-Conde and colleagues incorporated E-cadherin/β-catenin dynamics in an agent-based model to obtain a more realistic model of cell-cell adhesion mechanics [561]; β-catenin binds the membrane-bound E-cadherin to the cytoskeleton. Their detailed model could describe the detachment of cells from a primary tumor and the corresponding epithelial-to-mesenchymal transition. Galle et al. incorporated cell-ECM interactions and ECM contact-dependent cell regulation as well as cell differentiation [254]. They studied the effect of cancer stem cell organization on tumor growth, finding that tumors invade the host tissue much more rapidly when stem cells are on the tumor periphery, rather than confined to the interior.

Wang et al. developed a multiscale model of non-small cell lung cancer within a 2-D microenvironment, implementing a specific intracellular signal transduction pathway between the epidermal growth factor receptor (EGFR) and extracellular receptor kinase (ERK) at the molecular level [681]. Phenotypic changes at the cellular level were triggered through dynamical alterations of these molecules. The results indicated that for this type of cancer, downstream EGFR-ERK signaling may be processed more efficiently in the presence of a strong extrinsic chemotactic stimulus, leading to a migration-dominant cell phenotype and an accelerated rate of tumor expansion. Zhang et al. presented a 3-D multiscale agent-based model to simulate the cellular decision process to either proliferate or migrate in the context of brain tumors [721]. Each cell was equipped with an EGFR gene-protein interaction network module that also connected to a simplified cell cycle description. The results show that proliferative and migratory cell populations directly impact the spatiotemporal expansion patterns of the cancer. Zhang and co-workers later refined their model to incorporate mutations representing a simplified tumor progression pathway [722].

6.2 An agent-based cell modeling framework

To illustrate these concepts, we now introduce a discrete, cell-scale modeling framework that combines and extends the major features of the models introduced in Section 6.1. Our main objective is to develop a model that is sufficiently mechanistic that cellular and multicellular behavior manifest themselves as *emergent phenomena* of the modeling framework, rather than through computational rules that are imposed *a priori*. An additional design goal is that the model is modular (both in software and mathematics), allowing “sub-models” (e.g., molecular signaling, cell morphology) to be expanded, simplified, or outright replaced as necessary.

We use a lattice-free, agent-based approach to allows more accurate cell mechanics. We treat the cells (the agents) as physical objects subject to biophysically-justified forces. Cell-cell and cell-BM mechanical interactions are modeled with interaction potential functions, similarly to [188, 185, 186, 184, 104]. The balance of these forces explicitly determines the cell's velocity. The cells have nonzero, finite size, similar to the work by [188, 185, 186, 184]. We explicitly model mechanical interactions between the cells and the basement membrane, similarly to the work in [570]. As with many of the discrete models in Section 6.1.4, each cell has a phenotypic state, with transitions between those phenotypic states governed by stochastic processes. We note that we use the same model for both cancerous and non-cancerous cells. The cells differ primarily in the values of their proliferation, apoptosis, and other coefficients; this is analogous to modeling altered oncogenes and tumor suppressor genes [302].

We incorporate essential molecular biology through carefully-chosen constitutive relations. In particular, we attempt to model the mechanics, time duration, and biology of each phenotypic state as accurately as our data will allow; this should facilitate model calibration to molecular- and cellular data. As in preceding models (e.g., [28]), we incorporate the microenvironment using a composite discrete-continuum appproach: the microenvironment is modeled as a set of field variables (e.g., oxygen concentration, ECM density) governed by continuum equations that can be altered by the discrete cells. Cell agents interact with this microenvironment both mechanically and biochemically through surface receptors that are part of a molecular-scale signaling model.

This agent model introduces several new features to discrete modeling as part of our design philosophy. The cell states are chosen specifically to facilitate calibration to immunohistochemistry in patient-specific simulations. We explicitly link the phenotypic state transitions to the microenvironment and signaling models through functional relationships in the stochastic parameters. Our model differentiates between apoptosis and necrosis and introduces a model for necrotic cell calcification. To better facilitate a mechanistic understanding of the model and matching to experimental biology, we separate the forces into separate potential functions, rather than lump them together into a single function. We use interaction potential functions with compact support (are zero outside some finite maximum interaction distance) to more realistically model the finite interaction distances between cells and their neighbors. The adhesion model can differentiate between homophilic and heterophilic adhesion, and separates the effects of cell-cell, cell-BM, and cell-ECM adhesion.

In this discussion, cells are not polarized, and in particular, we assume an isotropic distribution of cell surface receptors; we discuss model extensions to address this in [436]. Also, we do not currently focus on stem cell dynamics, although this can readily be added by identifying cells as stem cells, progenitor cells, or differentiated cells, and assigning each class different proliferation and other phenotypic characteristics. We treat the cells as mostly-rigid spheres, with growth both in 2D and 3D; basement membranes are currently modeled as sharp boundaries using level set functions [437, 438, 439, 440, 230, 441]. We present applications of the model to breast cancer in in Section 6.6 and Chapter 10.

6.2.1 A brief review of exponential random variables and Poisson processes

Because we model transitions between cell states as stochastic processes, we begin with a brief review of the necessary preliminaries. This discussion necessarily only introduces the key concepts and does not explore the full richness of measure theory-based probability and stochastic processes. The interested reader can find more in widespread references (e.g., [612, 507]).

A random variable T is *exponentially distributed* with parameter α if for any $t > 0$, the probability $\Pr(T < t)$ is given by

$$\Pr(T < t) = 1 - \mathrm{e}^{-\alpha t}. \tag{6.1}$$

Also, T has expected value $\mathrm{Ex}[T] = \frac{1}{\alpha}$ (i.e, the mean $\langle T \rangle$ is $1/\alpha$) and variance $\mathrm{Var}[T] = \frac{1}{\alpha^2}$. The simple relationship between the mean $\langle T \rangle$ and α is useful for calibration by limited data. Exponential random variables are *memoryless.* For any $0 \leq t, \Delta t$, the probability that $T > t + \Delta t$ given that $T > t$ is

$$\Pr(T > t + \Delta t | T > t) = \Pr(T > \Delta t), \tag{6.2}$$

i.e., if the event T has not occurred by time t, then the probability that the event occurs within an additional Δt units of time is unaffected by the earlier times, and so we can "reset the clock" at time t. This is useful for modeling cell decision processes that depend upon the current subcellular and microenvironmental state, and not on previous times. Even if the current cell decisions do depend upon past times, that information can be built into the time evolution of the internal cell state.

A *stochastic process* N_t is a series of random variables indexed by the "time" t. In particular, N_t is a *counting process* if:

1. $N_0 \geq 0$. (The initial number of events N_0 is at least zero.)
2. $N_t \in \mathbb{Z}$ for all $t \geq 0$. (The current number of events N_t is an integer.)
3. If $s < t$, then $N_t - N_s \geq 0$. (N_t is the cummulative number of events, and the number of events occuring within $(s, t]$ is $N_t - N_s$.)

A *Poisson process* X_t is a particular type of counting process satisfying:

1. $X_0 = 0$. (The initial count is 0.)
2. If $[s, s + \Delta s]$ and $[t, t + \Delta t]$ are non-overlapping, then $X_{s+\Delta s} - X_s$ and $X_{t+\Delta t} - X_t$ are independent random variables. (What happens in the interval $(t, t + \Delta t)$ is independent of what happened in $(s, s + \Delta s)$.)
3. For any $0 \leq s < t$, the distribution of $X_t - X_s$ only depends upon the length of the interval (s, t) (stationary increments), and in particular, if $n \in \mathbb{N}$,

$$\Pr(X_t - X_s = n) = \frac{e^{-\alpha(t-s)}\alpha(t-s)}{n!}. \tag{6.3}$$

Poisson processes have a useful property that we rely upon in the model. If $A_n = \inf\{t : P_t = n\}$ is the *arrival time* of the n^{th} event (i.e., the first time at which $X_t = n$), and $T_{n+1} = A_{n+1} - A_n$ is the *interarrival time* between the n^{th}

and $(n+1)^{\text{st}}$ events for $n \in \mathbb{N}$, then T_n is an exponentially-distributed random variable with parameter α, and

$$\begin{aligned}\Pr\left(X_{t+\Delta t} - X_t \geq 1\right) &= \Pr\left(A_n \in (t, t+\Delta t] | A_n > t\right) \\ &= \Pr\left(T_n < \Delta t\right) = 1 - e^{-\alpha \Delta t}.\end{aligned} \tag{6.4}$$

Thus, for sequence of events governed by a Poisson process, the time between consecutive events are simple exponentially-distributed random variables. In the context of stochastic cell models, if X_t is a Poisson process that gives the cummulative number of phenotypic state changes experienced by the cell by time t, the time to the next phenotypic state change is exponentially distributed.

Lastly, we note that if $\alpha = \alpha(t)$ varies in time, then X_t is a *non-homogeneous* Poisson process with interarrival times given by

$$\begin{aligned}\Pr\left(X_{t+\Delta t} - X_t = n\right) &= \frac{e^{-\int_t^{t+\Delta t} \alpha(s)\, ds} \left(\int_t^{t+\Delta t} \alpha(s)\, ds\right)^n}{n!} \\ \Pr\left(T_n < \Delta t\right) &= \Pr\left(X_{t+\Delta t} - X_t \geq 1\right) \\ &= 1 - e^{-\int_0^{\Delta t} \alpha(s)\, ds} \\ &\approx 1 - e^{-\alpha(t)\Delta t}, \quad \Delta t \downarrow 0.\end{aligned}$$

In our work, the Poisson processes are non-homogeneous due to their dependencies upon microenvironmental and intracellular variables that vary in time. However, these can be approximated by homogeneous processes on small time intervals $[t, t+\Delta t]$ as above [435, 436].

6.2.2 A family of potential functions

As in the work by [188, 185, 186, 184, 104], we shall use potential functions to model biomechanical interactions between cells and the microenvironment. We now introduce the family of interaction potential functions $\varphi(\mathbf{x}; R, n)$ used in the agent model. Parameterized by R and n, they satisfy

$$\varphi(\mathbf{x}; R, n) = \begin{cases} -\frac{R}{n+2}\left(1 - \frac{|\mathbf{x}|}{R}\right)^{n+2} & \text{if } |\mathbf{x}| < R \\ 0 & \text{else,}\end{cases} \tag{6.5}$$

$$\varphi'(x; R, n) = \begin{cases} \left(1 - \frac{x}{R}\right)^{n+1} & \text{if } x < R \\ 0 & \text{else,}\end{cases} \tag{6.6}$$

$$\nabla\varphi(\mathbf{x}; R, n) = \begin{cases} \left(1 - \frac{|\mathbf{x}|}{R}\right)^{n+1} \frac{\mathbf{x}}{|\mathbf{x}|} & \text{if } |\mathbf{x}| < R \\ \mathbf{0} & \text{else,}\end{cases} \tag{6.7}$$

where R is the *maximum interaction distance* of φ, and n is the *exponent* of the potential. We use this form of potential function because:

1. The potential (and its derivatives) has *compact support*: it is zero outside a closed bounded set (in this case, the closed ball $\overline{B}(\mathbf{0}, R)$). This models finite cell-cell and cell-BM interaction distances.
2. For any R and n, and for any $0 < |\mathbf{x}| < R$, we have

$$0 = \varphi'(R; R, n) < \varphi'(|\mathbf{x}|\,; R, n) < \varphi'(0; R, n) = 1. \tag{6.8}$$

   The baseline case $n = 0$ is a linear ramping, and for higher n, the function tapers off to zero gradient smoothly.

A good discussion of the use of potential functions to mediate cell-cell adhesion and interaction for individual-based models can be found in [104].

6.2.3 Cell states

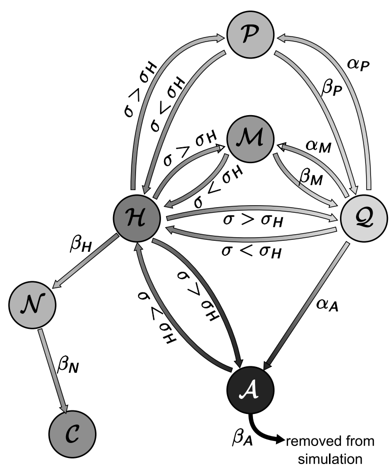

Figure 6.1 Flow between the cell states in the agent-based model. Reprinted with permission from [436].

We emulate the cells' biological function by endowing each agent with a state $\mathcal{S}(t)$ in the state space $\{\mathcal{Q}, \mathcal{P}, \mathcal{A}, \mathcal{H}, \mathcal{N}, \mathcal{C}, \mathcal{M}\}$. Quiescent cells ($\mathcal{Q}$) are in a "resting state" (G0, in terms of the cell cycle); this is the "default" cell state in the agent framework. We model the transitions between cell states as stochastic events governed by exponentially-distributed random variables. (Transition events are interarrival times modeling the elapsed time between proliferation and apoptosis events. See [436] for a discussion of the mathematical theory of this modeling construct.) Quiescent cells can become proliferative ($\mathcal{P}$), apoptotic ($\mathcal{A}$), or motile ($\mathcal{M}$). Cells in any state can become hypoxic ($\mathcal{H}$); hypoxic cells can recover to their previous state or become necrotic ($\mathcal{N}$), and necrotic cells are degraded and replaced by calcified debris ($\mathcal{C}$). See Figure 6.1. The subcellular scale is built into this framework by making the random exponential variables depend upon the microenvironment and the cell's internal properties. Cell cycle models have also been developed which can regulate the $\mathcal{P} \to \mathcal{Q}$ transition [2, 721], and protein signaling networks have been developed to regulate the $\mathcal{Q} \to \mathcal{P}$, $\mathcal{Q} \to \mathcal{A}$, and $\mathcal{Q} \to \mathcal{M}$ transitions. These can be directly integrated into the agent framework presented here by modifying the stochastic parameters; see Section 6.3. Further discussion of agent-based modeling with subcellular signaling components are in Section 6.1.4 and the excellent work done by [404, 176, 692, 697, 46, 719, 347, 691, 378, 681, 721, 134, 133, 170, 723].

Proliferation ($\mathcal{P}$):

Quiescent cells $\mathcal{Q}$ enter the proliferative state $\mathcal{P}$ with a probability that depends upon the microenvironment. We model the probability of a quiescent cell entering the proliferative state in the time interval $(t, t + \Delta t]$ as an exponential interarrival time with parameter $\alpha_P(\mathcal{S}, \bullet, \circ)$; $\bullet$ represents the cell's internal (genetic and proteomic) state, and $\circ$ denotes the local microenvironmental conditions. Hence[3],

$$\Pr\left(\mathcal{S}(t + \Delta t) = \mathcal{P} | \mathcal{S}(t) = \mathcal{Q}\right) = 1 - \mathrm{e}^{-\alpha_P \Delta t} \approx \alpha_P \Delta t. \tag{6.9}$$

Assuming a correlation between the microenvironmental oxygen level σ (nondimensionalized by σ_∞, the far-field oxygen level in non-diseased, "well-oxygenated" tissue) and proliferation (See Section 10.4.2), we expect α_P to increase with σ.[4] We model this by

$$\alpha_P = \alpha_P(\mathcal{S}(t), \sigma, \bullet, \circ) = \begin{cases} \overline{\alpha}_P(\bullet, \circ) \frac{\sigma - \sigma_H}{1 - \sigma_H} & \text{if } \mathcal{S}(t) = \mathcal{Q} \\ 0 & \text{else,} \end{cases} \tag{6.10}$$

where σ_H is a threshold oxygen value at which cells become hypoxic, and $\overline{\alpha}_P(\bullet, \circ)$ is the cell's $\mathcal{Q} \to \mathcal{P}$ transition rate when $\sigma = 1$ (i.e., in "well-oxygenated" tissue), which depends upon the cell's genetic profile and protein signaling state ($\bullet$) and the local microenvironment ($\circ$). For simplicity, we model $\overline{\alpha}_P$ as constant for and specific to each cell type. In Section 6.1.4, we discuss how to incorporate $\bullet$ (i.e., a cell's internal protein expression) and $\circ$ (as sampled by a cell's surface receptors) into α_P through a subcellular, molecular signaling model. We note that models have been developed that reduce the proliferation rate in response to mechanical stresses (e.g., see the excellent description by [613]); in the context of the model above, the cell samples these stresses from continuum-scale field variables or tensors (i.e., "$\circ$") to reduce α_P.

Once a cell has entered the proliferative state $\mathcal{P}$, it remains in that state for time β_P^{-1}, which may generally depend upon the microenvironment and the cell's

[3] The interarrival time normally gives the probability of having at least one proliferation event (rather than precisely one) during $(t, t + \Delta t]$. Our α_P in Eq. (6.10) precludes this because $\alpha_P \downarrow 0$ until completing proliferation.

[4] In Chapters 6 and 10, σ and g denote oxygen and glucose, which are generalized by the substrate n in the remainder of the book. In these chapters, n denotes an integer.

internal state, but which we currently model as fixed for both tumor and epithelial cells (with the same value). This models our assumption that both tumor and noncancerous cells use the same basic cellular machinery to proliferate, but with differing frequency due to altered oncogene expression [302]. Once the cell exits the proliferative state, we replace it with two identical daughter cells. Both inherit the parent cell's phenotypic properties, are randomly positioned adjacent to one another while conserving the parent cell's center of mass, and placed in the "default" quiescent state.

Apoptosis ($\mathcal{A}$):
Apoptotic cells are undergoing "programmed" cell death in response to internal protein signaling. As with proliferation, we model entry into $\mathcal{A}$ as an exponential interarrival time with parameter $\alpha_A(\mathcal{S}, \bullet, \circ)$. We assume no correlation between apoptosis and oxygen [195]. Hence, $\alpha_A(\mathcal{S}, \bullet)$ is fixed for each cell population:

$$\Pr\left(\mathcal{S}(t+\Delta t) = \mathcal{A} | \mathcal{S}(t) = \mathcal{Q}\right) = 1 - e^{-\alpha_A \Delta t}, \tag{6.11}$$

where

$$\alpha_A = \alpha_A(\mathcal{S}(t), \bullet, \circ) = \begin{cases} \overline{\alpha}_A(\bullet, \circ) & \text{if } \mathcal{S}(t) = \mathcal{Q} \\ 0 & \text{else,} \end{cases} \tag{6.12}$$

where $\circ$ does not include oxygen σ, but may include other microenvironmental stimuli such as chemotherapy or continuum-scale mechanical stresses that increase α_A, as in the work by [613]. Cells remain in the apoptotic state for a fixed amount of time β_A^{-1}. Cells leaving the apoptotic state are deleted from the simulation to model phagocytosis of apoptotic bodies by surrounding epithelial cells. Their previously-occupied volume is made available to the surrounding cells to model the release of the cells' water content after lysis.

Hypoxia ($\mathcal{H}$):
Cells enter the hypoxic state anytime $\sigma < \sigma_H$. Hypoxic cells have an exposure-dependent probability of becoming necrotic:

$$\Pr\left(\mathcal{S}(t+\Delta t) = \mathcal{N} | \mathcal{S}(t) = \mathcal{H}\right) = 1 - e^{-\beta_H \Delta t}, \tag{6.13}$$

where we currently model β_H as constant. If $\sigma > \sigma_H$ (i.e., normoxia is restored) at time $t + \Delta t$ and the cell has not become necrotic, it returns to its former state ($\mathcal{Q}$, $\mathcal{P}$, $\mathcal{A}$, or $\mathcal{M}$) and resumes its activity. For example, if the cell transitioned from $\mathcal{P}$ to $\mathcal{H}$ after spending τ time in the cycle, and normoxic conditions are restored before the cell transitions to $\mathcal{N}$, then it returns to $\mathcal{P}$ with τ time having ellapsed in its cell cycle progression. Because $\Pr\left(\mathcal{S}(t+\Delta t) = \mathcal{N} | \mathcal{S}(t) = \mathcal{H}\right) \approx \beta_H \Delta t$, the probability that a cell succumbs to hypoxia is approximately propotional to $\ell\left(t : \mathcal{S}(t) = \mathcal{H}\right)$, its cummulative exposure time to hypoxia. This construct could model cell response to other stressors (e.g., chemotherapy), similarly to "area under the curve" models (e.g., [197, 198]).

Necrosis ($\mathcal{N}$):

In our model, a hypoxic cell has a probability of irreversibly entering the necrotic state, simulating depletion of its ATP store. We can also simplify the model and neglect the hypoxic state by letting $\beta_H \to \infty$.

We assume that cells remain in the necrotic state for a fixed amount of time β_N^{-1}, during which time their surface receptors and subcellular structures degrade, they lose their liquid volume, and their solid component is calcified (replaced by calcium deposits). We define β_{NL}^{-1} to be the length of time for the cell to swell, lyse, and lose its water content, β_{NS}^{-1} the time for all surface adhesion receptors to degrade and become functionally inactive, and β_C^{-1} the time for the cell to fully calcify. Generally, $\beta_{NL}^{-1} \le \beta_{NS}^{-1} < \beta_C^{-1} = \beta_N^{-1}$. In [435], we found that a simplified model ($\beta_N^{-1} = \beta_{NS}^{-1} = \beta_{NL}^{-1} = \beta_C^{-1}$) could not reproduce certain aspects of the breast cancer microarchitecture.

If τ is the elapsed time spent in the necrotic state, we model the degradation of the surface receptor species S (scaled by the non-necrotic expression level) by exponential decay with rate constant $\beta_{NS} \log 100$; the constant is chosen so that $S(\beta_{NS}^{-1}) = 0.01\, S(0) = 0.01$, i.e., virtually all of the surface receptor is degraded by time $\tau = \beta_{NS}^{-1}$.

For a preliminary model of the necrotic cell's volume change, we neglect its early swelling and instead model it's volume change after lysis:

$$V(\tau) = \begin{cases} V & \text{if } 0 \le \tau < \beta_{NL}^{-1} \\ V_S & \text{if } \beta_{NL}^{-1} < \tau, \end{cases} \tag{6.14}$$

where V_S is the cell's solid volume.

Lastly, we assume a constant rate of cell calcification, with the necrotic cell 100% calcified by time β_C^{-1}. If C is the nondimensional degree of calcification, then $C(t) = \beta_C \tau$.

Calcified debris ($\mathcal{C}$):

Cells leaving the necrotic state $\mathcal{N}$ irreversibly enter the calcified debris state $\mathcal{C}$. Lacking functional adhesion receptors, these cells only adhere to other calcified debris. This is a simplified model of the crystalline bonds between calcium phosphate and/or calcium oxalate molecules in the microcalcification.

Motility ($\mathcal{M}$):

The transition of cells to the motile state (via α_M) is a complex "decision" that depends upon the cell's microenvironment as communicated to the cell by surface receptors and its internal signaling network. Once the cell enters $\mathcal{M}$, its speed (and hence β_M) and direction of motion depend upon its interaction with the microenvironment. Depending upon the sophistication of the model, the duration of motility can be fixed (constant β_M) or determined by the motility model (e.g., $\beta_M = 0$ until the cell reaches its destination, at which time we "force" an immediate $\mathcal{M} \to \mathcal{Q}$ transition). We discuss this further in Section 6.2.4.

6.2.4 Forces acting on the cells

Each cell is subject to competing forces that determine its motion within the microenvironment. Cells adhere to other cells (cell-cell adhesion: $\mathbf{F}_{\mathrm{cca}}$), the extracellular matrix (cell-ECM adhesion: $\mathbf{F}_{\mathrm{cma}}$), and the basement membrane (cell-BM adhesion: $\mathbf{F}_{\mathrm{cba}}$), calcified debris adheres to other calcified debris (debris-debris adhesion: $\mathbf{F}_{\mathrm{dda}}$), cells and calcified debris resist compression by other cells and debris (cell-cell repulsion: $\mathbf{F}_{\mathrm{ccr}}$), and the basement membrane resists its penetration and deformation by cells and debris (cell-BM repulsion: $\mathbf{F}_{\mathrm{cbr}}$). Motile cells experience a net locomotive force $\mathbf{F}_{\mathrm{loc}}$ along the direction of intended travel. See Figure 6.2, where we show the forces acting on cell 5. In addition, moving cells and debris experience a drag force $\mathbf{F}_{\mathrm{drag}}$ by the luminal and interstitial fluids, which we model by $\mathbf{F}_{\mathrm{drag}} = -\nu \mathbf{v}_i$. We express this balance of forces by Newton's second law acting on cell i:

$$m_i \dot{\mathbf{v}}_i = \sum_j \left(\mathbf{F}^{ij}_{\mathrm{cca}} + \mathbf{F}^{ij}_{\mathrm{ccr}} + \mathbf{F}^{ij}_{\mathrm{dda}} \right) + \mathbf{F}^{i}_{\mathrm{cma}} + \mathbf{F}^{i}_{\mathrm{cba}} + \mathbf{F}^{i}_{\mathrm{cbr}} + \mathbf{F}^{i}_{\mathrm{loc}} + \mathbf{F}^{i}_{\mathrm{drag}}. \tag{6.15}$$

Here, the sum is over all cells j in the computational domain.

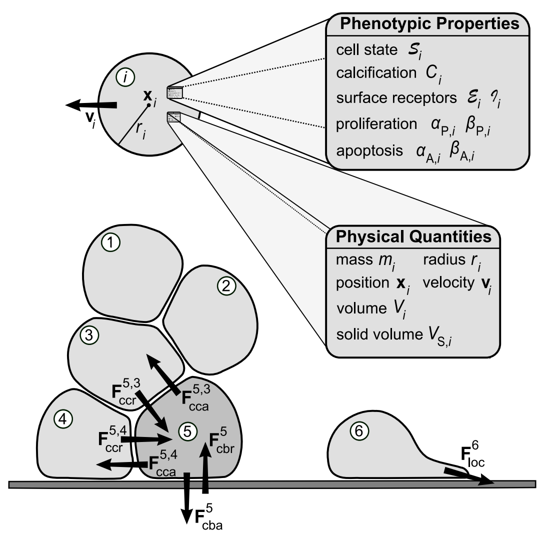

Figure 6.2 Basic schematic of the model. Key forces acting on cell 5 are labeled. Reprinted with permission from [436].

Cell-cell adhesion ($\mathbf{F}_{\mathrm{cca}}$):

Cell-cell adhesion can be both homophilic [524] and heterophilic [633, 657, 429].

Homophilic adhesion:
Adhesion molecules $\mathcal{E}$ on the cell surface bond with $\mathcal{E}$ molecules on neighboring cells. Hence, the strength of the adhesive force between the cells is proportional to the product of their respective $\mathcal{E}$ expressions. Furthermore, the strength of the adhesion increases as the cells are drawn more closely together, bringing more surface area and hence more adhesion molecules into direct contact. We model this adhesive force between cells i and j by

$$\mathbf{F}_{\mathrm{cca}}^{ij} = \alpha_{\mathrm{cca}} \mathcal{E}_i \mathcal{E}_j \nabla \varphi \left(\mathbf{x}_j - \mathbf{x}_i ; R_{\mathrm{cca}}^i + R_{\mathrm{cca}}^j , n_{\mathrm{cca}} \right) , \tag{6.16}$$

where $\mathcal{E}_i$ and R_{cca}^i are cell i's (nondimensionalized) adhesion receptor expression and maximum cell-cell adhesion interaction distance, respectively, r_i is the cell's radius, and n_{cca} is the cell-cell adhesion power for our potential function family in Section 6.2.2. We typically set $R_{\mathrm{cca}}^i > r_i$ to approximate the cell's ability to deform before breaking all adhesive bonds, with the strength of force decreasing as the cells are separated.

Heterophilic adhesion:
Adhesion molecules $\mathcal{I}_A$ on the cell surface bond with $\mathcal{I}_B$ molecules on neighboring cells. Hence, the strength of the adhesive force between the cells is proportional to the product of their $\mathcal{I}_A$ and $\mathcal{I}_B$ receptor expressions. Furthermore, the strength of the adhesion increases as the cells are drawn more closely together, bringing more surface area and hence more receptors into direct contact. We model this adhesive force between cells i and j by

$$\mathbf{F}_{\mathrm{cca}}^{ij} = \alpha_{\mathrm{cca}} \left(\mathcal{I}_{A,i} \mathcal{I}_{B,j} + \mathcal{I}_{B,i} \mathcal{I}_{A,j} \right) \nabla \varphi \left(\mathbf{x}_j - \mathbf{x}_i ; R_{\mathrm{cca}}^i + R_{\mathrm{cca}}^j , n_{\mathrm{cca}} \right) , \tag{6.17}$$

where $\mathcal{I}_{A,i}$ and $\mathcal{I}_{B,i}$ are cell i's (nondimensionalized) $\mathcal{I}_A$ and $\mathcal{I}_B$ receptor expressions, R_{cca}^i is the cell's maximum cell-cell adhesion interaction distance, and n_{cca} is the cell-cell adhesion power as before. As with homophilic cell-cell adhesion, we typically set $R_{\mathrm{cca}}^i > r_i$ to approximate the ability of cells to deform before breaking all adhesive bonds, with the strength of force decreasing as the cells are separated.

Cell-ECM adhesion ($\mathbf{F}_{\mathrm{cma}}$):
Integrins $\mathcal{I}_E$ on the cell surface form heterophilic bonds with suitable ligands $\mathcal{L}_E$ in the ECM. We assume that $\mathcal{L}_E$ is distributed proportionally to the (nondimensional) ECM density E. If we assume that $\mathcal{I}_E$ is distributed uniformly across the cell surface and E varies slowly relative to the spatial size of a single cell, then cells at rest encounter a uniform pull from $\mathbf{F}_{\mathrm{cma}}$ in all directions, resulting in zero net cell-ECM force. For cells in motion, $\mathbf{F}_{\mathrm{cma}}$ resists that motion similarly to drag due to the energy required to overcome $\mathcal{I} - \mathcal{L}$ bonds:

$$\mathbf{F}_{\mathrm{cma}} = -\alpha_{\mathrm{cma}} \mathcal{I}_{E,i} E \mathbf{v}_i . \tag{6.18}$$

If E or $\mathcal{L}_E$ varies with a higher spatial frequency, or if $\mathcal{I}_E$ is not uniformly distributed, then the finite half-life of $\mathcal{I}_E - \mathcal{L}_E$ bonds will lead to net haptotactictype migration up gradients of E [586]. We currently neglect this effect except by including it into the cell's (active) locomotive force $\mathbf{F}_{\mathrm{loc}}$.

Cell-BM adhesion ($\mathbf{F}_{\mathbf{cba}}$):
Integrin molecules on the cell surface form heterophilic bonds with specific ligands $\mathcal{L}_B$ (generally laminin and fibronectin [92]) on the basement membrane (with density $0 < B < 1$). We assume that $\mathcal{L}_B$ is distributed proportionally to the (nondimensional) BM density B. Hence, the strength of the cell-BM adhesive force is proportional to its integrin surface receptor expression and B. Furthermore, the strength of the adhesion increases as the cell approaches the BM, bringing more cell adhesion receptors in contact with their ligands on the BM. We model this adhesive force on cell i by

$$\mathbf{F}^i_{\mathrm{cba}} = \alpha_{\mathrm{cba}} \mathcal{I}_{B,i} B \nabla\varphi \left(d(\mathbf{x}_i); R^i_{\mathrm{cba}}, n_{\mathrm{cba}} \right), \tag{6.19}$$

where d is the distance to the basement membrane, $\mathcal{I}_{B,i}$ and R^i_{cba} are cell i's (nondimensionalized) integrin receptor expression and maximum cell-BM adhesion interaction distance, respectively, and n_{cba} is the cell-BM adhesion power. (See Section 6.2.2.) As with cell-cell adhesion, we typically set $R^i_{\mathrm{cba}} > r_i$ to approximate the cell's limited capacity to deform before breaking all its adhesive bonds.

(Calcified) debris-(calcified) debris adhesion ($\mathbf{F}_{\mathbf{dda}}$):
We model adhesion between calcified debris particles similarly to homophilic cell-cell adhesion; hence calcite crystals in the interacting calcified debris particles remain strongly bonded as part of the microcalcification. We model this adhesive force between the calcified debris particles i and j by

$$\mathbf{F}^{ij}_{\mathrm{dda}} = \alpha_{\mathrm{dda}} C_i C_j \nabla\varphi \left(\mathbf{x}_j - \mathbf{x}_i; R^i_{\mathrm{dda}} + R^j_{\mathrm{dda}}, n_{\mathrm{dda}} \right), \tag{6.20}$$

where C_i and R^i_{dda} are cell i's (nondimensionalized) degree of calcification and maximum debris-debris adhesion interaction distance, and n_{dda} is the debris-debris adhesion power. The α_{dda} can be interpreted as the adhesive force between two fully-calcified debris particles.

Cell-cell repulsion (including calcified debris) ($\mathbf{F}_{\mathbf{ccr}}$):
Cells resist compression by other cells due to the structure of their cytoskeletons, the incompressibility of their cytoplasm (fluid), and the surface tension of their membranes. We introduce a cell-cell repulsive force that is zero when cells are just touching, and then increases rapidly as the cells are pressed together. We approximate any pressure-induced cell deformation by allowing some overlap between cells. We model $\mathbf{F}_{\mathrm{ccr}}$ by

$$\mathbf{F}^{ij}_{\mathrm{ccr}} = -\alpha_{\mathrm{ccr}} \nabla\varphi \left(\mathbf{x}_j - \mathbf{x}_i; r_i + r_j, n_{\mathrm{ccr}} \right), \tag{6.21}$$

where n_{ccr} is the cell-cell repulsion power (Section 6.2.2) and α_{ccr} is the maximum repulsive force when the cells are completely overlapping.

Cell-BM repulsion (including debris) ($\mathbf{F}_{\mathbf{cbr}}$):
We model the basement membrane as rigid and non-deformable due to its relative stiffness and strength. Hence, it resists deformation and penetration by the cells and debris particles. We model the force by

$$\mathbf{F}^{i}_{\mathrm{cbr}} = -\alpha_{\mathrm{cbr}} B \nabla \varphi \left(d(\mathbf{x}_i); r_i, n_{\mathrm{cbr}} \right), \tag{6.22}$$

where n_{cbr} is the cell-BM repulsion power, d is the distance to the BM, and α_{cbr} is the maximum repulsive force when the cell's center is embedded in the basement membrane. Cells can secrete matrix metalloproteinases (MMPs) that degrade the BM (Section 2.2.3) and hence reduce $\mathbf{F}_{\mathrm{cbr}}$; we model this effect by making the cell-BM repulsive force proportional to the remaining BM density B. We discuss this further in Section 6.4.

Motile locomotive force ($\mathbf{F}_{\mathbf{loc}}$):
If $\mathcal{S} \neq \mathcal{M}$, then $\mathbf{F}_{\mathrm{loc}} = \mathbf{0}$. Otherwise, we can model the locomotive force with various levels of detail:

Imposed chemotaxis and haptotaxis:
For a simple motility model, we choose a deterministic direction of motion based upon biological hypotheses, such as chemotaxis in response to growth factors f and haptotaxis along gradients in the ECM E:

$$\mathbf{F}_{\mathrm{loc}} = \alpha_1 \nabla f + \alpha_2 \nabla E. \tag{6.23}$$

The coefficients α_1 and α_2 can be either fixed or altered to model energetic concerns such as oxygen availability, level of receptor activation, and expression of adhesive ligands necessary for traction. For instance, one could model

$$\alpha_1 = \overline{\alpha}_1 \left(\sigma, g \right) f f_r \mathcal{I}_{\mathrm{E},i} E, \tag{6.24}$$

where g is the cell's internal glucose level, $\overline{\alpha}_1(\sigma, g)$ models the rate of locomotion as a function of oxygen and glucose, f_r is the cell's surface expression of receptors to f; $f f_r$ denotes overall activation of f_r. Similarly, $\mathcal{I}_{\mathrm{E},i} E$ gives the overall level of binding of adhesion receptors $\mathcal{I}_{\mathrm{E},i}$ to their ligands in the ECM. We apply $\mathbf{F}_{\mathrm{loc}}$ for a fixed amount of time β_M^{-1}; afterwards, we set $\mathcal{S} = \mathcal{Q}$ and $\mathbf{F}_{\mathrm{loc}} = \mathbf{0}$. One could use similar functional forms for α_2.

Biased random motion:
Increasing the complexity somewhat, we choose a random direction of motion when the cell enters the motile state and fix it for the duration of motility, with distribution dependent upon the gradients of microenvironmental factors such

as oxygen (σ), growth factors (f), and ECM (E). One such method is

$$\mathbf{w} = r_1 \nabla \sigma + r_2 \nabla f + r_3 \nabla E, \qquad -1 \le r_1, r_2, r_3 \le 1 \tag{6.25}$$

$$\mathbf{F}_{\text{loc}} = \frac{\alpha_{\text{loc}}}{|\mathbf{w}|} \mathbf{w}, \tag{6.26}$$

where the distributions of the random variables r_1, r_2, and r_3 are chosen according to the desired weighting of oxygen taxis, chemotaxis, and haptotaxis. Random weightings can be used to model more complex signaling dynamics, where the cell must "choose" among competing signals, but the internal decision process is unknown. We apply the vector of travel for pseudotime $0 \le \tau \le \beta_M^{-1}$, after which $\mathcal{S} = \mathcal{Q}$ and $\mathbf{F}_{\text{loc}} = \mathbf{0}$.

Motion along the BM:
We can model motility along a basement membrane by extension and contraction of lamellipodia as follows: at any time t that the cell state changes to $\mathcal{M}$, we choose a random direction $\mathbf{w}$ (with $|\mathbf{w}| = 1$; see Figure 6.3a), and test the line segment between $\mathbf{x} + r\mathbf{w}$ (on the cell membrane) and $\mathbf{x} + (r + \ell_{\text{podium}})\mathbf{w}$ (the maximum extension of a lamellipodium) for intersection with the BM (labeled as $\mathbf{x}_{\text{loc}}$ in Figure 6.3b). If there is no intersection, we set $\mathcal{S} = \mathcal{Q}$. We assume that the cell adheres to the BM with a lamellipodium at $\mathbf{x}_{\text{loc}}$ and pulls towards this location until either (i) the cell's boundary reaches $\mathbf{x}_{\text{loc}}$ (Figure 6.3c), or (ii) the cell "gives up" at a maximum time $\beta_{M,\max}^{-1}$. Until then, we model

$$\mathbf{F}_{\text{loc}} = \alpha_{\text{loc}} \frac{\mathbf{x}_{\text{loc}} - \mathbf{x}}{|\mathbf{x}_{\text{loc}} - \mathbf{x}|}, \tag{6.27}$$

where α_{loc} gives the cell's speed of lamellipodium contraction. To avoid "double-counting" cell-BM adhesion, we set $\mathbf{F}_{\text{cba}} = \mathbf{0}$ during motility. See Figure 6.3. Once motility is complete, we set $\mathbf{F}_{\text{loc}} = \mathbf{0}$ and $\mathcal{S} = \mathcal{Q}$.

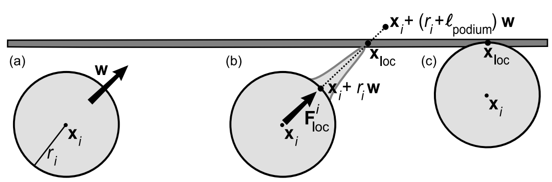

Figure 6.3 To simulate motility along a basement membrane, we **(a)** choose a random unit vector $\mathbf{w}$, **(b)** test for intersection with the BM along that direction, and apply $\mathbf{F}_{\text{loc}}$ towards that intersection point until **(c)** the cell membrane reaches the BM. Reprinted with permission from [436].

Mechanistic motility:
In a more rigorous motility model, we recognize locomotion as the combined effect of directed actin polymerization (drives protrusion of the cell membrane)

and differential cell-ECM adhesion [405]. Suppose that $a(\theta, \varphi, g, \sigma, f, f_r)$ gives the distribution of actin polymerization activity across the cell's surface, where $0 \le a \le 1$, and f and f_r also vary with position (θ, φ) on the cell surface. Let $\mathcal{I}(\theta, \varphi)$ and $E(\theta, \varphi)$ denote the distributions of surface adhesion receptor and nearby ligand, respectively, where these also vary between 0 and 1. Then the distribution of successful adhesion of cell membrane protrusions to the ECM can be modeled by

$$M(\theta, \varphi) = a(\theta, \varphi, g, \sigma, f, f_r)\mathcal{I}(\theta, \varphi)E(\theta, \varphi). \tag{6.28}$$

We set

$$\mathbf{F}_{\text{loc}} = \alpha_{\text{loc}}\mathbf{a}_{\max} \qquad \text{OR} \qquad \mathbf{F}_{\text{loc}} = \alpha_{\text{loc}}\nabla M, \tag{6.29}$$

where $\mathbf{a}_{\max}$ is the direction that maximizes a (or is randomly chosen if $\nabla M = \mathbf{0}$), and we apply this force until reaching a maximum motility duration β_M^{-1}. This approach could replace the explicit treatment of cell-cell, cell-BM, and cell-ECM adhesion. We are investigating this approach in a modified agent model that explicitly discretizes cell membrane extension and retraction [586].

This general form should capture oxygen/glucose taxis, chemotaxis and haptotaxis as emergent properties, as well as the effects of ECM anisotropy: if the rate of actin polymerization is assumed to correlate with local ATP availability (proportional to glucose and oxygen), then ∇a should correlate with ∇g and $\nabla \sigma$, thereby recovering nutrient taxis. If actin polymerization is assumed to occur as a result of an internal signaling response to a chemoattractant f and if the receptor f_r is roughly uniformly distributed, then ∇a should correlate with ∇f, giving chemotaxis as an emergent behavior. If a is uniform but the ECM has a local gradient, then $\mathbf{F}_{\text{loc}} \parallel \nabla E$, thus recovering haptotaxis. By incorporating a signaling model into a that connects with actin polymerization activity (e.g., as in [476, 456, 216, 707, 369, 593]), we can help make the model more mechanistic and less phenomenological, thereby improving the predictivity of the model. This is a key strength of multiscale modeling.

"Inertialess" assumption:

We assume that the forces equilibrate quickly, and so $|m_i \dot{\mathbf{v}}_i| \approx 0$. Hence, we approximate $\sum \mathbf{F} = \mathbf{0}$ and solve for the cell velocity from Eq. (6.15):

$$\mathbf{v}_i = \frac{1}{\nu + \alpha_{\text{cma}}\mathcal{I}_{E,i}E}\left(\sum_j \left(\mathbf{F}_{\text{cca}}^{ij} + \mathbf{F}_{\text{dda}}^{ij} + \mathbf{F}_{\text{ccr}}^{ij}\right) + \mathbf{F}_{\text{cba}}^{i} + \mathbf{F}_{\text{cbr}}^{i} + \mathbf{F}_{\text{loc}}^{i}\right). \tag{6.30}$$

This has a convenient interpretation: each term $\frac{1}{\nu+\alpha_{\text{cma}}\mathcal{I}_{E,i}E}\mathbf{F}_{\Box}$ is the "terminal" (equilibrium) velocity of the cell when fluid drag, cell-ECM adhesion, and $\mathbf{F}_{\Box}$ are the only forces acting upon it. (Here, "$\Box$" represents any individual force above, e.g., cba, cca, etc., and the summation is over all cells j in the computational domain.) This will be useful when calibrating cell motility in future work, as motility is generally measured as a cell velocity (e.g., [304]).

6.3 Subcellular modeling

We can incorporate a molecular-scale signaling model to improve the cell agent's "decision process." For example, in the context of the EGFR pathway, Deisboeck et al. modeled the PLCγ and ERK proteins to drive cell decisions on quiescence, proliferation, and motility based upon thresholding on the time derivatives of these proteins [169, 46, 45, 681, 721, 133, 723].

Taking an analogous approach, we may derive a generalized signaling model by introducing a set of proteins $\mathbf{P} = \left[P_1, P_2, \cdots\right]^T$ governed by a (nonlinear) system of ODEs. Because the cell's protein state depends upon sampling the microenvironment, we define a "stimulus" vector $\mathbf{S} = \left[S_1, S_2, \cdots\right]$, where the S_i may be oxygen, receptor ligands, and so forth. Furthermore, the signaling network topology depends upon the cell's genetic makeup, which we generically refer to as $\mathbf{G}$. Hence:

$$\dot{\mathbf{P}} = \mathbf{f}\left(\mathbf{G}, \mathbf{P}, \mathbf{S}\right). \tag{6.31}$$

The phenotypic transition probabilities then depend upon $\mathbf{P}$ and $\dot{\mathbf{P}}$.

We illustrate this idea with a rudimentary E-cadherin/β-catenin signaling model. Let P_1 be the cell's unligated E-cadherin, P_2 the ligated E-cadherin (bound to E-cadherin S_1 on neighboring cells, considered an external stimulus), P_3 the free cytoplasmic β-catenin, and P_4 the ligated E-cadherin-β-catenin complexes. Then a basic system of nonlinear ODEs that includes protein synthesis, binding, dissociation, and proteolysis is given by [436]

$$\dot{P}_1 = \overbrace{c_1}^{\text{synthesis}} - \overbrace{c_2 S_1 P_1}^{\text{homophilic binding}} + \overbrace{c_3 P_2}^{\text{dissociation}} - \overbrace{c_4 P_1}^{\text{proteolysis}} \tag{6.32}$$

$$\dot{P}_2 = c_2 S_1 P_1 - c_3 P_2 - \overbrace{c_5 P_2}^{\text{proteolysis}} - \overbrace{d_2 P_2 P_3}^{\beta\text{-catenin binding}} + \overbrace{d_3 P_4}^{\beta\text{-catenin dissociation}} \tag{6.33}$$

$$\dot{P}_3 = \overbrace{d_1}^{\text{synthesis}} - d_2 P_2 P_3 + d_3 P_4 - \overbrace{d_4 P_3}^{\text{proteolysis}} \tag{6.34}$$

$$\dot{P}_4 = d_2 P_2 P_3 - d_3 P_4 - \overbrace{d_5 P_4}^{\text{proteolysis}} \tag{6.35}$$

The first two equations describe E-cadherin *receptor trafficing*, and the second two give the interaction of cytoplasmic β-catenin with ligated E-cadherin. We assume that transcription of downstream targets of β-catenin is proportional to P_3 (see Section 2.1.5) and incorporate this molecular signaling into the phenotypic transformations by altering the $\mathcal{Q} \to \mathcal{P}$ transition parameter α_P:

$$\alpha_P = \overline{\alpha}_P f_P(P_3)\frac{\sigma - \sigma_H}{1 - \sigma_H}. \tag{6.36}$$

Here, f_P satisfies $f_P' > 0$ (transcription increases with P_3), $f_P(1) = 1$ (β-catenin is not a limiting factor if there is no E-cadherin binding), and $f_P(0) = 0$ (there is no downstream transcription if all β-catenin is bound).

6.4 Dynamic coupling with the microenvironment

As discussed throughout Section 6.2.3, a cell agent's behavior is inexorably linked to the microenvironment. We now integrate the agent model with the microenvironment as part of a discrete-continuum composite model. We do this by introducing field variables for key microenvironmental components (e.g., oxygen, signaling molecules, extracellular matrix, etc.) that are updated according to continuum equations. The distribution of these variables affects the cell agents' evolution as already described; simultaneously, the agents impact the evolution of the continuum variables. We give several key examples to illustrate the concept.

Oxygen:

All cell agents uptake oxygen as a part of metabolism. At the macroscopic scale, this is modeled by

$$\frac{\partial \sigma}{\partial t} = \nabla \cdot (D \nabla \sigma) - \lambda \sigma, \tag{6.37}$$

where σ is oxygen, D is its diffusion constant, and λ is the (spatiotemporally variable) uptake rate by the cells[5]. Suppose that tumor cells uptake oxygen at a rate λ_t, host cells at a rate λ_h, and elsewhere oxygen "decays" (by interacting chemically with the molecular landscape) at a low rate background rate λ_b. Suppose that in a small neighborhood B (a ball $B_\epsilon(\mathbf{x})$ of radius ϵ centered at $\mathbf{x}$), tumor cells, host cells, and stroma (non-cells) respectively occupy fractions f_t, f_h, and f_b of B, where $f_t + f_h + f_b = 1$. Then $\lambda(\mathbf{x})$ is given by

$$\lambda(\mathbf{x}) \approx f_t \lambda_t + f_h \lambda_h + f_b \lambda_b, \tag{6.38}$$

i.e., by averaging the uptake rates with weighting according to the combination of cell types and stroma present near $\mathbf{x}$. Note that we could further decompose f_t and f_h according to cell phenotype, if the uptake rates are expected to vary. In a numerical implementation, λ is calculated first on a high-resolution mesh (e.g., 1 mesh point is 1 cubic micron in 3D) and subsequently averaged to obtain λ at the continuum scale (e.g., 1000 cubic micron mesh points) [436]. In this

[5] In Chapters 6 and 10, σ and g denote oxygen and glucose, which are generalized by the substrate n in the remainder of the book. In these chapters, n denotes an integer.

formulation, the cell uptake rate varies with the tumor microstructure, which, in turn, evolves according to nutrient and oxygen availability.

Extracellular matrix:

Cell agents adhere to the extracellular matrix and require ECM for certain types of cell locomotion (Section 6.2.4). Cells can also affect the ECM by secreting matrix metalloproteinases that degrade the extracellular matrix, and possibly by also depositing new ECM (Section 2.2.3). If E is the concentration of ECM and M is the concentration of MMPs secreted by the cells, then we model this at the continuum scale similarly to our prior work in [441]:

$$\frac{\partial E}{\partial t} = \lambda^{E}_{\text{production}}(\mathbf{x}) - \lambda^{E}_{\text{degradation}} EM \tag{6.39}$$

$$\frac{\partial M}{\partial t} = \nabla \cdot (D_M \nabla M) + \lambda^{M}_{\text{production}}(\mathbf{x}) - \lambda^{M}_{\text{decay}} M, \tag{6.40}$$

where $\lambda^{\square}_{\text{production}}$ are production rates ($\square = E, M$), $\lambda^{E}_{\text{degradation}}$ is the rate ECM degradation by MMPs, $\lambda^{M}_{\text{decay}}$ is the MMP decay rate, and D_M is the MMP diffusion constant (generally low).

The production rates $\lambda^{\square}_{\text{production}}$ are upscaled from the cell scale analogously to the oxygen uptake rate, and generally are functions of E and M. Reference [441] used production rates of the form $\overline{\lambda}^{\square}_{\text{production}}(1-\square)$, $\square = E, M$ for a constant value of $\overline{\lambda}$ within the tumor viable rim. This was an approximation of subcellular signaling under the assumption that ECM and MDE production decrease as E and M approach an equilibrium value, here scaled to 1. In a multiscale, composite modeling context, however, these assumptions are not required, as the phenomena can emerge directly from subcellular signaling models.

Basement membrane:

In Section 6.2.4, the basement membrane impacts the cell agents through a balance of adhesive and repulsive forces. The cells can also impact the BM by deforming and degrading it (Section 2.2.3). We model the BM as a sharp, heterogeneous, deformable interface. The cell agents require information on (1) their distance to the basement membrane, and (2) the properties of the BM at that closest location. We satisfy these requirements using an augmented level set approach. For simplicity, we describe this method for simulations in 2D; the 3-D approach is analogous.

Let $\left\{\mathbf{x}^{BM}(s) : 0 \leq s \leq 1\right\}$ parameterize the basement membrane, let $\mathbf{n}(s)$ be normal to the BM at $\mathbf{x}^{BM}(s)$ for all s (facing towards the epithelial side of the BM), and let $\mathbf{b}(s) = \left(b^1(s), b^2(s), \ldots\right)$ be a set of properties along the basement membrane at position $\mathbf{x}(s)$. In our work, b^1 is the BM density and b^2 is the integrin concentration. For any point $\mathbf{x}$ in the computational domain, define

$$s(\mathbf{x}) = s \text{ that minimizes } \left\{\left|\mathbf{x} - \mathbf{x}^{BM}(s)\right| : 0 \leq s \leq 1\right\}, \tag{6.41}$$

that is, $\mathbf{x}^{BM}(s(\mathbf{x}))$ is the closest point on the BM to $\mathbf{x}$. Note that the minimum value in Eq. (6.41) is equal to $|d(\mathbf{x})|$. For notational simplicity, let $s_i = s(\mathbf{x}_i)$, $\mathbf{x}_i^{BM} = \mathbf{x}^{BM}(s_i)$, and $\mathbf{n}_i = \mathbf{n}(s_i)$ for any cell i.

Here, $d(\mathbf{x})$ is the signed distance function (first referenced in Section 6.2.4), satisfying:

$$\begin{aligned} d &= 0 \quad \text{on the basement membrane} \\ d &> 0 \quad \text{on the epithelial side of the BM} \\ d &< 0 \quad \text{on the stromal side of the membrane} \\ |\nabla d| &\equiv 1 \quad (d \text{ is a distance function}). \end{aligned}$$

We modify the cell-BM adhesive and repulsive forces to account for the heterogeneity introduced by $\mathbf{b}(s)$. The modified cell-BM adhesive force acting on cell i is

$$\mathbf{F}^i_{\mathrm{cba}} = \alpha_{\mathrm{cba}} \mathcal{I}_{B,i} b^2(s_i) \nabla\varphi\left(d(\mathbf{x}_i); R^i_{\mathrm{cba}}, n_{\mathrm{cba}}\right). \tag{6.42}$$

We modify the cell-BM repulsive force on cell i to

$$\mathbf{F}^i_{\mathrm{cbr}} = -\alpha_{\mathrm{cbr}} b^1(s_i) \nabla\varphi\left(d(\mathbf{x}_i); r_i, n_{\mathrm{cbr}}\right); \tag{6.43}$$

note that this assumes that the BM stiffness is proportional to its density.

The MMPs secreted by the cells ($M(\mathbf{x})$; see the previous section) degrade the BM. We model this by

$$\frac{db^1(s)}{dt} = -\lambda^E_{\mathrm{degradation}} b^1(s) M\left(\mathbf{x}^{BM}(s)\right) \text{ for each } 0 \le s \le 1. \tag{6.44}$$

Cells in contact with the basement membrane impart forces that deform it. In the simplest deformation model, the membrane acts like a semi-plastic material whose deformations remain even if the cell-imparted stresses are eliminated. Any cell contacting the BM with velocity directed towards it contributes locally to the membrane normal velocity $\mathbf{v}^{BM}(s)$. This membrane velocity varies according to the heterogeneous membrane stiffness. We model this by first defining the BM normal velocity wherever the cells are touching it:

$$\mathbf{v}^{BM}(s_i) = \frac{-\max\left(-\mathbf{v}_i \cdot \mathbf{n}_i, 0\right)}{b^1(s)} \text{ for any } i \text{ such that } d(\mathbf{x}_i) < r_i. \tag{6.45}$$

We then smoothly interpolate this function to obtain $\mathbf{v}^{BM}$ for other values of s. We update the boundary position using this extended normal velocity (e.g., by extending $\mathbf{v}^{BM}$ off the basement membrane and using level set techniques, as in [437, 438, 439, 440, 230, 441]).

More sophisticated models can also be applied to the membrane deformation. We could discretize $\mathbf{x}^{BM}$ and $\mathbf{b}$, connect the discrete membrane points with springs, and balance the forces at each membrane mesh point to model an elastic boundary; gradually reducing the strain in each virtual spring could then model relaxation in a viscoelastic material.

More sophsticated still, we could upscale the cells' velocities $\mathbf{v}_i$ to obtain the mean mechanical pressure in a coarsened spatial grid using Darcy's law $\langle \mathbf{v} \rangle = \mu \nabla p$, as in Chapter 3. Combined with proper material properties and boundary conditions, we could then solve for the basement membrane velocity. Ribba and co-workers have used similar approaches for continuum descriptions of membrane deformations under viscoelastic stresses [570]. Such an approach would be very well-suited to hybrid models, where both discrete and continuum representations of the cell velocities are already present. In fact, membrane deformations are better suited to continuum descriptions that are well-developed for solid material mechanics, while membrane heterogeneity can be well-characterized by the localized alterations by the discrete cells; this is a good example where a hybrid model would be stronger than either a discrete or continuum approach alone. Chapter 7 will explore hybrid models in greater detail.

6.5 A brief analysis of the volume-averaged model behavior

Let us fix a volume Ω contained within the viable rim (i.e., any cell i in Ω satisfies $\mathcal{S}_i \notin \{\mathcal{H}, \mathcal{N}, \mathcal{C}\}$). We analyze the population dynamics in the simplified $\mathcal{Q}$-$\mathcal{A}$-$\mathcal{P}$ cell state network (we assume no motility); this analysis is the basis of the model calibration in Section 10.3. Let $P(t)$, $A(t)$, and $Q(t)$ denote the number of proliferating, apoptosing, and quiescent cells in Ω at time t, respectively. Let $N(t) = P + A + Q$ be the total number of cells in Ω. If $\langle \alpha_P \rangle (t) = \frac{1}{|\Omega|} \int_\Omega \alpha_P \, dV$ is the mean value of α_P at time t throughout Ω, then the net number of cells entering state $\mathcal{P}$ in the time interval $[t, t + \Delta t)$ is approximately

$$\begin{aligned} P(t+\Delta t) &= P(t) + \Pr\left(\mathcal{S}(t+\Delta t) = \mathcal{P} | \mathcal{S}(t) = \mathcal{Q}\right) Q(t) - \beta_P P(t) \Delta t \\ &\approx P(t) + \left(1 - e^{-\langle \alpha_P \rangle \Delta t}\right) Q(t) - \beta_P P(t) \Delta t, \end{aligned} \tag{6.46}$$

whose limit as $\Delta t \downarrow 0$ (after some rearrangement) is

$$\dot{P} = \langle \alpha_P \rangle Q - \beta_P P. \tag{6.47}$$

Similarly,

$$\dot{A} = \alpha_A Q - \beta_A A \tag{6.48}$$

$$\dot{Q} = 2\beta_P P - \left(\langle \alpha_P \rangle + \alpha_A\right) Q. \tag{6.49}$$

Summing these, we obtain

$$\dot{N} = \beta_P P - \beta_A A. \tag{6.50}$$

Next, define $\mathrm{PI} = P/N$ and $\mathrm{AI} = A/N$ to be the *proliferative* and *apoptotic indices*, respectively. We can express the equations above in terms of AI and PI by dividing by N and using Eq. 6.50 to properly treat $\frac{d}{dt}(P/N)$ and $\frac{d}{dt}(A/N)$.

After simplifying, we obtain a nonlinear system of ODEs for PI and AI:

$$\dot{\mathrm{PI}} = \langle \alpha_P \rangle (1 - \mathrm{AI} - \mathrm{PI}) - \beta_P \left(\mathrm{PI} + \mathrm{PI}^2\right) + \beta_A \mathrm{AI} \cdot \mathrm{PI} \tag{6.51}$$

$$\dot{\mathrm{AI}} = \alpha_A (1 - \mathrm{AI} - \mathrm{PI}) - \beta_A \left(\mathrm{AI} - \mathrm{AI}^2\right) - \beta_P \mathrm{AI} \cdot \mathrm{PI}. \tag{6.52}$$

These equations are far simpler to compare to immunohistochemical measurements, which are generally given in terms of AI and PI.

Lastly, let us nondimensionalize the equations by letting $t = \hat{t}\,\overline{t}$, where $\hat{t}$ is dimensionless. Then if $f' = \frac{d}{d\hat{t}} f$, we have

$$\frac{1}{\overline{t}} \mathrm{PI}' = \langle \alpha_P \rangle (1 - \mathrm{AI} - \mathrm{PI}) - \beta_P \left(\mathrm{PI} + \mathrm{PI}^2\right) + \beta_A \mathrm{AI} \cdot \mathrm{PI} \tag{6.53}$$

$$\frac{1}{\overline{t}} \mathrm{AI}' = \alpha_A (1 - \mathrm{AI} - \mathrm{PI}) - \beta_A \left(\mathrm{AI} - \mathrm{AI}^2\right) - \beta_P \mathrm{AI} \cdot \mathrm{PI}. \tag{6.54}$$

The cell cycle length β_P^{-1} is on the order of 1 day (e.g., as in [515]), and in Section 10.4.1, we determine that β_A is of similar magnitude. Thus, if we choose $\overline{t} \sim \mathcal{O}\,(10 \text{ day})$ or greater, then we can assume that $\frac{1}{\overline{t}}\mathrm{PI}' = \frac{1}{\overline{t}}\mathrm{AI}' = 0$ and conclude that the local cell state dynamics reach steady state after after 10-100 days. This is significant, because it allows us to calibrate the population dynamic parameters (α_A, α_P, β_A, and β_P) without the inherent difficulty of estimating temporal derivatives from often noisy *in vitro* and immunohistochemistry data.

6.6 Numerical examples from breast cancer

We now present numerical examples of the agent model applied to ductal carcinoma in situ: a type of breast cancer where the cells are confined to growth and motion in a breast duct. We focus on the simulation results and defer a biological discussion of breast cancer and model calibration to Chapter 10.

For simulation in 2D, consider cells growing in a fluid-filled domain Ω (representing a rigid-walled duct) of length ℓ (1 mm in our simulations) and width $2R$ (340 μm in our simulations). We "cap" the left edge of the simulated duct with a semicircle of radius R. Cells are removed from the simulation if they cross the right edge of the computational boundary. We represent the duct wall with a signed distance function d satisfying $d > 0$ inside the duct.

Cell states (see Figure 6.1) include the proliferative ($\mathcal{P}$), quiescent ($\mathcal{Q}$), apoptotic ($\mathcal{A}$), hypoxic ($\mathcal{H}$), necrotic ($\mathcal{N}$), calcified debris ($\mathcal{C}$) and motile ($\mathcal{M}$) states. We use the simplified model of motility along a basement membrane in randomly-selected directions. See Figure 6.3. For simplicity, we neglect membrane degradation, membrane deformation, and molecular-scale signaling, allowing us to instead focus upon the effects of the various cell states and forces. We assume there is no ECM in the duct ($\mathbf{F}_{\mathrm{cma}} = \mathbf{0}$), and cells adhere to one another with E-cadherin (homophilic adhesion) and to the BM with integrins. We assume the surface adhesion receptors and BM adhesion ligands are distributed uniformly on the cell surfaces and BM, respectively.

We model oxygen transport within the duct by

$$\begin{cases} \frac{\partial \sigma}{\partial t} = D\nabla^2\sigma - \lambda\sigma & \text{if } \mathbf{x} \in \Omega \\ \sigma = \sigma_B & \text{if } \mathbf{x} \in \partial\Omega, \end{cases} \tag{6.55}$$

where λ is the locally-averaged oxygen uptake rate discussed in Section 6.4. We use a Neumann condition $\partial\sigma/\partial n = 0$ on the righthand side of the duct. The parameter values for the simulations are given in Table 6.1. The duct size, population parameters (α_A, $\overline{\alpha}_P$, β_A, and β_P), balance of cell-cell adhesion and repulsion (α_{cca} vs. α_{ccr}), and oxygen boundary value σ_B are calibrated to the patient data presented in Chapter 10; more detail is given there. Further detail on the numerical implementation can be found in Section 10.2.4 and [436].

Parameter	Physical Meaning	Value
$2\,R_{\text{duct}}$	duct diameter	340 μm
L_{duct}	duct length	1 mm
R	Cell radius	9.953 μm
σ_H	hypoxic oxygen threshold	0.2
σ_B	duct boundary O_2 value	0.263717 if $\lambda_b = 0.001$ 0.277491 if $\lambda_b = 0.01$ 0.386095 if $\lambda_b = 0.1$
$\langle\lambda\rangle$	mean oxygen uptake rate	0.1 min^{-1}
λ_t	tumor cell O_2 uptake rate	0.1 min^{-1}
λ_b	background O_2 decay rate	0.001, 0.01, or 0.1 min^{-1}
$\langle\lambda\rangle\ L$	oxygen diffusion length scale	100 μm
α_A^{-1}	mean time to apoptosis	786.61 hours
$\overline{\alpha}_P^{-1}$	mean time to proliferation (when $\sigma = 1$)	115.27 min if $\lambda_b = 0.001$ 151.21 min if $\lambda_b = 0.01$ 434.53 min if $\lambda_b = 0.1$
β_A^{-1}	time to complete apoptosis	8.6 hours
β_P^{-1}	time to complete cell cycle	18 hours
β_{NC}^{-1}	time to complete calcification	15 days
β_H^{-1}	mean survival time for hypoxic cells	0 or 5 hours
β_{NL}^{-1}	time for necrotic cells to lyse	2, 24, 120, or 360 hours
β_{NS}^{-1}	necrotic cell surface receptor degradation time	5 or 15 days
V_S/V	solid cell fraction	10%
$\alpha_{\text{cca}}, \alpha_{\text{cba}}, \alpha_{\text{dda}}$	cell-cell, cell-BM, debris adhesive forces	0.391531ν (μm/min)
α_{ccr}	cell-cell repulsive force	8ν (μm/min)
α_{cbr}	cell-BM repulsive force	5ν (μm/min)
α_{loc}	locomotive (motile) force	5ν (μm/min)
α_M^{-1}	mean time between migration events	120, 300, or ∞ min
$\beta_{M,\max}^{-1}$	maximum motility time	15 min
ℓ_{podium}	maximum lamellipodium length	15 or 20 μm
$n_{\text{cca}}, n_{\text{cba}}, n_{\text{dda}}$	adhesion potential parameters	1
$n_{\text{ccr}}, n_{\text{nbr}}$	repulsion potential parameters	1
$R_{\text{cca}}, R_{\text{ccr}}, R_{\text{cba}}, R_{\text{cbr}}$	maximum interaction distances	12.083 μm

Table 6.1. Main parameters used for the agent model DCIS simulations.

6.6.1 Baseline calibrated run

We first simulate DCIS with simplified hypoxia ($\beta_H^{-1} = 0$) and no motility ($\alpha_M = 0$). We apply a simplified model of necrosis: $\beta_{NS}^{-1} = \beta_{NL}^{-1} = \beta_{NC}^{-1}$. We set $\lambda_b = 0.01\lambda_t$. The dynamic simulation is presented in Figure 6.4.

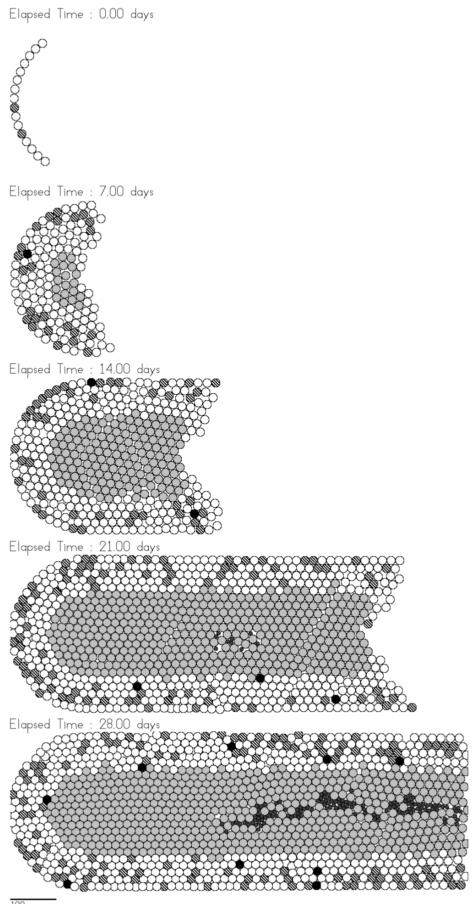

Figure 6.4 Dynamic agent-based simulation of DCIS in a 1 mm duct. **Legend:** quiescent cells are white, apoptotic cells are black, proliferating cells are diagonally striped, necrotic cells are light gray, and calcified cell debris is dark gray. Reprinted with permission from [436].

In the simulation, a small initial population begins proliferating into the duct (0 days). As the tumor grows along the duct, oxygen uptake by the cells leads to the formation of an oxygen gradient (not shown). At time 5.04 days, the oxygen level drops below σ_H in the center of the duct near the leading edge of the tumor, causing the first instance of necrosis (light gray cells). By 7 to 14 days, a viable rim of nearly uniform thickness (approximately 80 μm thick) can be observed, demonstrating the overall oxygen gradient decreasing from σ_B at the duct boundary to σ_H at the edge of the necrotic core. (See also Section 10.3.3.) This is consistent with the prediction in Section 6.5 that the cell state dynamics reach a local steady state by 10 to 100 days.

Consistent with the assumed functional form of the $\mathcal{Q} \to \mathcal{P}$ transition, proliferating cells (diagonally striped) are most abundant near the duct wall where the oxygen level is highest, with virtually no proliferation at the peri-necrotic boundary. Because oxygen can diffuse into the tumor from the duct lumen (with low decay rate λ_b), viable tumor cells are also observed along the tumor's leading edge near the center of the duct. See Figure 6.4 at times 7, 14, and 21 days.

Cells begin to lyse at 20.04 days, and because $\beta_{NC} = \beta_{NL}$, they immediately calcify (dark gray cells). By 28 days, another characteristic length emerges: the trailing edge of the microcalcification maintains a distance of approximately 500 μm from the end of the duct. Several features combine to cause this. We do not model contact inhibition, and so cells at the end of the duct continue to proliferate and push cells toward's the tumor's leading edge. Because the end of the duct has reached a local dynamic equilibrium by this time (see the discussion above and [439]), a steady flux of tumor cells into the necrotic region has emerged. Because the lysis and calcification times (β_{NL}^{-1} and β_{NC}^{-1}) are fixed, the cells are pushed a fixed distance along the necrotic core before lysing and calcifying, leading to the observed "standing wave" pattern.

The viable rim of the tumor reaches the end of the simulated 1 mm stretch of the duct by time 22.5 days, and the necrotic core reaches this computational boundary by approximately 24 days. Cells that exit the computational domain are removed from the simulation, leading to an artificial drop in mechanical resistance to growth, particularly as cells from the trailing edge of the tumor continue to proliferate and push into the lumen. Thus, the simulation is more valuable for examining the radial tumor dynamics than the rate of progression through the duct after this time.

6.6.2 Impact of hypoxic survival time

We next examined the impact of β_H^{-1}, the mean time hypoxic cells survive before necrosing. We found that increasing β_H^{-1} from 0 to 5 hours has a minimal impact on the simulation, principally by delaying calcification (because cells wait a few more hours before necrosing). (Results not shown.)

The minimal impact of β_H on the current model behavior is not surprising: hypoxic cells are not motile in this model implementation, and the overall flux of cells is from the proliferating rim towards the center of the duct. Hence, there is no opportunity for hypoxic cells to take advantage of their increased survival time to return to the viable rim. Thus, increasing β_H^{-1} merely delays necrosis (in this model formulation). Furthermore, the hypoxic cells are not glycemic in this model, and so they do not lower the pH (acidosis) in the nearby viable rim; hence, the increased hypoxic survival time does not impact the survivability and behavior of cells in the viable rim. We expect that β_H would have a greater impact if:

1. hypoxic cells were allowed to switch to anaerobic glycolysis, thus making the viable rim microenvironment acidic and giving the hypoxic cells a competitive advantage over nearby non-resistent tumor cell strains;

2. hypoxic cells were allowed to migrate out of the hypoxic region, thereby propogating their phenotypic adaptations into the tumor viable rim;
3. continuing the previous point, hypoxic cells could reach the basement membrane and initiate invasive carcinoma; and
4. hypoxic cells may experience increased genetic instability due to the harsh environment. This tends to accelerate the previous points.

Taken together, hypoxia would be expected to increased tumor invasiveness if these aspects were incorporated in the model.

6.6.3 Impact of the cell lysis time

Next, we investigate the impact of the necrotic cell lysis time β_{NL}^{-1} on the overall tumor evolution. We varied β_{NL}^{-1} with values 15 days, 5 days, 1 day, and 2 hours. Because surface receptor degradation is likely a faster process than cell calcification, we set β_{NS}^{-1} to 5 days. However, we found that varying β_{NS} had little impact on the mechanical behavior due to the dense cell packing in the simulated tumors.

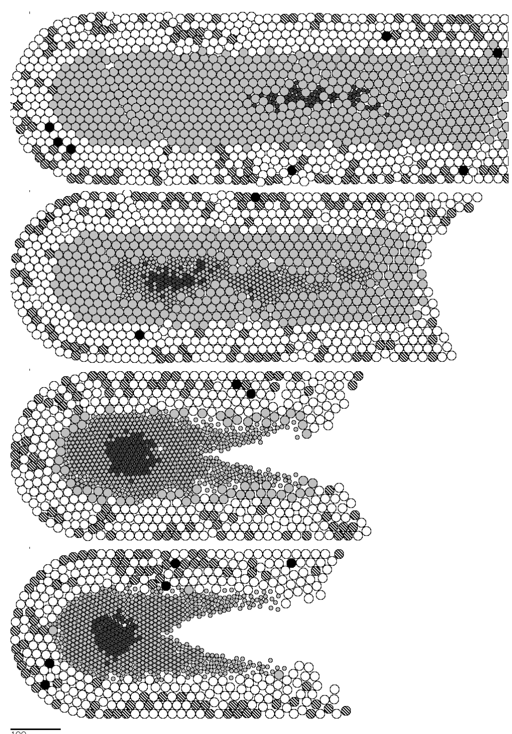

Figure 6.5 Impact of the necrotic cell lysis timescale: We plot the DCIS progression at time 25 days for $\beta_{NL}^{-1} = 15$ days (top), 5 days (second from top), 1 day (second from bottom), and 2 hours (bottom). Reprinted with permission from [436].

In Figure 6.5, we plot the DCIS simulations at time 25 days for each of these lysis parameter values. The parameter has a great effect on the rate of tumor advance through the duct: as the lysis time is decreased, the rate of tumor advance through the duct slows. This is because the necrotic core acts as a volume sink when the cells lyse, thereby relieving mechanical pressure. In turn, more of the cell flux is directed towards the center of the duct, rather than forward towards the tumor leading edge. Once $\beta_{NL}^{-1} < 1$ day, further reductions have little additional impact on the tumor progression, because the time the cells spend in an unlysed state is much smaller than the growth time scale.

In addition, the size of the microcalcification grows as β_{NL}^{-1} decreases. This is because more cells are pushed into the necrotic core rather than forward for small values of β_{NL}^{-1}, whereby a greater number of cells have been in the necrotic region longer than the calcification time β_{NC}^{-1}. Furthermore, the microcalcification appears to have a rounder morphology for the shorter lysis times. This topic is still under investigation, but it appears to be due to the more uniform packing of the lysed necrotic cells, owing to their occupying a greater percentage of the necrotic core for small values of β_{NL}^{-1}. Furthermore, the microcalcifications appear to occupy a larger percentage of the duct cross section due to the slower rate of tumor advance through the duct.

Similarly to the "standing wave" calcification pattern in the baseline simulation (and for similar reasons), a characteristic length emerges between the end of the duct and the start of the lysed cell region. This length is shorter than the distance from the end of the duct to the trailing edge of the calcification. These lengths both decrease as β_{NL}^{-1} decreases, due to the faster progression from viable cells to necrotic cells to lysed cells to calcified cells.

In a detailed comparison of these simulation results to breast histopathology, we find that 1 day $\leq \beta_{NL}^{-1} \leq 5$ day yields the best match between the simulated and actual necrotic core morphological features, including the rough distribution of lysed and unlysed cells and the general appearance of the necrotic cross sections [436].

6.6.4 Impact of background oxygen decay rate

We varied λ_b with values 0.001 min^{-1}, 0.01 min^{-1}, and 0.1 min^{-1} to investigate its impact on the simulation results. Aside from eliminating the viable cells from the center of the tumor's leading edge (see the baseline run), there was very little impact on the simulations (not shown). This is because the tumor necrotic centers were densely packed for all values of λ_b, and since necrotic cells uptake oxygen at rate $\lambda_t = \langle\lambda\rangle$, the oxygen uptake rate is equal throughout the bulk of the computational domain. Thus, the oxygen profile is similar for all three cases, leading to comparable amounts of cell proliferation in all cases; i.e., the extra viable cells in the leading edge did not contribute substantially to the tumor's advance through the duct. However, λ_b may have a greater impact in less dense tumors, such as cribriform DCIS (see Section 10.1.2).

6.6.5 Impact of cell motility

When next allowed random cell motility along the basement membrane, as described in Section 6.2.4. We set $\beta_{NL}^{-1} = 2$ hours, $\beta_H^{-1} = 5$ hours, and investigated the role of the mean time to migration ($\alpha_M^{-1} = 300$ min, 120 min) and that of the maximum lamellipodium length (15 or 20 μm). We set the maximum migration speed (α_{loc}/ν) to 5 μm/min and the maximum duration of migration to 15 min. All simulations set $\lambda_b = 0.001$ min^{-1}.

In Figure 6.6, we plot the simulations at time 30 days for 15 μm maximum lamellipodium length, for $\alpha_M = 0$ (top), $\alpha_M^{-1} = 300$ min (middle), and $\alpha_M^{-1} = 120$ min (bottom). In additional to the earlier figure legends, hypoxic cells are light gray with black dots. As α_M^{-1} is decreased from infinite (top) to 120 min (bottom), the tumor leading edge morphology becomes less blunt, and the tumor advances slightly farther along the duct. Thus, even random motility can increase the rate of a tumor's advance through a breast duct. We expect that this effect will be more pronounced if the cells instead move in a directed manner (e.g., chemotactically, as in Paget's disease [166]).

We also increased the maximum lamellipodium length ℓ_{podium} from 15 μm to 20 μm for $\alpha_M^{-1} = 120$ min. Similarly to decreasing α_M^{-}, increasing ℓ_{podium} accentuates the effect of motility because the motile cells can travel farther per migration event (simulation not shown). Note that these effects are subtle, and so further analysis and simulations (with different random seeds) are required to fully quantify them and confirm their statistical significance.

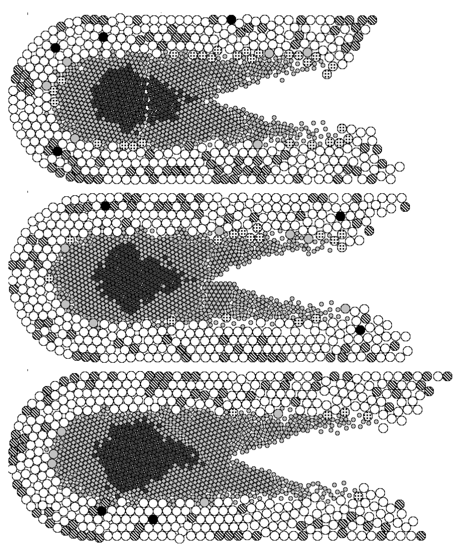

Figure 6.6 Impact of cell motility: As the mean time to migration is decreased from infinite (top) to 300 minutes (middle) to 120 minutes (bottom), the rate of tumor advance through the duct is slightly increased, with the leading edge more spread out. Reprinted with permission from [436].

6.7 Conclusions

In this chapter, we reviewed the major discrete modeling approaches currently employed in mathematical cancer cell biology, with particular focus on a generalized agent-based cell modeling framework. After a brief analysis of the model's population dynamics, we closed by presenting numerical examples of the model applied to breast cancer; this application is explored in greater depth in Chapter 10. We found that the specific modeling of the necrotic volume loss can have a major impact on the rate of tumor advance through the duct. Furthermore, even random cell motility along the basement membrane can speed a tumor's spread through the duct system, and the effect should be much more pronounced in cases of directed motility, such as Paget's disease (chemotactic motion along the ducts towards chemoattractants released by keratinocytes in the breast nipple [166]). On the other hand, we found that if hypoxia is modeled merely as a delayed progression to necrosis, then it has little impact on DCIS progression; instead, glycolysis, acidosis, and motility must be considered. This finding is consistent with previous modeling results by Gatenby and co-workers (e.g., [264, 629, 265, 268, 630, 627, 628]).

References

[1] A. C. Abajian and J. S. Lowengrug. An agent-based hybrid model for avascular tumor growth. *UCI Undergrad. Res. J.*, 11, 2008.

[2] R. Abbott, S. Forrest, and K. Pienta. Simulating the hallmarks of cancer. *Art. Lif*, 12(4):617–34, 2006.

[3] H. Acker, J. Carlsson, W. Mueller-Klieser, and R. Sutherland. Comparative po2 measurements in cell spheroids cultured with different techniques. *Br. J. Cancer*, 56:325–327, 1987.

[4] D. Adalsteinsson and J. A. Sethian. The Fast Construction of Extension Velocities in Level Set Methods. *J. Comput. Phys.*, 148(1):2–22, 1999.

[5] J. Adam. General aspects of modeling tumor growth and the immune response. In J. Adam and N. Bellomo, editors, *A Survey of Models on Tumor Immune Systems Dynamics*, pages 15–87. Birkhaeuser, Boston, 1996.

[6] T. L. Adamovich and R. M. Simmons. Ductal carcinoma in situ with microinvasion. *Am. J. Surg.*, 186(2):112–6, 2003.

[7] B. Addison-Smith, D. McElwain, and P. Maini. A simple mechanistic model of sprout spacing in tumour-associated angiogenesis. *J. Theor. Biol.*, 250:1–15, 2008.

[8] L. Ai, W.-J. Kim, T.-Y. Kim, C. R. Fields, N. A. Massoll, K. D. Robertson, and K. D. Brown. Epigenetic silencing of the tumor suppressor cystatin m occurs during breast cancer progression. *Canc. Res.*, 66:7899–909, 2006.

[9] T. Alarcón, H. Byrne, and P. Maini. A cellular automaton model for tumour growth in inhomogeneous environment. *J. Theor. Biol.*, 225:257–274, 2003.

[10] T. Alarcón, H. Byrne, and P. Maini. A multiple scale model for tumor growth. *Multiscale Model. Sim.*, 3:440–475, 2005.

[11] M. Alber, M. Kiskowski, J. Glazier, and Y. Jiang. On cellular automaton approaches to modeling biological cells. In R. Rosenthal and D. Gilliam, editors, *IMA Series on Mathematical systems theory in biology, communication and finance*, volume 142, pages 1–40. Springer, New York, 2002.

[12] B. Alberts, A. Johnson, J. Lewis, M. Raff, K. Roberts, and P. Walter. *Molecular Biology of the Cell*. Garland Science, New York, fifth edition, 2007.

[13] J. W. Allen, S. R. Khetani, R. S. Johnson, and S. Bhatia. *In Vitro* Liver Tissue Model Established from Transgenic Mice: Role of HIF-1alpha on Hypoxic Gene Expression. *Tissue Engineering*, 12(11):3135–47, 2006.

[14] M. Amar and A. Goriely. Growth and instability in soft tissues. *J. Mech. Phys. Solids*, 53:2284–2319, 2005.

[15] D. Ambrosi, F. Bussolino, and L. Preziosi. A review of vasculogenesis models. *Comp. Math. Meth. Med.*, 6:1–19, 2005.

[16] D. Ambrosi, A. Duperray, V. Peschetola, and C. Verdier. Traction patterns of tumor cells. *J. Math. Biol.*, 58(1-2):163–81, 2009.

[17] D. Ambrosi, A. Gamba, and G. Serini. Cell directional and chemotaxis in vascular morphogenesis. *Bull. Math. Biol.*, 66:1851–1873, 2004.

[18] D. Ambrosi and F. Guana. Mechanical aspects of growth in soft tissues. *Boll. Unione Mat. Ital.*, 7:775–781, 2004.

[19] D. Ambrosi and F. Guana. Stress-modulated growth. *Math. Mech. Solids*, 12:319–343, 2007.

[20] D. Ambrosi, A. Guillou, and E. DiMartino. Stress-modulated remodeling of a non-homogeneous body. *Biomech. Model. Mechanobiol.*, 7:63–76, 2008.

[21] D. Ambrosi and F. Mollica. On the mechanics of a growing tumor. *Int. J. Eng. Sci.*, 40:1297–1316, 2002.

[22] D. Ambrosi and F. Mollica. The role of stress in the growth of a multicell spheroid. *J. Math. Biol.*, 48:477–499, 2004.

[23] D. Ambrosi and L. Preziosi. On the closure of mass balance models for tumor growth. *Math. Mod. Meth. Appl. Sci.*, 12:737–754, 2002.

[24] D. Ambrosi and L. Preziosi. Cell adhesion mechanisms and elasto-viscoplastic mechanics of tumours. *Mech. Model. Mechanobiol.*, 8:397–413, 2009. 10.1007/s10237-008-145-y.

[25] American Cancer Society. American cancer society breast cancer facts and figures 2007-2008. *Atlanta: American Cancer Society, Inc.*, 2007. http://www.cancer.org/downloads/STT/BCFF-Final.pdf.

[26] A. Anderson. A hybrid mathematical model of solid tumour invasion: The importance of cell adhesion. *Math. Med. Biol.*, 22:163–186, 2005.

[27] A. Anderson and M. Chaplain. Continuous and discrete mathematical models of tumor-induced angiogenesis. *Bull. Math. Biol.*, 60:857–900, 1998.

[28] A. Anderson, M. Chaplain, E. Newman, R. Steele, and A. Thompson. Mathematical modeling of tumour invasion and metastasis. *J. Theor. Med.*, 2:129–154, 2000.

[29] A. Anderson, M. Chaplain, K. Rejniak, and J. Fozard. Single-cell based models in biology and medicine. *Math. Med. Biol.*, 25(2):185–6, 2008.

[30] A. Anderson and V. Quaranta. Integrative mathematical oncology. *Nature Reviews Cancer*, 8:227–244, 2008.

[31] A. Anderson, K. Rejniak, P. Gerlee, and V. Quaranta. Microenvironment driven invasion: a multiscale multimodel investigation. *J. Math. Biol.*, 58:579–624, 2009.

[32] A. Anderson, A. Weaver, P. Commmings, and V. Quaranta. Tumor morphology and phenotypic evolution driven by selective pressure from the microenvironment. *Cell*, 127:905–915, 2006.

[33] E. Anderson. Cellular homeostasis and the breast. *Maturitas*, 48(S1):13–7, 2004.

[34] M. Anderson, D. Srolovitz, G. Grest, and P. Sahini. Computer simulation of grain growth- i. kinetics. *Acta Metall.*, 32:783–791, 1984.

[35] E. D. Angelis and L. Preziosi. Advection-diffusion models for solid tumour evolution in vivo and related free boundary problem. *Math. Models Meth. Appl. Sci.*, 10:379–407, 2000.

[36] R. Araujo and D. McElwain. A history of the study of solid tumour growth: The contribution of mathematical modelling. *Bull. Math. Biol.*, 66:1039–1091, 2004.

[37] R. Araujo and D. McElwain. A linear-elastic model of anisotropic tumor growth. *Eur. J. Appl. Math.*, 15:365–384, 2004.

[38] R. Araujo and D. McElwain. New insights into vascular collapse and growth dynamics in solid tumors. *J. Theor. Biol.*, 228:335–346, 2004.

[39] R. Araujo and D. McElwain. A mixture theory for the genesis of residual stresses in growing tissues I: A general formulation. *SIAM J. Appl. Math.*, 65:1261–1284, 2005.

[40] R. Araujo and D. McElwain. A mixture theory for the genesis of residual stresses in growing tissues II: Solutions to the biphasic equations for a multicell spheroid. *SIAM J. Appl. Math.*, 66:447–467, 2005.

[41] R. Araujo and D. McElwain. The nature of the stresses induced during tissue growth. *Appl. Math. Lett.*, 18:1081–1088, 2005.

[42] N. Armstrong, K. Painter, and J. Sherratt. A continuum approach to modeling cell-cell adhesion. *J. Theor. Biol.*, 243:98–113, 2006.

[43] P. Armstrong. Light and electron microscope studies of cell sorting in combinations of chick embryo and neural retina and retinal pigment epithelium. *Willhelm Roux Archiv.*, 168:125–141, 1971.

[44] S. Astanin and L. Preziosi. Multiphase models of tumour growth. In N. Bellomo, M. Chaplain, and E. DeAngelis, editors, *Selected Topics on Cancer Modelling: Genesis - Evolution - Immune Competition - Therapy*. Birkhaeuser, Boston, 2007.

[45] C. Athale and T. Deisboeck. The effects of egf-receptor density on multiscale tumor growth patterns. *J. Theor. Biol.*, 238:771–779, 2006.

[46] C. Athale, Y. Mansury, and T. Deisboeck. Simulating the impact of a molecular 'decision-process' on cellular phenotype and multicellular patterns in brain tumors. *J. Theor. Biol.*, 233:469–481, 2005.

[47] H. Augustin. Tubes, branches, and pillars: The many ways of forming a new vasculature. *Circ. Research*, 89:645–647, 2001.

[48] D. H. Ausprunk and J. Folkman. Migration and proliferation of endothelial cells in preformed and newly formed blood vessels during tumour angiogenesis. *Microvasc. Res.*, 14(1):53–65, 1977.

[49] D. Balding and D. McElwain. A mathematical model of tumor-induced capillary growth. *J. Theor. Biol.*, 114:53–73, 1985.

[50] A. Bardelli, M. Basile, E. Audero, S. Giordano, S. Wennström, S. Ménard, P. Comoglio, and C. Ponzetto. Concomitant activation of pathways downstream of grb2 and pi 3-kinase is required for met-mediated metastasis. *Oncogene*, 18:1139–1146, 1999.

[51] L. F. Barros, T. Hermosilla, and J. Castro. Necrotic volume increase and the early physiology of necrosis. *Comp. Biochem. Physiol. A. Mol. Integr. Physiol.*, 130:401–9, 2001.

[52] U. Bartels, C. Hawkins, M. Jing, M. Ho, P. Dirks, J. Rutka, D. Stephens, and E. Bouffet. Vascularity and angiogenesis as predictors of growth in optic pathway/hypothalamic gliomas. *J. Neurosurg.*, 104:314–320, 2006.

[53] K. Bartha and H. Rieger. Vascular network remodeling via vessel cooption, regression and growth in tumors. *J. Theor. Biol.*, 241:903–918, 2006.

[54] R. J. Basaraba, H. Bielefeldt-Ohmann, E. K. Eschelbach, C. Reisenhauer, A. E. Tolnay, L. C. Taraba, C. A. Shanley, E. A. Smith, C. L. Bedwell, E. A. Chlipala, and I. A. Orme. Increased expression of host iron-binding proteins precedes iron accumulation and calcification of primary lung lesions in experimental tuberculosis in the guinea pig. *Tuberculosis*, 88(1):69–79, 2008.

[55] A. Bauer, T. Jackson, and Y. Jiang. A cell-based model exhibiting branching and anastomosis during tumor-induced angiogenesis. *Biophys. J.*, 92:3105–3121, 2007.

[56] F. O. Baxter, K. Neoh, and M. C. Tevendale. The beginning of the end: Death signaling in early involution. *J. Mamm. Gland Biol. Neoplas.*, 12(1):3–13, 2007.

[57] B. Bazaliy and A. Friedman. A free boundary problem for an elliptic-parabolic system: Application to a model of tumor growth. *Comm. Partial Diff. Eq.*, 28:517–560, 2003.

[58] P. A. Beachy, S. S. Karhadkar, and D. M. Berman. Tissue repair and stem cell renewal in carcinogenesis. *Nature*, 432(7015):324–331, 2004.

[59] E. Bearer, J. Lowengrub, Y. Chuang, H. Frieboes, F. Jin, S. Wise, M. Ferrari, D. Agus, and V. Cristini. Multiparameter computational modeling of tumor invasion. *Cancer Res.*, 69:4493–4501, 2009.

[60] L. Bello, V. Lucini, F. Costa, M. Pluderi, C. Giussani, F. Acerbi, G. Carrabba, M. Pannacci, D. Caronzolo, S. Grosso, S. Shinkaruk, F. Colleoni, X. Canron, G. Tomei, G. Deleris, and A. Bikfalvi. Combinatorial administration of molecules that simultaneously inhibit angiogenesis and invasion leads to increased therapeutic efficacy in mouse models of malignant glioma. *Clin. Cancer Res.*, 10:4527–4537, 2004.

[61] N. Bellomo, E. de Angelis, and L. Preziosi. Multiscale modeling and mathematical problems related to tumor evolution and medical therapy. *J. Theor. Medicine*, 5:111–136, 2003.

[62] N. Bellomo, N. Li, and P. Maini. On the foundations of cancer modelling: selected topics, speculations, and perspectives. *Math. Models Meth. Appl. Sci.*, 4:593–646, 2008.

[63] N. Bellomo and L. Preziosi. Modelling and mathematical problems related to tumor evolution and its interaction with the immune system. *Math. Comput. Modelling*, 32:413–542, 2000.

[64] M. Ben-Amar and A. Goriely. Growth and instability in elastic tissues. *J. Mech. Phys. Solids*, 53:2284–2319, 2005.

[65] R. Benjamin, J. Capparella, and A. Brown. Classification of glioblastoma multiforme in adults by molecular genetics. *The Cancer Journal*, 9:82–90, 2003.

[66] J. R. Berenson, L. Rajdev, and M. Broder. Pathophysiology of Bone Metastases. *Cancer Biol. Ther.*, 5(9):1078–1081, 2006.

[67] M. Berger and I. Rigoutsos. An algorithm for point clustering and grid generation. *IEEE Trans. Syst. Man. Cybern.*, 21:1278–1286, 1991.

[68] H. Bernsen and A. van der Kogel. Antiangiogenic therapy in brain tumor models. *J. Neuro-oncology*, 45:247–255, 1999.

[69] R. Betteridge, M. Owen, H. Byrne, T. Alarcón, and P. Maini. The impact of cell crowding and active cell movement on vascular tumour growth. *Networks Heterogen. Media*, 1:515–535, 2006.

[70] Y. Bi, C. H. Stuelten, T. Kilts, S. Wadhwa, R. V. Iozzo, P. G. Robey, X.-D. Chen, and M. F. Young. Extracellular matrix proteoglycans control the fate of bone marrow stromal cells. *J. Biol. Chem.*, 280:30481–9, 2005.

[71] M. Bienz and H. Clevers. Linking colorectal cancer to Wnt signaling. *Cell*, 103:311–20, 2000.

[72] M. V. Blagosklonny and A. B. Pardee. The restriction point of the cell cycle. *Cell Cycle*, 1(2):103–110, 2002.

[73] C. Blanpain and E. Fuchs. Epidermal Stem Cells of the Skin. *Annu. Rev. Cell Dev. Biol.*, 22:339–73, 2006.

[74] H. Bloemendal, T. Logtenberg, and E. Voest. New strategies in anti-vascular cancer therapy. *Euro J. Clin. Invest.*, 29:802–809, 1999.

[75] C. Boccaccio, M.Andò, L. Tamagnone, A. Bardelli, P. Michieli, C. Battistini, and P. Comoglio. Induction of epithelial tubules by growth factor hgf depends on the stat pathway. *Nature*, 391:285–288, 1998.

[76] K. Bold, Y. Zou, I. Kevrekidis, and M. Henson. An equation-free approach to analyzing heterogeneous cell population dynamics. *J. Math. Biol.*, 55:331–352, 2007.

[77] A. Brandt. Multi-level adaptive solutions to boundary-value problems. *Math. Comput.*, 31:333–390, 1977.

[78] B. Brandt, D. Kemming, J. Packeisen, R. Simon, M. Helms, U. Feldmann, A. Matuschek, C. Kersting, B. Hinrichs, J.-M. Midart, D. Bellet, K. Bartkowiak, N. Dankbar, T. Dittmar, G. Sauter, W. Boecker, and H. Buerger. Expression of early placenta insulin-like growth factor in breast cancer cells provides an autocrine loop that preodominantly enhances invasiveness and motility. *Endocrine-Related Canc.*, 12(4):823–7, 2005.

[79] A. Bredel-Geissler, U. Karbach, S. Walenta, L. Vollrath, and W. Mueller-Klieser. Proliferation-associated oxygen consumption and morphology of tumor cells in monolayer and spheroid culture. *J. Cell Phys.*, 153:44–52, 1992.

[80] D. Bresch, T. Colin, E. Grenier, and B. Ribba. A viscoelastic model for avascular tumor growth. inria-00267292, version 2, 2008.

[81] D. Bresch, T. Colin, E. Grenier, B. Ribba, and O. Saut. Computational modeling of solid tumor growth: the avascular stage. unpublished, 2007.

[82] C. Breward, H. Byrne, and C. Lewis. The role of cell-cell interactions in a two-phase model for avascular tumour growth. *J. Math. Biol.*, 45:125–152, 2002.

[83] C. Breward, H. Byrne, and C. Lewis. A multiphase model describing vascular tumor growth. *Bull. Math. Biol.*, 65:609–640, 2003.

[84] D. Brizel, S. Scully, J. Harrelson, L. Layfield, J. Bean, L. Prosnitz, and M. Dewhirst. Tumor oxygenation predicts for the likelihood of distant metastases in human soft tissue sarcoma. *Cancer Res.*, 56:941–943, 1996.

[85] D. Brizel, G. Sibley, L. Prosnitz, R. Scher, and M. Dewhirst. Tumor hypoxia adversely affects the prognosis of carcinoma of the head and neck. *Int. J. Radiat. Oncol. Biol. Phys.*, 38:285–289, 1997.

[86] J. Brown and L. Lowe. Multigrid elliptic equation solver with adaptive mesh refinement. *J. Comput. Phys.*, 209:582–598, 2005.

[87] R. K. Bruick and S. L. McKnight. A conserved family of Prolyl-4-Hydroxylases that modify HIF. *Science*, 294(5545):1337–40, 2001.

[88] H. Bueno, G. Ercole, and A. Zumpano. Asymptotic behaviour of quasi-stationary solutions of a nonlinear problem modelling the growth of tumours. *Nonlinearity*, 18:1629–1642, 2005.

[89] E. Bullitt, D. Zeng, G. Gerig, S. Aylward, S. Joshi, J. Smith, W. Lin, and M. Ewend. Vessel tortuosity and brain tumor malignance: a blinded study. *Acad. Radiol.*, 12:1232–1240, 2005.

[90] A. Burton. Rate of growth of solid tumours as a problem of diffusion. *Growth*, 30:157–176, 1966.

[91] F. Bussolino, M. Arese, E. Audero, E. Giraudo, S. Marchiò, S. Mitola, L. Primo, and G. Serini. *Cancer Modelling and Simulation*, chapter 1: Biological Aspects of Tumour Angiogenesis, pages 1–22. Chapman and Hall/CRC, London, 2003.

[92] L. M. Butler, S. Khan, G. E. Rainger, and G. B. Nash. Effects of endothelial basement membrane on neutrophil adhesion and migration. *Cell. Immun.*, 251:56–61, 2008.

[93] S. Byers, C. Sommers, B. Hoxter, A. Mercurio, and A. Tozeren. Role of e-cadherin in the response of tumor cell aggregates to lymphatic, venous and arterial flow: measurement of cell-cell adhesion strength. *J. Cell Sci.*, 108:2053–2064, 1995.

[94] H. Byrne. The effect of time delays on the dynamics of avascular tumor growth. *Math. Biosci.*, 144:83–117, 1997.

[95] H. Byrne. The importance of intercellular adhesion in the development of carcinomas. *IMA J. Math. Med. Biol.*, 14:305–323, 1997.

[96] H. Byrne. A comparison of the roles of localized and nonlocalised growth factors in solid tumour growth. *Math. Models Meth. Appl. Sci.*, 9:541–568, 1999.

[97] H. Byrne. A weakly nonlinear analysis of a model of avascular solid tumour growth. *J. Math. Biol.*, 39:59–89, 1999.

[98] H. Byrne, T. Alarcón, M. Owen, S. Webb, and P. Maini. Modeling aspects of cancer dynamics: A review. *Phi. Trans. R. Soc. A*, 364:1563–1578, 2006.

[99] H. Byrne and M. Chaplain. Growth of nonnecrotic tumors in the presence and absence of inhibitors. *Mathl. Biosci.*, 130:151–181, 1995.

[100] H. Byrne and M. Chaplain. Mathematical models for tumour angiogenesis: Numerical simulations and nonlinear wave solutions. *Bull. Math. Biol.*, 57:461–486, 1995.

[101] H. Byrne and M. Chaplain. Growth of necrotic tumors in the presence and absence of inhibitors. *Mathl. Biosci.*, 135:187–216, 1996.

[102] H. Byrne and M. Chaplain. Modelling the role of cell-cell adhesion in the growth and development of carcinomas. *Mathl. Comput. Modelling*, 24:1–17, 1996.

[103] H. Byrne and M. Chaplain. Free boundary value problems associated with the growth and development of multicellular spheroids. *Eur. J. Appl. Math.*, 8:639–658, 1997.

[104] H. Byrne and D. Drasdo. Individual-based and continuum models of growing cell populations: A comparison. *J. Math. Biol.*, 58(4-5):657–87, 2009.

[105] H. Byrne, J. King, D. McElwain, and L. Preziosi. A two-phase model of solid tumour growth. *Appl. Math. Letters*, 16:567–573, 2003.

[106] H. Byrne and P. Matthews. Asymmetric growth of models of avascular solid tumors: exploiting symmetries. *IMA J. Math. Appl. Med. Biol.*, 19:1–29, 2002.

[107] H. Byrne and L. Preziosi. Modelling solid tumour growth using the theory of mixtures. *Math. Med. Biol.*, 20:341–366, 2003.

[108] N. Cabioglu, K. K. Hunt, A. A. Sahin, H. M. Kuerer, G. V. Babiera, S. E. Singletary, G. J. Whitman, M. I. Ross, F. C. Ames, B. W. Feig, T. A. Buchholz, and F. Meric-Bernstam. Role for intraoperative margin assessment in patients undergoing breast-conserving surgery. *Ann. Surg. Oncol.*, 14(4):1458–71, 2007.

[109] J. Cahn and J. Hilliard. Free energy of a nonuniform system. i. interfacial free energy. *J. Chem. Phys.*, 28:258–267, 1958.

[110] R. Cairns, T. Kalliomaki, and R. Hill. Acute (cyclic) hypoxia enhances spontaneous metastasis of kht murine tumors. *Cancer Res.*, 61:8903–8908, 2001.

[111] D. Q. Calcagno, M. F. Leal, A. D. Seabra, A. S. Khayat, E. S. Chen, S. Demachki, P. P. Assumpcao, M. H. G. Faria, S. H. B. Rabenhorst, M. V. P. Ferreira, M. D. C. Smith, and R. R. Burbano. Interrelationship between chromosome 8 aneuploidy, C-MYC amplification and increased expression in individuals from northern Brazil with gastric adenocarcinoma. *World J. Gastroenterol.*, 12(38):6027–211, 2006.

[112] V. Capasso and D. Morale. Stochastic modelling of tumour-induced angiogenesis. *J. Math. Biol.*, 58:219–233, 2009.

[113] J. Carlsson and H. Acker. Relations ph, oxygen partial pressure and growth in cultured cell spheroids. *Int. J. Cancer*, 42:715–720, 1988.

[114] P. Carmeliot and R. Jain. Angiogenesis in cancer and other diseases. *Nature*, 407:249–257, 2000.

[115] L. Carreras, P. Macklin, J. Kim, S. Sanga, V. Cristini, and M. E. Edgerton. Oxygen uptake in quiescent versus cycling cells in a model of DCIS. *U.S. Canadian Acad. Path.*, 2010 Annual Meeting, 2010. (submitted).

[116] J. Casciari, S. Sotirchos, and R. Sutherland. Glucose diffusivity in multicellular tumor spheroids. *Cancer Res.*, 48:3905–3909, 1988.

[117] J. Casciari, S. Sotirchos, and R. Sutherland. Variations in tumor cell growth rates and metabolism with oxygen concentration, glucose concentration, and extracellular ph. *J. Cell. Physiol.*, 151:386–394, 1992.

[118] M. Castro, C. Molina-Paris, and T. Deisboeck. Tumor growth instability and the onset of invasion. *Phys. Rev. E*, 72:041907, 2005.

[119] P. Castro, P. Soares, L. Gusmo, R. Seruca, and M. Sobrinho-Simes. H-*RAS* 81 polymorphism is significantly associated with aneuploidy in follicular tumors of the thyroid. *Oncogene*, 25:4620–7, 2006.

[120] M. Chaplain. Reaction-diffusion prepatterning and its potential role in tumour invasion. *J. Biol. Sys.*, 3:929–936, 1995.

[121] M. Chaplain. Avascular growth, angiogenesis and vascular growth in solid tumours: The mathematical modelling of the stages of tumour development. *Mathl. Comput. Modelling*, 23:47–87, 1996.

[122] M. Chaplain. Pattern formation in cancer. In M. Chaplain, G. Singh, and J. MacLachlan, editors, *On Growth and Form: Spatio-Temporal Pattern Formation in Biology*. Wiley, New York, 2000.

[123] M. Chaplain, M. Ganesh, and I. Graham. Spatio-temporal pattern formation on spherical surfaces: numerical simulation and application to solid tumour growth. *J. Math. Biol.*, 42:387–423, 2001.

[124] M. Chaplain, L. Graziano, and L. Preziosi. Mathematical modelling of the loss of tissue compression responsiveness and its role in solid tumor development. *Math. Med. Biol.*, 23:197–229, 2006.

[125] M. Chaplain and G. Lolas. Mathematical modeling of cancer cell invasion of tissue: The role of the urokinase plasminogen activation system. *Math. Models Meth. Appl. Sci.*, 15:1685–1734, 2005.

[126] M. Chaplain, S. McDougall, and A. Anderson. Mathematical modeling of tumor-induced angiogenesis. *Ann. Rev. Biomed. Eng.*, 8:233–257, 2006.

[127] M. Chaplain and B. Sleeman. Modelling the growth of solid tumours and incorporating a method for their classification using nonlinear elasticity theory. *J. Math. Biol.*, 31:431–479, 1993.

[128] M. Chaplain and A. Stuart. A model mechanism for the chemotactic response of endothelial cells to tumor angiogenesis factor. *IMA J. Math. Appl. Med. Biol.*, 10:149–168, 1993.

[129] A. Chauvier and L. Preziosi. A mathematical framework to model migration of a cell population in the extracellular matrix. In A. Chauvier, L. Preziosi, and C. Verdier, editors, *Cell mechanics: From single cell scale-based models to multiscale modeling*. Chapman and Hall/CRC Press, Boca Raton, 2009.

[130] A. Chauviere, T. Hillen, and L. Preziosi. Modeling cell movement in anisotropic and heterogeneous tissues. *Networks Hetero. Media*, 2:333–357, 2007.

[131] A. Chauviere, L. Preziosi, and T. Hillen. Modeling the motion of a cell population in the extracellular matrix. *Discrete Cont. Dyn. Syst. B*, Supp:250–259, 2007.

[132] C. Chen, H. Byrne, and J. King. The influence of growth-induced stress from the surrounding medium on the development of multicell spheroids. *J. Math. Biol.*, 43:191–220, 2001.

[133] L. L. Chen, L. Zhang, J. Yoon, and T. S. Deisboeck. Cancer cell motility: optimizing spatial search strategies. *Biosys.*, 95(3):234–42, 2009.

[134] W. W. Chen, B. Schoeberl, P. J. Jasper, M. Niepel, D. A. Nielsen, U B andLauffenburger, et al. Input-output behavior of ErbB signaling pathways as revealed by a mass action model trained against dynamic data. *Mol. Syst. Biol.*, 5:239ff, 2009.

[135] X. Chen, S. Cui, and A. Friedman. A hyperbolic free boundary problem modeling tumor growth: asymptotic behavior. *Trans. Am. Math. Soc.*, 357:4771–4804, 2005.

[136] L. Cheng, N. K. Al-Kaisi, N. H. Gordon, A. Y. Liu, F. Gebrail, and R. R. Shenk. Relationship between the size and margin status of ductal carcinoma in situ of the breast and residual disease. *J. Natl. Cancer Inst.*, 89(18):1356–60, 1997.

[137] J. H. Choi, Y. Y. Jeong, S. S. Shin, H. S. Lim, and H. K. Kang. Primary calcified T-cell lymphoma of the urinary bladder: a case report. *Korean J. Radiol.*, 4(4):252–4, 2003.

[138] Y.-L. Chuang, M. E. Edgerton, P. Macklin, S. Wise, J. S. Lowengrub, and V. Cristini. Clinical predictions of bulk DCIS properties based on a duct-scale mixture model. (in preparation), 2009.

[139] S. Ciatto, S. Bianchi, and V. Vezzosi. Mammographic appearance of calcifications as a predictor of intraductal carcinoma histologic subtype. *Eur. Radiology*, 4(1):23–6, 1994.

[140] R. G. Clyde, J. L. Brown, T. R. Hupp, N. Zhelev, and J. W. Crawford. The role of modelling in identifying drug targets for diseases of the cell cycle. *J. R. Soc. Interface*, 3(10):617–627, 2006.

[141] D. Coffey. Self-organization, complexity and chaos: the new biology for medicine. *Nature Med.*, 4:882, 1998.

[142] P. Colella, D. T. Graves, T. J. Ligocki, D. F. Martin, D. Modiano, D. B. Serafini, and B. V. Straalen. CHOMBO software package for AMR applications: design document. Technical report, Lawrence Berkeley National Laboratory, Applied Numerical Algrithms Group; NERSC Division, Berkeley, CA, USA, 2003.

[143] B. Coleman and W. Noll. Thermodynamics of elastic materials with conduction and viscosity. *Arch. Rat. Mech.*, 13:167–178, 1963.

[144] M. Conacci-Sorrell, J. Zhurinsky, and A. Ben-Zeév. The cadherin-catenin adhesion system in signaling and cancer. *J. Clin. Invest.*, 109(8):987–91, 2002.

[145] J. Condeelis, R. Singer, and J. Segall. The great escape: When cancer cells hijack the genes for chemotaxis and motility. *Annu. Rev. Cell Dev. Biol.*, 21:695–718, 2005.

[146] A. Coniglio, A. deCandia, S. DiTalia, and A. Gamba. Percolation and burgers' dynamics in a model of capillary formation. *Phys. Rev. E*, 69:051910, 2004.

[147] V. Cristini, H. Frieboes, R. Gatenby, S. Caserta, M. Ferrari, and J. Sinek. Morphologic instability and cancer invasion. *Clin. Cancer Res.*, 11:6772–6779, 2005.

[148] V. Cristini, H. Frieboes, X. Li, J. Lowengrub, P. Macklin, S. Sanga, S. Wise, and X. Zheng. Nonlinear modeling and simulation of tumor growth. In N. Bellomo, M. Chaplain, and E. de Angelis, editors, *Modelling and simulation in science, engineering and technology*. Birkhäuser, Boston, 2008.

[149] V. Cristini, X. Li, J. Lowengrub, and S. Wise. Nonlinear simulations of solid tumor growth using a mixture model: invasion and branching. *J. Math. Biol.*, 58(4-5):723–763, 2009.

[150] V. Cristini and J. Lowengrub. Three-dimensional crystal growth. i. linear analysis and self-similar evolution. *J. Crystal Growth*, 240:267–276, 2002.

[151] V. Cristini, J. Lowengrub, and Q. Nie. Nonlinear simulation of tumor growth. *J. Math. Biol.*, 46:191–224, 2003.

[152] S. Cui. Analysis of a mathematical model for the growth of tumors under the action of external inhibitors. *J. Math. Biol.*, 44:395–426, 2002.

[153] S. Cui. Analysis of a free boundary problem modeling tumor growth. *Acta Math. Sinica*, 21:1071–1082, 2005.

[154] S. Cui. Well-posedness of a multidimensional free boundary problem modelling the growth of nonnecrotic tumors. *J. Func. Analysis*, 245:1–18, 2007.

[155] S. Cui. Lie group action and stability analysis of stationary solutions for a free boundary problem modelling tumor growth. *J. Diff. Eq.*, 246(5):1845–1882, 2009.

[156] S. Cui and J. Escher. Asymptotic behaviour of solutions of a multidimensional moving boundary problem modeling tumor growth. *Comm. Partial Diff. Equations*, 33:636–655, 2008.

[157] S. Cui and J. Escher. Well-posedness and stability of a multi-dimensional tumor growth model. *Arch. Rat. Mech. Analysis*, 191:173–193, 2009.

[158] S. Cui and A. Friedman. Analysis of a mathematical model of the effect of inhibitors on the growth of tumors. *Math. Biosci.*, 164:103–137, 2000.

[159] S. Cui and A. Friedman. A free boundary problem for a singular system of differential equations: An application to a model of tumor growth. *Trans. Amer. Math. Soc.*, 255:3537–3590, 2003.

[160] S. Cui and A. Friedman. Formation of necrotic cores in the growth of tumors: analytic results. *Acta Matematica Scientia*, 26:781–796, 2006.

[161] S. Cui and X. Wei. Global existence for a parabolic-hyperbolic free boundary problem modelling tumor growth. *Acta Math. Appl. Sinica*, 21:597–614, 2005.

[162] S. Cui and S. Xu. Analysis of mathematical models for the growth of tumors with time delays in cell proliferation. *J. Math. Analysis Appl.*, 336:523–541, 2007.

[163] J. Dallon and H. Othmer. How cellular movement determines the collective force generated by the dictyostelium discoideum slug. *J. Theor. Biol.*, 231:299–306, 2004.

[164] C. G. Danes, S. L. Wyszomierski, J. Lu, C. L. Neal, W. Yang, and D. Yu. 14-3-3ζ down-regulates p53 in mammary epithelial cells and confers luminal filling. *Canc. Res.*, 68:1760–7, 2008.

[165] K. Date, K. Matsumoto, K. Kuba, H. Shimura, M. Tanaka, and T. Nakamura. Inhibition of tumor growth and invasion by a four-kringle antagonist (hgf/nk4) for hepatocyte growth factor. *Oncogene*, 17:3045–3054, 1998.

[166] C. R. De Potter, I. Eeckhout, A.-M. Schelfhout, M.-L. Geerts, and H. J. Roelsh. Keratinocyte induced chemotaxis in the pathogenesis of Paget's disease of the breast. *Histopath.*, 24(4):349–56, 1994.

[167] J. Debnath and J. Brugge. Modelling glandular epithelial cancers in three-dimensional cultures. *Nature Rev. Cancer*, 5:675–688, 2005.

[168] J. Debnath, K. Mills, N. Collins, M. Reginato, S. Muthuswarmy, and J. Brugge. The role of apoptosis in creating and maintaining luminal space within normal and oncogene-expressing mammary acini. *Cell*, 111:29–40, 2002.

[169] T. Deisboeck, M. Berens, A. Kansal, S. Torquato, A. Stemmer-Rachamimov, and E. Chiocca. Pattern of self-organization in tumour systems: Complex growth dynamics in a novel brain tumour spherical model. *Cell Proliferation*, 34:115–134, 2001.

[170] T. Deisboeck, L. Zhang, J. Yoon, and J. Costa. In silico cancer modeling: is it ready for prime time? *Nature Clin. Practice Oncol.*, 6(1):34–42, 2009.

[171] K. DeJaeger, M. Kavanagh, and R. Hill. Relationship of hypoxia to metastatic ability in rodent tumors. *Br. J. Cancer*, 84:1280–1285, 2001.

[172] H. D. Dell. Milestone 1 (1889) Seed and soil hypothesis: Observations from a ploughman. *Nat. Rev. Cancer*, 6:S7, 1989. http://www.nature.com/milestones/milecancer/index.html.

[173] R. Demicheli, G. Pratesi, and R. Foroni. The exponential-gompertzian growth model : data from six tumor cell lines in vitro and in vivo. estimate of the transition point from exponential to gompertzian growth and potential clinical applications. *Tumori*, 77:189–195, 1991.

[174] B. Desai, T. Ma, and M. A. Chellaiah. Invadopodia and matrix degradation, a new property of prostate cancer cells during migration and invasion. *J. Biol. Chem.*, 283(20):13856–66, 2008.

[175] A. Deutsch and S. Dormann. *Cellular automaton modeling of biological pattern formation*. Birkhäuser, New York, 2005.

[176] A. E. DeWitt, J. Y. Dong, H. S. Wiley, and D. A. Lauffenburger. Quantitative analysis of the EGF receptor autocrine system reveals cryptic regulation of cell response by ligand capture. *J. Cell. Sci.*, 114(Pt 12):2301–13, 2001.

[177] J. Diaz and J. Tello. On the mathematical controllability in a simple growth tumors model by the internal localized action of inhibitors. *Nonlinear Analysis*, 4:109–125, 2003.

[178] A. DiCarlo and S. Quiligotti. Growth and balance. *Mech. Res. Comm.*, 29:449–456, 2002.

[179] M. F. Dillon, A. A. Maguire, E. W. McDermott, C. Myers, A. D. Hill, A. O'Doherty, and C. M. Quinn. Needle core biopsy characteristics identify patients at risk of compromised margins in breast conservation surgery. *Mod. Pathol.*, 21(1):39–45, 2008.

[180] M. F. Dillon, E. W. McDermott, A. O'Doherty, C. M. Quinn, A. D. Hill, and N. O'Higgins. Factors affecting successful breast conservation for ductal carcinoma in situ. *Ann. Surg. Oncol.*, 14(5):1618–28, 2007.

[181] R. Dillon, M. Owen, and K. Painter. A single-cell based model of multicellular growth using the immersed interface method. In B. Khoo, Z. Li, and P. Lin, editors, *Contemporary mathematics: Moving interface problems and applications in fluid dynamics*, volume 466, chapter 1, pages 1–15. AMS, Providence, 2008.

[182] S. Dormann and A. Deutsch. Modeling of self-organized avascular tumor growth with a hybrid cellular automaton. *In Silico Biology*, 2:393–406, 2002.

[183] D. Drasdo. On selected individual-based approaches to the dynamics of multicellular systems. In W. Alt, M. Chaplain, and M. Griebel, editors, *Multiscale modeling*. Birkhaeuser, Basel, 2003.

[184] D. Drasdo. Coarse graining in simulated cell populations. *Adv. Complex Sys.*, 8:319–363, 2005.

[185] D. Drasdo and S. Höhme. Individual-based approaches to birth and death in avascular tumors. *Math. Comput. Modelling*, 37:1163–1175, 2003.

[186] D. Drasdo and S. Höhme. A single-scale-based model of tumor growth in vitro: monolayers and spheroids. *Phys. Biol.*, 2:133–147, 2005.

[187] D. Drasdo and S. Höhme. On the role of physics in the growth and pattern of multicellular systems: What we learn from individual-cell based models? *J. Stat. Phys.*, 128:287–345, 2007.

[188] D. Drasdo, R. Kree, and J. McCaskill. Monte-carlo approach to tissue cell populations. *Phys. Rev. E*, 52:6635–6657, 1995.

[189] F. Drees, S. Pokutta, S. Yamada, W. J. Nelson, and W. T. Weis. Alpha-catenin is a molecular switch that binds E-cadherin-beta-catenin and regulates actin-filament assembly. *Cell*, 123:903–15, 2005.

[190] W. R. Duan, D. S. Garner, S. D. Williams, C. L. Funckes-Shippy, I. S. Spath, and E. A. G. Blomme. Comparison of immunohistochemistry for activated caspase-3 and cleaved cytokeratin 18 with the TUNEL method for quantification of apoptosis in histological sections of PC-3 subcutaneous xenografts. *J. Pathol.*, 199(2):221–8, 2003.

[191] M. Ducasse and M. A. Brown. Epigenetic aberrations and cancer. *Mol. Cancer*, 5:60, 2006.

[192] H. S. Earp, T. L. Dawson, X. Li, and H. Yu. Heterodimerization and functional interaction between EGF receptor family members: a new signaling paradigm with implications for breast cancer research. *Breast Canc. Res. Treat.*, 35(1):115–132, 1995.

[193] D. A. Eberhard, B. E. Johnson, L. C. Amler, et al. Mutations in the epidermal growth factor receptor and in KRAS are predictive and prognostic indicatorsin patients with non-small-cell lung cancer treated with chemotherapy alone and in combination with erlotinib. *J. Clin. Oncol.*, 23:5900–09, 2005.

[194] M. Edgerton, Y.-L. Chuang, J. Kim, G. Tomaiuolo, P. Macklin, S. Sanga, W. Yang, A. Broom, K.-A. Do, and V. Cristini. Using mathematical models to understand the time dependence of the growth of ductal carcinoma in situ. *31st Annual San Antonio Breast Cancer Symposium.*, Supplement to Volume 68(24):Abstract 1165, 2008.

[195] M. Edgerton, Y.-L. Chuang, J. Kim, G. Tomaiuolo, P. Macklin, S. Sanga, W. Yang, A. Broom, K.-A. Do, and V. Cristini. Using mathematical models to understand time-dependence of growth DCIS: Implications for clinical detection and IDC. (in preparation), 2009.

[196] M. Edgerton, P. Macklin, Y.-L. Chuang, G. Tomaiuolo, W. Yang, J. Kim, S. Sanga, A. Broom, K.-A. Do, and V. Cristini. A multiscale model of ductal carcinoma in situ. *Cancer Res.*, 2010. (submitted).

[197] A. W. El-Kareh and T. W. Secomb. A mathematical model for cisplatin cellular pharmacodynamics. *Neoplasia*, 5(2):161–9, 2003.

[198] A. W. El-Kareh and T. W. Secomb. Two-mechanism peak concentration model for cellular pharmacodynamics of doxorubicin. *Neoplasia*, 7(7):705–13, 2005.

[199] C. Elliot and S. Luckhaus. A generalized diffusion equation for phase separation of a multi-component mixture with interfacial free energy. Technical report, Univ. Sussex and Univ. Bonn, 1991. Inst. Math. Appl., report 887.

[200] Y. I. Elshimali and W. W. Grody. The Clinical Significance of Circulating Tumor Cells in the Peripheral Blood. *Diagn. Mol. Pathol.*, 15(4):187–194, 2006.

[201] P. Elvin and A. Garner. Tumour invasion and metastasis: challenges facing drug discovery. *Curr. Opin. Pharmacol.*, 5:374–381, 2005.

[202] S. Enam, M. Rosenblum, and K. Edvardsen. Role of extracellular matrix in tumor invasion: migration of glioma cells along fibronectinpositive mesenchymal cell processes.

Neurosurgery, 42:599–608, 1998.

[203] R. Erban, I. Kevrekidis, and H. Othmer. An equation-free computational approach for extracting population-level behavior from individual-based models of biological dispersal. *Physica D*, 215:1–24, 2006.

[204] R. Erban and H. Othmer. From individual to collective behavior in bacterial chemotaxis. *SIAM J. Appl. Math.*, 65:361–391, 2004.

[205] R. Erban and H. Othmer. From signal transduction to spatial pattern formation in *E. coli*: A paradigm for multi-scale modeling in biology. *Multiscale Model. Simul.*, 3:362–394, 2005.

[206] B. Erbas, E. Provenzano, J. Armes, and D. Gertig. The natural history of ductal carcinoma *in situ* of the breast: a review. *Breast Canc. Res. Treat.*, 97(2):135–44, 2006.

[207] J. Erler, K. Bennewith, M. Nicolau, N. Dornhoefer, C. Kong, Q.-T. Le, J.-T. Chi, S. Jeffrey, and A. Giaccia. Lysyl oxidase is essential for hypoxia-induced metastasis. *Nature*, 440:1222–1226, 2006.

[208] M. Esteban and P. Maxwell. If, a missing link between metabolism and cancer. *Nature Med.*, 11:1047–1048, 2005.

[209] J. Fang, R. Gillies, and R. Gatenby. Adaptation to hypoxia and acidosis in carcinogenesis and tumor progression. *Semin. Cancer Biol.*, 18:330–337, 2008.

[210] A. Fasano, A. Bertuzzi, and A. Gandolfi. *Complex systems in biomedicine*, chapter Mathematical modelling of tumour growth and treatment, pages 71–108. Springer, Milan, 2006.

[211] L. Ferrante, S. Bompadre, L. Possati, and L. Leone. Parameter estimation in a gompertzian stochastic model for tumor growth. *Biometrics*, 56:1076–1081, 2000.

[212] M. Ferrari. Cancer nanotechnology: opportunities and challenges. *Nature Rev. Cancer*, 5:161–171, 2005.

[213] R. Filion and A. Popel. A reaction-diffusion model of basic fibroblast growth factor interactions with cell surface receptors. *Annals Biomed. Eng.*, 32:645–663, 2004.

[214] I. Fischer, J.-p. Gagner, M. Law, E. W. Newcomb, and D. Zagzag. Angiogenesis in Gliomas: Biology and Molecular Pathophysiology. *Brain Pathol.*, 15(4):297–310, 2005.

[215] A. B. Fisher, S. Chien, A. I. Barakat, and R. M. Nerem. Endothelial cellular response to altered shear stress. *Am. J. Physiol. Heart Circ. Physiol.*, 281(3):L529–L533, 2001.

[216] B. Flaherty, J. P. McGarry, and P. E. McHugh. Mathematical models of cell motility. *Cell. Biochem. Biophys.*, 49(1):14–28, 2007.

[217] G. B. Fogarty, N. M. Conus, J. Chu, and G. McArthur. Characterization of the expression and activation of the epidermal growth factor receptor in squamous cell carcinoma of the skin. *Brit. J. Derm.*, 156(1):92–98, 2007.

[218] J. Folkman. Angiogenesis in cancer, vascular, rheumatoid and other disease. *Nat. Med.*, 1:27–30, 1995.

[219] J. Forsythe, B. Jiang, N. Iyer, S. L. F. Agani, R. Koos, and G. Semenza. Activation of vascular endothelial growth factor gene transcription by hypoxia-inducible factor 1. *Mol. Cell. Biol.*, 16:4604–4613, 1996.

[220] L. M. Franks and M. A. Knowles. What is Cancer? In Knowles and Selby [386], chapter 1, pages 1–24.

[221] S. Franks, H. Byrne, J. King, J. Underwood, and C. Lewis. Modeling the early growth of ductal carcinoma in situ of the breast. *J. Math. Biol.*, 47:424–452, 2003.

[222] S. Franks, H. Byrne, H. Mudhar, J. Underwood, and C. Lewis. Mathematical modeling of comedo ductal carcinoma in situ of the breast. *Math. Med. Biol.*, 20:277–308, 2003.

[223] S. Franks and J. King. Interactions between a uniformly proliferating tumor and its surrounding. uniform material properties. *Math. Med. Biol.*, 20:47–89, 2003.

[224] J. Freyer and R. Sutherland. Determination of diffusion constants for metabolites in multicell tumor spheroids. *Adv. Exp. Med. Biol.*, 159:463–475, 1983.

[225] J. Freyer and R. Sutherland. A reduction in the in situ rates of oxygen and glucose consumption of cells in emt6/ro spheroids during growth. *J. Cell. Physiol.*, 124:516–524, 1985.

[226] J. Freyer and R. Sutherland. Regulation of growth saturation and development of necrosis in emt6/ro multicellular spheroids by the glucose and oxygen supply. *Cancer Res.*, 46:3504–3512, 1986.

[227] J. P. Freyer. Decreased mitochondrial function in quiescent cells isolated from multicellular tumor spheroids. *J. Cell. Physiol.*, 176(1):138–49, 1998.

[228] H. Frieboes, M. Edgerton, J. Fruehauf, F. Rose, L. Worrall, R. Gatenby, M. Ferrari, and V. Cristini. Prediction of drug response in breast cancer using integrative experimental/computational modeling. *Cancer Research*, 69:4484–4492, 2009.

[229] H. Frieboes, J. Fang, Y.-L. Chuang, S. Wise, J. Lowengrub, and V. Cristini. Nonlinear simulations of three-dimensional multispecies tumor growth -ii: Tumor invasion and angiogenesis. *J. Theor. Biol.*, in review.

[230] H. Frieboes, J. Lowengrub, S. Wise, X. Zheng, P. Macklin, E. Bearer, and V. Cristini. Computer simulation of glioma growth and morphology. *NeuroImage*, 37:S59–S70, 2007.

[231] H. Frieboes, X. Zheng, C.-H. Sun, B. Tromberg, R. Gatenby, and V. Cristini. An integrated computational/experimental model of tumor invasion. *Cancer Res.*, 66:1597–1604, 2006.

[232] P. Friedl. Prespecification and plasticity: shifting mechanisms of cell migration. *Curr. Opin. Cell Biol.*, 16:14–23, 2004.

[233] P. Friedl, E. Brocker, and K. Zanker. Integrins, cell matrix interactions and cell migration strategies: fundamental differences in leukocytes and tumor cells. *Cell Adhes. Commun.*, 6:225–236, 1998.

[234] P. Friedl, Y. Hegerfeldt, and M. Tilisch. Collective cell migration in morphogenesis and cancer. *Int. J. Dev. Biol.*, 48:441–449, 2004.

[235] P. Friedl, P. Noble, P. Walton, D. Laird, P. Chauvin, R. Tabah, M. Black, and K. Zaenker. Migration of coordinated cell clusters in mesenchymal and epithelial cancer explants in vitro. *Cancer Res.*, 55:4557–4560, 1995.

[236] P. Friedl and A. Wolf. Tumor cell invasion and migration: diversity and escape mechanisms. *Nat. Rev. Cancer*, 3:362–374, 2003.

[237] A. Friedman. A hierarchy of cancer models and their mathematical challenges. *Discrete Cont. Dyn. Systems Ser. B*, 4:147–159, 2004.

[238] A. Friedman, N. Bellomo, and P. Maini. Mathematical analysis and challenges arising from models of tumor growth. *Math. Models Meth. Appl. Sci.*, 17:1751–1772, 2007.

[239] A. Friedman and B. Hu. Asymptotic stability for a free boundary problem arising in a tumor model. *J. Diff. Equations*, 227:598–639, 2005.

[240] A. Friedman and B. Hu. Bifurcation from stability to instability for a free boundary problem arising in a tumor model. *Arch. Rat. Mech. Analysis*, 180:293–330, 2006.

[241] A. Friedman and B. Hu. Bifurcation from stability to instability for a free boundary problem modeling tumor growth by stokes equation. *J. Math. Analysis Appl.*, 327:643–664, 2007.

[242] A. Friedman and F. Reitich. Analysis of a mathematical model for the growth of tumors. *J. Math. Biol.*, 38:262–284, 1999.

[243] A. Friedman and F. Reitich. On the existence of spatially patterned dormant malignancies in a model for the growth of non-necrotic vascular tumors. *Math. Models Meth. Appl. Sci.*, 11:601–625, 2001.

[244] A. Friedman and F. Reitich. Symmetry-breaking bifurcation of analytic solutions to free boundary problems: an application to a model of tumor growth. *Trans. Am. Math. Soc.*, 353:1587–1634, 2001.

[245] S. H. Friend, R. Bernards, S. Rogelj, R. A. Weinberg, J. M. Rapaport, D. M. Albert, and T. P. Dryja. A human DNA segment with properties of the gene that predisposes to retinoblastoma and osteosarcoma. *Nature*, 323:643–6, 1986.

[246] S. M. Frisch and H. Francis. Disruption of epithelial cell-matrix interactions induces apoptosis. *J. Cell Biol.*, 124:619–26, 1994.

[247] R. Fukuda, H. Zhang, J.-W. Kim, L. Shimoda, C. V. Dang, and G. L. Semenza. HIF-1 regulates cytochrome oxidase subunits to optimize efficiency of respiration in hypoxic cells. *Cell*, 129(1):111–22, 2007.

[248] D. Fukumura and R. Jain. Tumor microenvironment abnormalities: causes, consequences, and strategies to normalize. *J. Cell. Biochem.*, 101:937–949, 2007.

[249] Y. Fung. *Biomechanics: motion, flow, stress and growth*. Springer, New York, 1990.

[250] Y. Fung. *Biomechanics: material properties of living tissues*. Springer, New York, 1993.

[251] A.-P. Gadeau, H. Chaulet, D. Daret, M. Kockx, J.-M. Daniel-Lamaziè, and C. Desgranges. Time course of osteopontin, osteocalcin, and osteonectin accumulation and calcification after acute vessel wall injury. *J. Histochem. Cytochem.*, 49:79–86, 2001.

[252] D. Galaris, A. Barbouti, and P. Korantzopoulos. Oxidative stress in hepatic ischemia-reperfusion injury: The role of antioxidants and iron chelating compounds. *Curr. Pharma. Design*, 12:2875–2890, 2006.

[253] J. Galle, G. Aust, G. Schaller, T. Beyer, and D. Drasdo. Individual cell-based models of the spatial temporal organization of multicellular systems- achievements and limitations. *Cytometry*, 69A:704–710, 2006.

[254] J. Galle, M. Hoffmann, and G. Aust. From single cells to tissue architecture-a bottom-up approach to modeling the spatio-temporal organization of complex multicellular systems. *J. Math. Biol.*, 58:261–283, 2009.

[255] J. Galle, M. Loeffler, and D. Drasdo. Modeling the effect of deregulated proliferation and apoptosis on the growth dynamics of epithelial cell populations in vitro. *Biophys. J.*, 88:62–75, 2005.

[256] J. Galle, L. Preziosi, and A. Tosin. Contact inhibition of growth described using a multiphase model and an individual cell based model. *Appl. Math. Lett.*, 2009. in press.

[257] A. Gamba, D. Ambrosi, A. Coniglio, A. deCandia, S. DiTalia, E. Giraudo, G. Serini, L. Preziosi, and F. Bussolino. Percolation, morphogenesis and burgers dynamics in blood vessels formation. *Phys. Rev. Lett.*, 90:118101, 2003.

[258] J. Ganghoffer. Some issues related to growth and goal functions for continuum biological systems. *Phil. Mag.*, 85:4353–4391, 2005.

[259] M. Garbey and G. Zouridakis. Modeling tumor growth: from differential deformable models to growth prediction of tumors detected in pet images. *Eng. Med. Biol. Soc.*, 3:2687–2690, 2003.

[260] H. Garcke, M. Rumpf, and U. Weikard. The Cahn-Hilliard equation with elasticity: finite element approximation and qualitative studies. *Interfaces Free Bound*, pages 101–

118, 2001.

[261] M. Gardner. The fantastic combinations of john conway's new solitaire game "life". *Scientific American*, 223:120–3, Oct. 1970.

[262] K. Garikipati, E. Arruda, K. Grosh, H. Narayanan, and S. Calve. A continuum treatment of growth in biological tissue: the coupling of mass transport and mechanics. *J. Mech. Phys. Solids*, 52:1595–1625, 2004.

[263] L. Garner, Y. Lau, T. Jackson, M. Uhler, D. Jordan, and R. Gilgenbach. Incorporating spatial dependence into a multicellular tumor spheroid growth model. *J. Appl. Phys.*, 98:124701, 2005.

[264] R. Gatenby and E. Gawlinski. The glycolytic phenotype in carcinogenesis and tumor invasion: insights through mathematical models. *Cancer Res.*, 63:3847–3854, 2003.

[265] R. Gatenby, E. Gawlinski, A. Gmitro, B. Kaylor, and R. Gillies. Acid-mediated tumor invasion: a multidisciplinary study. *Cancer Res.*, 66:5216–5223, 2006.

[266] R. Gatenby and E. Gawlinsky. *The tumour microenvironment*, chapter Mathematical models of tumour invasion mediated by transformation-induced alteration of microenvironmental pH, pages 85–99. Wiley, London, 2003.

[267] R. Gatenby and R. Gillies. A microenvironmental model of carcinogenesis. *Nat. Rev. Cancer*, 8:56–61, 2008.

[268] R. Gatenby, K. Smallbone, P. Maini, F. Rose, J. Averill, R. Nagle, L. Worrall, and R. Gillies. Cellular adaptations to hypoxia and acidosis during somatic evolution of breast cancer. *Br. J. Cancer*, 97:646–653, 2007.

[269] R. Gatenby and T. Vincent. An evolutionary model of carcinogenesis. *Cancer Res.*, 63:6212–6220, 2003.

[270] C. W. Gear and I. G. Kevrekidis. Projective methods for stiff differential equations: problems with gaps in the eigenvalue spectrum. *SIAM J. Sci. Comput.*, 24:1091–1106, 2003.

[271] C. W. Gear, I. G. Kevrekidis, and C. Theodoropoulos. 'Coarse' integration/bifurcation analysis via microscopic simulators: micro-Galerkin methods. *Comput. Chem. Engineer.*, 26:941–963, 2002.

[272] A. Gerisch and M. Chaplain. Mathematical modelling of cancer cell invasion of tissue: local and non-local models and the effect of adhesion. *J. Theor. Biol.*, 250:684–704, 2008.

[273] P. Gerlee and A. Anderson. An evolutionary hybrid cellular automaton model of solid tumor growth. *J. Theor. Biol.*, 246:583–603, 2007.

[274] P. Gerlee and A. Anderson. Stability analysis of a hybrid cellular automaton model of cell colony growth. *Phys. Rev. E*, 75:051911, 2007.

[275] P. Gerlee and A. Anderson. A hybrid cellular automaton model of clonal evolution in cancer: The emergence of the glycolytic phenotype. *J. Theor. Biol.*, 250:705–722, 2008.

[276] P. Gerlee and A. Anderson. A hybrid cellular automaton model of clonal evolution in cancer: The emergence of the glycolytic phenotype. *J. Theor. Biol.*, 250:705–722, 2008.

[277] J. Gevertz and S. Torquato. Modeling the effects of vasculature evolution on early brain tumor growth. *J. Theor. Biol.*, 243:517–531, 2006.

[278] F. G. Giancotti and E. Ruoslahti. Integrin signaling. *Science*, 285(5430):1028–32, 1999.

[279] J. W. Gibbs. Fourier's series. *Nature*, 59:200–200, 1898.

[280] M. Z. Gilcrease. Integrin signaling in epithelial cells. *Canc. Lett.*, 247(1):1–25, 2007.

[281] R. Gillies and R. Gatenby. Adaptive landscapes and emergent phenotypes: why do cancers have high glycolysis? *J. Bioenerg. Biomem.*, 39:251–257, 2007.

[282] R. Gillies and R. Gatenby. Hypoxia and adaptive landscapes in the evolution of carcinogenesis. *Cancer Metastasis Rev.*, 26:311–317, 2007.

[283] R. Gillies, Z. Liu, and Z. Bhujwalla. 31p-mrs measurements of extracellular ph of tumors using 3- aminopropylphosphonate. *Am. J. Physiol.*, 267:195–203, 1994.

[284] R. Gillies, I. Robey, and R. Gatenby. Causes and consequences of increased glucose metabolism of cancers. *J. Nuclear Med.*, 49:24S–42S, 2008.

[285] M. Gimbrone, R. Cotran, S. Leapman, and J. Folkman. Tumor growth and neovascularization: an experimental model using the rabbit cornea. *J. Nat. Cancer Inst.*, 52:413–427, 1974.

[286] J. Glazier and F. Garner. Simulation of the differential adhesion driven rearrangement of biological cells. *Phys. Rev. E*, 47:2128–2154, 1993.

[287] R. Godde and H. Kurz. Structural and biophysical simulation of angiogenesis and vascular remodeling. *Dev. Dyn.*, 220(4):387–401, 2001.

[288] J. J. Going and T. J. Mohun. Human breast duct anatomy, the 'sick lobe' hypothesis and intraductal approaches to breast cancer. *Breast. Canc. Res. and Treat.*, 97(3):0167–6806, 2006.

[289] J. D. Gordan, J. A. Bertout, C.-J. Hu, J. A. Diehl, and M. C. Simon. HIF-2α promotes hypoxic cell proliferation by enhancing c-Myc transcriptional activity. *Canc. Cell*, 11(4):335–47, 2007.

[290] V. Gordon, M. Valentine, M. Gardel, D. Andor-Ardó, S. Dennison, A. Bogdanov, D. Weitz, and T. Deisboeck. Measuring the mechanical stress induced by an expanding multicellular tumor system: a case study. *Exp. Cell Res.*, 289:58–66, 2003.

[291] T. Graeber, C. Osmanian, T. Jacks, and *et al.* Hypoxia-mediated selection of cells with diminished apoptotic potential in solid tumors. *Nature*, 379:88–91, 1996.

[292] F. Graner and J. Glazier. Simulation of biological cell sorting using a two-dimensional extended potts model. *Phys. Rev. Lett.*, 69:2013–2016, 1992.

[293] L. Graziano and L. Preziosi. Mechanics in tumor growth. In F. Mollica, L. Preziosi, and K. Rajagopal, editors, *Modeling of Biological Materials*, pages 267–328. Birkhaeuser, New York, 2007.

[294] H. Greenspan. Models for the growth of a solid tumor by diffusion. *Stud. Appl. Math.*, 51:317–340, 1972.

[295] H. Greenspan. On the growth and stability of cell cultures and solid tumors. *J. Theor. Biol.*, 56:229–242, 1976.

[296] A. Grin, G. Horne, M. Ennis, and F. P. O'Malley. Measuring extent of ductal carcinoma in situ in breast excision specimens: a comparison of 4 methods. *Arch. Pathol. Lab. Med.*, 133:31–7, 2009.

[297] K. Groebe, S. Erz, and W. Mueller-Klieser. Glucose diffusion coefficients determined from concentration profiles in emt6 tumor spheroids incubated in radioactively labeled l-glucose. *Adv. Exp. Med. Biol.*, 361:619–625, 1994.

[298] J. Guck, S. Schinkinger, B. Lincoln, F. Wottawah, S. Ebert, M. Romeyke, D. Lenz, H. M. Erickson, R. Ananthakrishnan, D. Mitchell, J. Käs, S. Ulvick, and C. Bilby. Optical deformability as an inherent cell marker for testing malignant transformation and metastatic competence. *Biophys. J.*, 88(5):3689–98, 2005.

[299] C. Guiot, P. D. Santo, and T. Deisboeck. Morphological instability and cancer invasion: a 'splashing water drop' analogy. *Theor. Biol. Med. Model.*, 4:4, 2007.

[300] G. P. Gupta and J. Massagu. Cancer Metastasis: Building a Framework. *Cell*, 127(4):679–695, 2006.

[301] G. Hamilton. Multicellular spheroids as an in vitro tumor model. *Cancer Letters*, 131:29–34, 1998.

[302] D. Hanahan and R. Weinberg. The hallmarks of cancer. *Cell*, 100:57–70, 2000.

[303] R. K. Hansen and M. J. Bissell. Tissue architecture and breast cancer: the role of extracellular matrix and steroid hormones. *Endocrine-Related Cancer*, 7(2):95–113, 2000.

[304] B. D. Harms, G. M. Bassi, A. R. Horwitz, and D. A. Lauffenburger. Directional persistence of EGF-induced cell migration is associated with stabilization of lamellipodial protrusions. *Biophys. J.*, 88(2):1479–88, 2005.

[305] A. Harris. Hypoxia-a key regulatory factor in tumor growth. *Nat. Rev. Cancer*, 2:38–47, 2002.

[306] A. Harten, B. Engquist, S. Osher, and S. R. Chakravarthy. Uniformly high order accurate essentially non-oscilatory schemes, III. *J. Comput. Phys.*, 71:231–303, 1987.

[307] H. Hashizume, P. Baluk, S. Morikawa, J. McLean, G. Thurston, S. Roberge, R. Jain, and D. McDonald. Openings between defective endothelial cells explain tumor vessel leakiness. *Am. J. Pathol.*, 156:1363–1380, 2000.

[308] H. Hatzikirou, L. Brusch, and A. Deutsch. From cellular automaton rules to an effective macroscopic mean field description. *Math. Biosci.*, 2009. in review.

[309] H. Hatzikirou, A. Deutsch, C. Schaller, M. Simon, and K. Swanson. Mathematical modeling of glioblastoma tumour development: A review. *Math. Models Meth. Appl. Sci.*, 15:1779–1794, 2005.

[310] M. A. Hayat. *Methods of Cancer Diagnosis, Therapy, and Prognosis: Liver Cancer.* Springer, New York, fifth edition, 2009.

[311] Y. Hegerfeldt, M. Tusch, E. Brocker, and P. Friedl. Collective cell movement in primary melanoma explants: plasticity of cell-cell interaction, 1-integrin function, and migration strategies. *Cancer Res.*, 62:2125–2130, 2002.

[312] G. Helmlinger, P. Netti, H. Lichtenbeld, R. Melder, and R. Jain. Solid stress inhibits the growth of multicellular tumor spheroids. *Nat. Biotech.*, 15:778–783, 1997.

[313] G. Helmlinger, F. Yuan, M. Dellian, and R. Jain. Interstitial ph and po2 gradients in solid tumors in vivo: high-resolution measurements reveal a lack of correlation. *Nat. Med.*, 3:177–182, 1997.

[314] R. S. Herbst. Review of epidermal growth factor receptor biology. *Int. J. Rad. Oncol. Biol. Phys.*, 59(2 (S1)):S21–S26, 2004.

[315] S.-i. Hino, C. Tanji, K. I. Nakayama, and A. Kikuchi. Phosphorylation of β-catenin by cyclic AMP-dependent protein kinase stabilizes β-catenin through inhibition of its ubiquitination. *Molec. Cell. Biol.*, 25(20):9063–72, 2005.

[316] S. Hiratsuka, K. Nakamura, S. Iwai, M. Murakami, T. Itoh, H. Kijima, J. M. Shipley, R. M. Senior, and M. Shibuya. MMP9 induction by vascular endothelial growth factor receptor-1 is involved in lung-specific metastasis. *Cancer Cell*, 2(4):289–300, 2002.

[317] M. Höckel, K. Schlenger, B. Aral, M. Mitze, U. Schaffer, and P. Vaupel. Association between tumor hypoxia and malignant progression in advanced cancer of the uterine cervix. *Cancer Res.*, 56:4509–4515, 1996.

[318] M. Höckel, K. Schlenger, S. Hoeckel, and P. Vaupel. Hypoxic cervical cancers with low apoptotic index are highly aggressive. *Cancer Res.*, 59:4525–4528, 1999.

[319] M. Höckel, K. Schlenger, and P. Vaupel. Tumor hypoxia: definitions and current clinical, biologic, and molecular aspects. *J. Natl. Cancer Inst.*, 93:266–276, 2001.

[320] C. Hogea, B. Murray, and J. Sethian. Simulating complex tumor dynamics from avascular to vascular growth using a general level-set method. *J. Math. Biol.*, 53:86–134,

2006.

[321] P. Hogeweg. Evolving mechanisms of morphogenesis: On the interplay between differential adhesion and cell-differentiation. *J. Theor. Biol.*, 203:317–333, 2000.

[322] J. Holash, P. Maisonpierre, D. Compton, P. Boland, C. Alexander, D. Zagzag, G. Yancopoulos, and S. Wiegand. Vessel cooption, regression, and growth in tumors mediated by angiopoietins and vegf. *Science*, 284:1994–1998, 1999.

[323] J. Holash, S. Wiegand, and G. Yancopoulos. New model of tumor angiogenesis: dynamic balance between vessel regression and growth mediated by angiopoietins and vegf. *Oncogene*, 18:5356–5362, 1999.

[324] M. Holmes and B. Sleeman. A mathematical model of tumor angiogenesis incorporating cellular traction and viscoelastic effects. *J. Theor. Biol.*, 202:95–112, 2000.

[325] J. M. Horowitz, D. W. Yandell, S.-H. Park, S. Canning, P. Whyte, K. Buchkovich, E. Harlow, R. A. Weinberg, and T. P. Dryja. Point mutational inactivation of the retinoblastoma antioncogene. *Science*, 243(4893):937–940, 1989.

[326] D. Horstmann, K. Painter, and H. Othmer. Aggregation under local reinforcement: From lattice to continuum. *Eur. J. Appl. Math.*, 15:545–576, 2004.

[327] K. B. Hotary, E. D. Allen, P. C. Brooks, N. S. Datta, M. W. Long, and S. J. Weiss. Membrane type 1 matrix metalloproteinase usurps tumour growth control imposed by the three-dimensional extracellular matrix. *Cell*, 114(1):33–45, 2003.

[328] M. Hu, J. Yao, L. Cai, K. E. Bachman, F. van den Brle, V. Velculescu, and K. Polyak. Distinct epigenetic changes in the stromal cells of breast cancers. *Nat. Genet.*, 37(8):899–905, 2005.

[329] Z. Hu, K. Yuri, H. Ozawa, H. Lu, and M. Kawata. The *In Vivo* time course for elimination of adrenalectomy-induced apoptotic profiles from the granule cell layer of the rat hippocampus. *J. Neurosci.*, 17(11):3981–9, 1997.

[330] J. Humphrey. Continuum biomechanics of soft biological tissues. *Proc. Roy. Soc. London A*, 459:3–46, 2003.

[331] J. Humphrey and K. Rajagopal. A constrained mixture model for growth and remodeling of soft tissues. *Math. Mod. Meth. Appl. Sci.*, 12:407–430, 2002.

[332] D. Ilic, E. A. Almeida, D. D. Schlaepfer, P. Dazin, S. Aizawa, and C. H. Damsky. Extracellular matrix survival signals transduced by focal adhesion kinase suppress p53-mediated apoptosis. *J. Cell Biol.*, 143:547–60, 1998.

[333] J. H. Irving and J. G. Kirkwood. The statistical mechanical theory of transport processes. IV. The equations of hydrodynamics. *J. Chem. Phys.*, 18:817–829, 1950.

[334] N. Ishii, D. Maier, A. Merlo, M. Tada, Y. Sawamura, A. Diserens, and E. V. Meir. Frequent co-alterations of tp53, p16/cdkn2a, p14arf, pten tumor suppressor genes in human glioma cell lines. *Brain Pathol.*, 9:469–479, 1999.

[335] T. Ishii, J. Murakami, K. Notohara, H. M. Cullings, H. Sasamoto, T. Kambara, Y. Shirakawa, Y. Naomoto, M. Ouchida, K. Shimizu, N. Tanaka, J. R. Jass, and N. Matsubara. Oeophageal squamous cell carcinoma may develop within a background of accumulating DNA methylation in normal and dysplastic mucosa. *Gut*, 56(1):13–19, 2007.

[336] T. Ishikawa, Y. Kobayashi, A. Omoto, Y. Adachi, S. Nakagawa, T. Kaneko, K. Nishida, Y. Miyamoto, Y. Chimori, T. Yoshikawa, and M. Kondo. Calcification in untreated non-Hodgkin's lymphoma of the jejunum. *Acta Haematol.*, 102(4):185–9, 1999.

[337] T. Jackson. Intracellular accumulation and mechanism of action of doxorubicin in a spatio-temporal tumor model. *J. Theor. Biol.*, 220:201–213, 2003.

[338] T. Jackson. A mathematical investigation of the multiple pathways to recurrent prostate cancer: Comparison with experimental data. *Neoplasia*, 6:697–704, 2004.

[339] T. Jackson. A mathematical model of prostate tumor growth and androgen-independent relapse. *Disc. Cont. Dyn. Sys. B*, 4:187–201, 2004.

[340] T. Jackson and H. Byrne. A mechanical model of tumor encapsulation and transcapsular spread. *Math. Biosci.*, 180:307–328, 2002.

[341] R. Jain. Determinants of tumor blood flow: a review. *Cancer Res.*, 48:2641–2658, 1988.

[342] R. Jain. Physiological barriers to delivery of monoclonal antibodies and other macromolecules in tumors. *Cancer Res.*, 50:814s–819s, 1990.

[343] R. Jain. Delivery of molecular medicine to solid tumors: lessons from in vivo imaging of gene expression and function. *J. Control. Release*, 74:7–25, 2001.

[344] R. Jain. Normalizing tumor vasculature with anti-angiogenic therapy: a new paradigm for combination therapy. *Nat. Med.*, 7:987–989, 2001.

[345] R. Jain. Molecular regulation of vessel maturation. *Nature Med.*, 9:685–693, 2003.

[346] R. Jain. Normalization of tumor vasculature: An emerging concept in antiangiogenic therapy. *Science*, 307:58–62, 2005.

[347] K. A. Janes and D. A. Lauffenburger. A biological approach to computational models of proteomic networks. *Curr. Opin. Chem. Biol.*, 10(1):73–80, 2006.

[348] A. Jemal, R. Siegel, E. Ward, T. Murray, J. Xu, and M. J. Thun. Cancer statistics, 2007. *CA Cancer J. Clin.*, 57(1):43–66, 2007.

[349] R. Jensen. Hypoxia in the tumorigenesis of gliomas and as a potential target for therapeutic measures. *Neurosurg. Focus*, 20:E24, 2006.

[350] B. Jian, N. Narula, Q.-Y. Li, E. R. Mohler III, and R. J. Levy. Progression of aortic valve stenosis: TGF-β1 is present in calcified aortic valve cusps and promotes aortic valve interstitial cell calcification via apoptosis. *Ann. Thoracic Surg.*, 75(2):457–65, 2003.

[351] G.-S. Jiang and C.-W. Shu. Efficient implementation of weighted ENO schemes. *J. Comput. Phys.*, 126:202–228, 1996.

[352] T. X. Jiang and C. M. Chuong. Mechanism of skin morphogenesis I: Analyses with antibodies to adhesion molecules tenascin, NCAM, and integrin. *Dev. Biol.*, 150:82–98, 1992.

[353] Y. Jiang, J. Pjesivac-Grbovic, C. Cantrell, and J. Freyer. A multiscale model for avascular tumor growth. *Biophys. J.*, 89:3884–3894, 2005.

[354] A. Jones, H. Byrne, J. Gibson, and J. Dold. Mathematical model for the stress induced during avascular tumor growth. *J. Math. Biol.*, 40:473–499, 2000.

[355] P. Jones and B. Sleeman. Angiogenesis-understanding the mathematical challenge. *Angiogenesis*, 9:127–138, 2006.

[356] P. A. Jones and S. B. Baylin. The fundamental role of epigenetic events in cancer. *Nat. Rev. Genet*, 3(6):415–28, 2002.

[357] P. A. Jones and P. W. Laird. Cancer epigenetics comes of age. *Nat. Genet.*, 21(2):163–7, 1999.

[358] R. E. Jr., K. O'Connor, D. Lacks, D. Schwartz, and R. Dotson. Dynamics of spheroid self-assembly in liquid-overlay culture of du 145 human prostate cancer cells. *Biotech. Bioeng.*, 72:579–591, 2001.

[359] K. Kaibuchi, S. Kuroda, and M. Amano. Regulation of the cytoskeleton and cell adhesion by the Rho family GTPases in mammalian cells. *Annu. Rev. Biochem.*, 68:459–86, 1999.

[360] F. Kallinowski, P. Vaupel, S. Runkel, G. Berg, H. Fortmeyer, K. Baessler, K. Wagner, W. Mueller-Klieser, and S. Walenta. Glucose uptake, lactate release, ketone body turnover, metabolic milieu and ph distributions in human cancer xenografts in nude rats. *Cancer Res.*, 48:7264–7272, 1988.

[361] K. Kaneko, K. Satoh, and A. Masamune. T. myosin light chain kinase inhibitors can block invasion and adhesion of human pancreatic cancer cell lines. *Pancreas*, 24:34–41, 2002.

[362] R. N. Kaplan, S. Rafii, and D. Lyden. Preparing the "Soil": The Premetastatic Niche. *Cancer Res.*, 66(23):11089–93, 2006.

[363] P. I. Karecla, S. J. Green, S. J. Bowden, J. Coadwell, and P. J. Kilshaw. Identification of a binding site for integrin $\alpha e \beta 7$ in the N- terminal domain of E-cadherin. *J. Biol. Chem.*, 271:30909–15, 1996.

[364] B. Kaur, F. Khwaja, E. Severson, S. Matheny, D. Brat, and E. VanMeir. Hypoxia and the hypoxia-inducible-factor pathway in glioma growth and angiogenesis. *Neuro-Oncol.*, 7:134–153, 2005.

[365] D. Kay and R. Welford. A multigrid finite element solver for the Cahn-Hilliard equation. *J. Comput. Phys.*, 212:288–304, 2006.

[366] P. Keller, F. Pampaloni, and E. Stelzer. Life sciences require the third dimension. *Curr. Op. Cell Biol.*, 18:117–124, 2006.

[367] T. Kelly, Y. Yan, R. L. Osborne, A. B. Athota, T. L. Rozypal, J. C. Colclasure, et al. Proteolysis of extracellular matrix by invadopodia facilitates human breast cancer cell invasion and is mediated by matrix metalloproteinases. *Clin. Exp. Metastasis*, 16(6):501–12, 1998.

[368] P. Kenny, G. Lee, and M. Bissell. Targeting the tumor microenvironment. *Front. Biosci.*, 12:3468–3474, 2007.

[369] K. Keren, Z. Pincus, G. M. Allen, E. L. Barnhart, G. Marriott, A. Mogilner, et al. Mechanism of shape determination in motile cells. *Nature*, 453(7194):475–80, 2008.

[370] K. Kerlikowske, A. Molinaro, I. Cha, B. M. Ljung, V. L. Ernster, K. Stewart, K. Chew, D. H. Moore 2nd, and F. Waldman. Characteristics associated with recurrence among women with ductal carcinoma in situ treated by lumpectomy. *J. Natl. Cancer Inst.*, 95(22):1692–702, 2003.

[371] J. F. R. Kerr, C. M. Winterford, and B. V. Harmon. Apoptosis. its significance in cancer and cancer therapy. *Cancer*, 73(8):2013–26, 1994.

[372] I. Kevrekidis, , C. Gear, J. Hyman, P. Kevrekidis, O. Runborg, and K. Theodoropoulos. Equation-free, coarse-grained multiscale computation: Enabling microscopic simulators to perform system-level analysis. *Comm. Math. Sci.*, 1:715–762, 2003.

[373] P. Kevrekidis, N. Whitaker, D. Good, and G. Herring. Minimal model for tumor angiogenesis. *Phys. Rev. E*, 73:061926, 2006.

[374] E. Khain and L. Sander. Generalized cahn-hilliard equation for biological applications. *Phys. Rev. E*, 77:051129, 2008.

[375] E. Khain, L. Sander, and C. Schneider-Mizell. The role of cell-cell adhesion in wound healing. *J. Stat. Phys.*, 128:209–218, 2007.

[376] S. Khan, M. Rogers, K. Khurana, M. Meguid, and P. Numann. Estrogen receptor expression in benign breast epithelium and breast cancer risk. *J. Natl. Canc. Inst.*, 90:37–42, 1998.

[377] S. Khan, A. Sachdeva, S. Naim, M. Meguid, W. Marx, H. Simon, et al. The normal breast epithelium of women with breast cancer displays an aberrant response to estra-

diol. *Canc. Epidemiol. Biomarkers Prev.*, 8:867–72, 1999.

[378] S. Kharait, S. Hautaniemi, S. Wu, A. Iwabu, D. A. Lauffenburger, and A. Wells. Decision tree modeling predicts effects of inhibiting contractility signaling on cell motility. *BMC Syst. Biol.*, 1:9ff, 2007.

[379] B. N. Kholodenko, O. V. Demin, G. Moehren, and J. B. Hoek. Quantification of short term signaling by the epidermal growth factor receptor. *J. Biol. Chem.*, 274(42):30169–81, 1999.

[380] J. Kim. Three-dimensional tissue culture models in cancer biology. *J. Biomol. Screening*, 15:365–77, 2005.

[381] J. Kim, K. Kang, and J. Lowengrub. Conservative multigrid methods for Cahn-Hilliard fluids. *J. Comput. Phys.*, 193:511–543, 2003.

[382] J. Kim, K. Kang, and J. Lowengrub. Conservative multigrid methods for ternary Cahn-Hilliard systems. *Comm. Math. Sci.*, 2:53–77, 2004.

[383] J. Kim and J. Lowengrub. Phase field modeling and simulation of three phase flows. *Int. Free Bound.*, 7:435–466, 2005.

[384] Y. Kim, M. Stolarska, and H. Othmer. A hybrid model for tumor spheroid growth in vitro i: Theoretical development and early results. *Math. Meth. App. Sci.*, 17:1773–1798, 2007.

[385] R. Kloner and R. Jennings. Consequences of brief ischemia: stunning, preconditioning, and their clinical implications: part 1. *Circulation*, 104:2981–2989, 2001.

[386] M. Knowles and P. Selby, editors. *Introduction to the Cellular and Molecular Biology of Cancer*. Oxford University Press, Oxford, UK, fourth edition, 2005.

[387] K. A. Knudsen, A. P. Soler, K. R. Johnson, and M. J. Wheelock. Interaction of α-actin with the cadherin/catenin cell-cell adhesion complex via α-catenin. *J. Cell. Biol.*, 130:66–77, 1995.

[388] A. G. Knudson. Mutation and cancer: statistical study of retinoblastoma. *Proc. Natl. Acad. Sci. USA*, 68(4):820–3, 1971.

[389] A. G. Knudson. Two genetic hits (more or less) to cancer. *Nat. Rev. Cancer*, 1(2):157–62, 2001.

[390] L. Kopfstein and G. Christofori. Metastasis: cell-autonomous mechanisms versus contributions by the tumor microenvironment. *Cell. Mol. Life Sci.*, 63:449–468, 2006.

[391] D. V. Krysko, T. V. Berghe, K. D'Herde, and P. Vandenabeele. Apoptosis and necrosis: Detection, discrimination and phagocytosis. *Methods*, 44:205–21, 2008.

[392] E. Kuhl and G. Holzapfel. A continuum model for remodeling in living structures. *J. Mater. Sci.*, 42:8811–8823, 2007.

[393] R. Kuiper, J. Schellens, G. Blijham, J. Beijnen, and E. Voest. Clinical research on antiangiogenic therapy. *Pharmacol. Res.*, 37:1–16, 1998.

[394] P. Kunkel, U. Ulbricht, P. Bohlen, R. F. M.A. Brockmann, D. Stavrou, M. Westphal, and K. Lamszus. Inhibition of glioma angiogenesis and growth in vivo by systemic treatment with a monoclonal antibody against vascular endothelial growth factor receptor-2. *Cancer Res.*, 61:6624–6628, 2001.

[395] L. Kunz-Schughart, J. P. Freyer, F. Hofstaedter, and R. Ebner. The use of 3-d cultures for high-throughput screening: The multicellular spheroid model. *J. Biomol. Screening*, 9:273–85, 2004.

[396] R. Küppers and R. Dalla-Favera. Mechanisms of chromosomal translocations in B cell lymphomas. *Oncogene*, 20(40):5580–94, 2001.

[397] A. Lal, C. Glazer, H. Martinson, H. Friedman, G. Archer, J. Sampson, and G. Riggins. Mutant epidermal growth factor receptor up-regulates molecular effectors of tumor invasion. *Cancer Res.*, 62:3335–3339, 2002.

[398] C. R. Lamb. Diagnosis of calcification on abdominal radiographs. *Vet. Rad. Ultrasound*, 32(5):211–20, 1991.

[399] O. T. Lampejo, D. M. Barnes, P. Smith, and R. R. Millis. Evaluation of infiltrating ductal carcinomas with a DCIS component: correlation of the histologic type of the in situ component with grade of the infiltrating component. *Semin. Diagn. Pathol.*, 11(3):215–22, 1994.

[400] K. Lamszus, P. Kunkel, and M. Westphal. Invasion as limitation to anti-angiogenic glioma therapy. *Acta Neurochir Suppl.*, 88:169–177, 2003.

[401] K. Landman and C. Please. Tumour dynamics and necrosis: Surface tension and stability. *IMA J. Math. Appl. Medicine Biol.*, 18:131–158, 2001.

[402] M. C. Lane, M. A. Koehl, F. WIlt, and R. Keller. A role for regulated secretion of apical extracellular matrix during epithelial invagination in the sea urchin. *Development*, 117(3):1049–60, 1993.

[403] H. Larjava, T. Salo, K. Haapasalmi, R. H. Kramer, and J. Heino. Expression of integrins and basement membrane components by wound keratinocytes. *J. Clin. Invest.*, 92(3):1425–35, 1993.

[404] D. A. Lauffenburger. Cell signaling pathways as control modules: complexity for simplicity? *Proc. Natl. Acad. Sci. USA*, 97(10):5031–3, 2000.

[405] C. Le Clainche and M. F. Carlier. Regulation of actin assembly associated with protrusion and adhesion in cell migration. *Physiol. Rev.*, 88(2):489–513, 2008.

[406] D. Lee, H. Rieger, and K. Bartha. Flow correlated percolation during vascular remodeling in growing tumors. *Phys. Rev. Lett.*, 96:058104, 2006.

[407] J. S. Lee, D. M. Basalyga, A. Simionescu, J. C. Isenburg, D. T. Sinionescu, and N. R. Vyavahare. Elastin calcification in the rate subdermal model is accompanied by upregulation of degradative and osteogenic cellular responses. *Am. J. Pathol.*, 168:490–8, 2006.

[408] S. Lee, S. K. Mohsin, S. Mao, S. G. Hilsenbeck, D. Medina, and D. C. Allred. Hormones, receptors, and growth in hyperplastic enlarged lobular units: early potential precursors of breast cancer. *Breast Canc. Res.*, 8(1):R6, 2006.

[409] S. Lehoux and A. Tedgui. Signal transduction of mechanical stresses in the vascular wall. *Hypertension*, 32(2):338–345, 1998.

[410] J. Less, T. Skalak, E. Sevick, and R. Jain. Microvascular architecture in a mammary carcinoma: branching patterns and vessel dimensions. *Cancer Res.*, 51:265–273, 1991.

[411] H. Levine and M. Nilsen-Hamilton. Angiogenesis- a biochemical/mathematical perspective. *Tutorials in Math. Biosci. III*, 1872:23–76, 2006.

[412] H. Levine, S. Pamuk, B. Sleeman, and M. Nilsen-Hamilton. Mathematical modeling of capillary formation and development in tumor angiogenesis: penetration into the stroma. *Bull. Math. Biol.*, 63:801–863, 2001.

[413] H. Levine and B. Sleeman. Modelling tumour-induced angiogenesis. In L. Preziosi, editor, *ancer modelling and simulation*, pages 147–184. Chapman&Hall/CRC, Boca Raton, Florida, 2003.

[414] H. Levine, B. Sleeman, and M. Nilsen-Hamilton. Mathematical modeling of the onset of capillary formation initiating angiogenesis. *J. Math. Biol.*, 42:195–238, 2001.

[415] H. Levine, M. Smiley, A. Tucker, and M. Nilsen-Hamilton. A mathematical model for the onset of avascular tumor growth in response to the loss of p53 function. *Cancer Informatics*, 2:163–188, 2006.

[416] H. Levine, A. Tucker, and M. Nilsen-Hamilton. A mathematical model for the role of cell signal transduction in the initiation and inhibition of angiogenesis. *Growth Factors*, 20:155–175, 2002.

[417] J. Li, P. Kevrekidis, C. Gear, and I. Kevrekidis. Deciding the nature of the coarse equation through microscopic simulations: The baby-bathwater scheme. *SIAM Review*, 49:469–487, 2007.

[418] X. Li, V. Cristini, Q. Nie, and J. Lowengrub. Nonlinear three-dimensional simulation of solid tumor growth. *Disc. Dyn. Contin. Dyn. Syst. B*, 7:581–604, 2007.

[419] S.-Y. Lin, W. Xia, J. C. Wang, K. Y. Kwong, and B. Spohn. β-Catenin, a novel prognostic marker for breast cancer: Its roles in Cyclin D1 expression and cancer progression. *Proc. Natl. Acad. Sci. USA*, 97(8):4262–6, 2000.

[420] L. Liotta and E. Kohn. The microenvironment of the tumour-host interface. *Nature*, 411:375–379, 2001.

[421] A. Lipton. Pathophysiology of Bone Metastases: How This Knowledge May Lead to Therapeutic Intervention. *J. Support. Oncol.*, 2(3):205–220, 2004.

[422] X. D. Liu, S. Osher, and T. Chan. Weighted essentially non-oscillatory schemes. *J. Comput. Phys.*, 115:200–212, 1994.

[423] B. Lloyd, D. Szczerba, M. Rudin, and G. Szekely. A computational framework for modeling solid tumour growth. *Phil. Trans. Roy. Soc. A*, 366:3301–3318, 2008.

[424] B. Lloyd, D. Szczerba, and G. Szekely. A coupled finite element model of tumor growth and vascularization. In N. Ayache, S. Ourselin, and A. Maeder, editors, *Medical image computing and computer-assisted intervention-MICCA 2007: 10th international conference*, volume 4792 of *Lecture Notes in Computer Science*, pages 874–881. Springer, New York, 2007.

[425] J. Lotem and L. Sachs. Epigenetics and the plasticity of differentiation in normal and cancer stem cells. *Oncogene*, 25(59):7663–7672, 2006.

[426] R. M. B. Loureiro and P. A. D'Amore. Transcriptional regulation of vascular endothelial growth factor in cancer. *Cytokine Growth Factor Rev.*, 16(1):77–89, 2005.

[427] J. Lowengrub, H. Frieboes, F. Jin, Y. Chuang, X. Li, P. Macklin, S. Wise, and V. Cristini. Nonlinear modeling of cancer: Bridging the gap between cells and tumors. *Nonlinearity*, 2010. in press.

[428] V. Lubarda and A. Hoger. On the mechanics of solids with a growing mass. *Int. J. Solids Structures*, 39:4627–4664, 2002.

[429] P. J. Lucio, M. T. Faria, A. M. Pinto, M. R. da Silva, M. E. Correia Jr., R. J. da Costa, and A. B. Parreira. Expression of adhesion molecules in chronic B-cell lymphoproliferative disorders. *Haematologica*, 83(2):104–11, 1998.

[430] B. Lustig, B. Jerchow, M. Sachs, S. Wiler, T. Pietsch, U. Karsten, M. van de Wetering, H. Clevers, P. M. Schlag, W. Birchmeier, and J. Behrens. Negative feedback loop of Wnt signaling through upregulation of conductin/axin2 in colorectal and liver tumors. *Mol. Cell. Biol.*, 22:1184–93, 2002.

[431] B. MacArthur and C. Please. Residual stress generation and necrosis formation in multi-cell tumour spheroids. *J. Math. Biol.*, 49:537–552, 2004.

[432] P. Macklin. Numerical Simulation of Tumor Growth and Chemotherapy. M.S. thesis, University of Minnesota School of Mathematics, September 2003.

[433] P. Macklin. *Toward Computational Oncology: Nonlinear Simulation of Centimeter-Scale Tumor Growth in Complex, Heterogeneous Tissues.* Ph.D. dissertation, University of California, Irvine Department of Mathematics, June 2007.

[434] P. Macklin, L. Carreras, J. Kim, S. Sanga, V. Cristini, and M. E. Edgerton. Mathematical analysis of histopathology indicates comparable oxygen uptake rates for quiescent and proliferating breast cancer cells in DCIS. (in preparation), 2009.

[435] P. Macklin, J. Kim, G. Tomaiuolo, M. E. Edgerton, and V. Cristini. Agent-Based Modeling of Ductal Carcinoma in Situ: Application to Patient-Specific Breast Cancer Modeling. In T. Pham, editor, *Computational Biology: Issues and Applications in Oncology*, chapter 4, pages 77–112. Springer, New York, NY, 2009.

[436] P. Macklin, J. Kim, G. Tomaiuolo, M. E. Edgerton, and V. Cristini. An agent-based cell model, with application to patient-specific ductal carcinoma in situ modeling. (in preparation), 2010.

[437] P. Macklin and J. Lowengrub. Evolving interfaces via gradients of geometry-dependent interior Poisson problems: Application to tumor growth. *J. Comput. Phys.*, 203:191–220, 2005.

[438] P. Macklin and J. Lowengrub. An improved geometry-aware curvature discretization for level set methods: Application to tumor growth. *J. Comput. Phys.*, 215:392–401, 2006.

[439] P. Macklin and J. Lowengrub. Nonlinear simulation of the effect of microenvironment on tumor growth. *J. Theor. Biol.*, 245:677–704, 2007.

[440] P. Macklin and J. Lowengrub. A new ghost cell/level set method for moving boundary problems: Application to tumor growth. *J. Sci. Comp.*, 35(2-3):266–99, 2008.

[441] P. Macklin, S. McDougall, A. Anderson, M. Chaplain, V. Cristini, and J. Lowengrub. Multiscale modeling and nonlinear simulation of vascular tumour growth. *J. Math. Biol.*, 58(4-5):765–98, 2009.

[442] A. D. C. Macknight, D. R. DiBona, A. Leaf, and M. C. Mortimer. Measurement of the composition of epithelial cells from the toad urinary bladder. *J. Membrane Biol.*, 6(2):108–26, 1971.

[443] S. Madsen, E. Angell-Petersen, S. Spetalen, S. Carper, S. Ziegler, and H. Hirschberg. Photodynamic therapy of newly implanted glioma cells in the rat brain. *Lasers Surg. Med.*, 38:540–548, 2006.

[444] S. Maggelakis and J. Adam. Mathematical model of prevascular growth of a spherical carcinoma. *Math. Comput. Modelling*, 13:23–38, 1990.

[445] E. Maher, F. Furnari, R. Bachoo, D. Rowitch, D. Louis, W. Cavenee, and R. De-Pinho. Malignant glioma: genetics and biology of a grave matter. *Genes Dev.*, 15:1311–1333, 2001.

[446] G. Majno and I. Joris. *Cells, Tissues, and Disease: Principles of General Pathology.* Oxford University Press, New York, second edition, 2004.

[447] A. G. Makeev, D. Maroudas, and I. G. Kevrekidis. 'Coarse' stability and bifurcation analysis using stochastic simulators: Kinetic Monte Carlo examples. *J. Chem. Phys.*, 116:10083–10091, 2002.

[448] A. G. Makeev, D. Maroudas, A. Z. Panagiotopoulos, and I. G. Kevrekidis. Coarse bifurcation analysis of kinetic Monte Carlo simulations: A lattice-gas model with lateral interactions. *J. Chem. Phys.*, 117:8229–8240, 2002.

[449] R. Malladi, J. A. Sethian, and B. C. Vemuri. Shape Modeling with Front Propagation: A Level Set Approach. *IEEE Trans. Pattern Anal. Mach. Intell.*, 17(2), 1995.

[450] R. Malladi, J. A. Sethian, and B. C. Vemuri. A fast level set based algorithm for topology-independent shape modeling. *J. Math. Imaging Vision*, 6(2-3):269–289, 1996.

[451] M. Malumbres and M. Barbacis. RAS oncogenes: the first 30 years. *Nat. Rev. Cancer*, 3(6):459–465, 2001.

[452] L. Malvern. *Introduction of the mechanics of a continuous medium*. Prentice Hall, Englewood Cliffs, 1969.

[453] D. Manoussaki, S. Lubkin, R. Vernon, and J. Murray. A mechanical model for the formation of vascular networks in vitro. *Acta Biotheor.*, 44:271–282, 1996.

[454] N. Mantzaris, S. Webb, and H. Othmer. Mathematical modeling of tumor-induced angiogenesis. *J. Math. Biol.*, 49:111–187, 2004.

[455] B. Marchant, J. Norbury, and J.A.Sherratt. Travelling wave solutions to a haptotaxis-dominated model of malignant invasion. *Nonlinearity*, 14:1653–1671, 2001.

[456] A. F. Maree, A. Jilkine, A. Dawes, V. A. Grieneisen, and L. Edelstein-Keshet. Polarization and movement of keratocytes: a multiscale modelling approach. *Bull. Math. Biol.*, 68(5):1169–1211, 2006.

[457] D. Martin and P. Colella. A cell-centered adaptive projection method for the incompressible Euler equations. *J. Comput. Phys.*, 163:271–312, 2000.

[458] M. Marusic, Z. Baizer, J. Freyer, and S. Vuk-Pavlovic. Analysis of growth of multicellular tumour spheroids by mathematical models. *Cell Prolif.*, 27:73–94, 1994.

[459] K. Matsumoto and T. Nakamura. Hepatocyte growth factor and the Met system as a mediator of tumor-stromal interactions. *Int. J. Cancer*, 119(3):477–483, 2006.

[460] B. McArthur and C. Please. Residual stress generation and necrosis formation in multicell tumor spheroids. *J. Math. Biol.*, 49:537–552, 2004.

[461] S. McDougall, A. Anderson, and M. Chaplain. Mathematical modelling of dynamic adaptive tumour-induced angiogenesis: Clinical applications and therapeutic targeting strategies. *J. Theor. Biol.*, 241:564–589, 2006.

[462] S. McDougall, A. Anderson, M. Chaplain, and J. Sherratt. Mathematical modelling of flow through vascular networks: implications for tumour-induced angiogenesis and chemotherapy strategies. *Bull. Math. Biol.*, 64:673–702, 2002.

[463] D. McElwain and L. Morris. Apoptosis as a volume loss mechanism in mathematical models of solid tumor growth. *Math. Biosci.*, 39:147–157, 1978.

[464] C. Medrek, G. Landberg, and K. Andersson, T adn Leandersson. Wnt-5a-CKIα signaling promotes β-Catenin/E-Cadherin complex formation and intercellular adhesion in human breast epithelial cells. *J. Biol. Chem.*, 284:10968–79, 2009.

[465] A. Menzel. Modelling of anisotropic growth in biological tissues- a new approach and computational aspects. *Biomech. Model. Mechanobiol.*, 3:147–171, 2005.

[466] R. Merks, S. Brodsky, M. Goligorksy, S. Newman, and J. Glazier. Cell elongation is key to in silico replication of in vitro vasculogenesis and subsequent remodeling. *Dev. Biol.*, 289:44–54, 2006.

[467] R. Merks and J. Glazier. Dynamic mechanisms of blood vessel growth. *Nonlinearity*, 19:C1–C10, 2006.

[468] R. Merks, E. P. A. Shirinifard, and J. Glazier. Contact-inhibited chemotaxis in de novo and sprouting blood-vessel growth. *PloS Comp. Biol.*, 4:e1000163, 2008.

[469] A. Merlo. Genes and pathways driving glioblastomas in humans and murine disease models. *Neurosurg. Rev.*, 26:145–158, 2003.

[470] N. Metropolis, A. Rosenbluth, M. Rosenbluth, A. Teller, and E. Teller. Equation of state calculations by fast computing machines. *J. Chem. Phys.*, 21:1087–1092, 1953.

[471] P. Michieli, C. Basilico, S. Pennacchietti, A. Maffè, L. Tamagnone, S. Giordano, A. Bardelli, and P. Comoglio. Mutant met mediated transformation is ligand-dependent and can be inhibited by hgf antagonists. *Oncogene*, 18:5221–5231, 1999.

[472] L. P. Middleton, G. Vlastos, N. Q. Mirza, S. Eva, and A. A. Sahin. Multicentric mammary carcinoma: evidence of monoclonal proliferation. *Cancer*, 94(7):1910–6, 2002.

[473] F. Milde, M. Bergdorf, and P. Koumoutsakos. A hybrid model for three-dimensional simulations of sprouting angiogenesis. *Biophys. J.*, 95:3146–3160, 2008.

[474] S. Mitran. *BEARCLAW a code for multiphysics applications with embedded boundaries: user's manuel*. Department of Mathematics, University of North Carolina, http://www.amath.unc.edu/Faculty/mitran/bearclaw.html, 2006.

[475] D. F. Moffat and J. J. Going. Three dimensional anatomy of complete duct systems in human breast: pathological and developmental implications. *J. Clin. Pathol.*, 49:48–52, 1996.

[476] A. Mogilner and L. Edelstein-Keshet. Regulation of actin dynamics in rapidly moving cells: a quantitative analysis. *Biophys. J.*, 83(3):1237–58, 2002.

[477] R. Montesano, K. Matsumoto, T. Nakamura, and L. Orci. Identification of a fibroblast-derived epithelial morphogen as hepatocyte growth factor. *Cell*, 67:901–908, 1991.

[478] J. Moreira and A. Deutsch. Cellular automaton models of tumor development: A critical review. *Adv. Complex Sys.*, 5:247–267, 2002.

[479] A. Morotti, S. Mila, P. Accornero, E. Tagliabue, and C. Ponzetto. K252a inhibits the oncogenic properties of met, the hgf receptor. *Oncogene*, 21:4885–4893, 2002.

[480] K. Morton and D. Mayers. *Numerical Solution of Partial Differential Equations*. Cambridge, Cambridge, UK, second edition, 2005.

[481] B. Mosadegh, W. Saadi, S. J. Wang, and N. L. Jeon. Epidermal growth factor promotes breast cancer cell chemotaxis in CXCL12 gradients. *Biotech. Bioeng.*, 100(6):1205–13, 2008.

[482] W. Mueller-Klieser. Multicellular spheroids: a review on cellular aggregates in cancer research. *J. Cancer Res. Clin. Oncol.*, 113:101–122, 1987.

[483] W. Mueller-Klieser. Three-dimensional cell cultures: from molecular mechanisms to clinical applications. *Am. J. Physiol. Cell Physiol.*, 273:C1109–C1123, 1997.

[484] W. Mueller-Klieser, J. Freyer, and R. Sutherland. Influence of glucose and oxygen supply conditions on the oxygenation of multicellular spheroids. *Br. J. Cancer*, 53:345–353, 1986.

[485] G. Müller and J.-J. Métois. *Crystal Growth: From Fundamentals to Technology*. Elsevier, 2004.

[486] W. Mullins and R. Sekerka. Morphological instability of a particle growing by diffusion or heat flow. *J. Appl. Phys.*, 34:323–329, 1963.

[487] G. R. Mundy. Metastasis to bone: causes, consequences and therapeutic opportunities. *Nat. Rev. Cancer*, 2(8):584–93, 2002.

[488] J. Murray and G. Oster. Cell traction models for generation of pattern and form in morphogenesis. *J. Math. Biol.*, 33:489–520, 1984.

[489] V. R. Muthukkaruppan, L. Kubai, and R. Auerbach. Tumor-induced neovascularization in the mouse eye. *J. Natl. Cancer Inst.*, 69(3):699–705, 1982.

[490] K. Nabeshima, T. Moriyama, Y. Asada, N. Komada, T. Inoue, H. Kataoka, A. Sumiyoshi, and M. Koono. Ultrastructural study of TPA-induced cell motility: human well-differentiated rectal adenocarcinoma cells move as coherent sheets via localized modulation of cell–cell adhesion. *Clin. Exp. Med.*, 13(6):499–508, 1995.

[491] M. Nagane, A. Levitzki, A. Gazit, W. Cavenee, and H. Huang. Drug resistance of human glioblastoma cells conferred by a tumor-specific mutant epidermal growth factor receptor through modulation of bcl-x l and caspase-3-like proteases. *Proc. Natl. Acad. Sci. USA*, 95:5724–5729, 1998.

[492] H. Naganuma, R. Kimurat, A. Sasaki, A. Fukamachi, H. Nukui, and K. Tasaka. Complete remission of recurrent glioblastoma multiforme following local infusions of lymphokine activated killer cells. *Acta Neurochir.*, 99:157–160, 1989.

[493] J. Nagy. The ecology and evolutionary biology of cancer: A review of mathematical models of necrosis and tumor cell diversity. *Math. Biosci. Eng.*, 2:381–418, 2005.

[494] M. N. Nakatsu, R. C. A. Sainson, J. N. Aoto, K. L. Taylor, M. Aitkenhead, S. Prez-del Pulgard, P. M. Carpenter, and C. C. W. Hughes. Angiogenic sprouting and capillary lumen formation modeled by human umbilical vein endothelial cells (HUVEC) in fibrin gels: the role of fibroblasts and Angiopoietin-1. *Microvasc. Res.*, 66:102–112, 2003.

[495] M. A. H. Navarrete, C. M. maier, R. Falzoni, L. G. d. A. Quadros, E. C. Baracat, and A. C. P. Nazário. Assessment of the proliferative, apoptotic, and cellular renovation indices of the human mammary epithelium during the follicular and luteal phases of the menstrual cycle. *Breast Cancer Res.*, 7:R306–13, 2005.

[496] C. Nelson and M. Bissell. Of extracellular matrix, scaffolds, and signaling: tissue architecture regulates development, homeostasis, and cancer. *Annu. Rev. Cell Dev. Biol.*, 22:287–309, 2006.

[497] P. Netti, L. Baxter, Y. Boucher, R. Skalak, and R. Jain. Time dependent behavior of interstitial fluid pressure in solid tumors: Implications for drug delivery. *Cancer Res.*, 55:5451–5458, 1995.

[498] A. Neville, P. Matthews, and H. Byrne. Interactions between pattern formation and domain growth. *Bull. Math. Biol.*, 68:1975–2003, 2006.

[499] G. Ngwa and P. Maini. Spatio-temporal patterns in a mechanical model for mesenchymal morphogenesis. *J. Math. Biol.*, 33:489–520, 1995.

[500] M. Nichols and T. Foster. Oxygen diffusion and reaction kinetics in the photodynamic therapy of multicell tumour spheroids. *Phys. Med. Biol.*, 39:2161–2181, 1994.

[501] R. Nishikawa, X. Ji, R. Harmon, C. Lazar, G. Gill, W. Cavenee, and H. Huang. A mutant epidermal growth factor receptor common in human glioma confers enhanced tumorigenicity. *Proc. Natl. Acad. Sci. USA*, 91:7727–7731, 1994.

[502] J. Nor, J. Christensen, J. Liu, M. Peters, D. Mooney, R. Strieter, and P. Polverini. Up-regulation of bcl-2 in microvascular endothelial cells enhances intratumoral angiogenesis and accelerates tumor growth. *Cancer Res.*, 61:2183–2188, 2001.

[503] M. A. Nowak, N. L. Komarova, A. Sengupta, J. V. Prasad, I.-M. Shih, B. Vogelstein, and C. Lengauer. The role of chromosomal instability in tumor initiation. *Proc. Natl. Acad. Sci. USA*, 99(25):16226–16231, 2002.

[504] J. O'Connor, A. Jackson, G. Parker, and G. Jayson. Dce-mri biomarkers in the clinical evaluation of antiangiogenic and vascular disrupting agents. *Br. J. Cancer*, 96:189–195, 2007.

[505] K. Oda, Y. Matsuoka, A. Funahashi, and H. Kitano. A comprehensive pathway map of epidermal growth factor receptor signaling. *Mol. Syst. Biol.*, 1, 2005.

[506] T. Ohtake, I. Kimijima, T. Fukushima, M. Yasuda, K. Sekikawa, S. Takenoshita, and R. Abe. Computer-assisted complete three-dimensional reconstruction of the mammary ductal/lobular systems. *Cancer*, 91:2263–72, 2001.

[507] B. Øksendal. *Stochastic Differential Equations: An Introduction with Applications.* Springer, New York, 6th edition, 2007.

[508] M. Orme and M. Chaplain. Two-dimensional models of tumour angiogenesis and anti-angiogenesis strategies. *Math. Med. Biol.*, 14:189–205, 1997.

[509] S. Osher and R. Fedkiw. Level Set Methods: An Overview and Some Recent Results. *J. Comput. Phys.*, 169(2):463–502, 2001.

[510] S. Osher and R. Fedkiw. *Level Set Methods and Dynamic Implicit Surfaces*. Springer, New York, NY, 2002.

[511] S. Osher and J. Sethian. Fronts propagating with curvature-dependent speed: algorithms based on hamilton-jacobi formulation. *J. Comput. Phys.*, 79:12, 1988.

[512] H. Othmer and A. Stevens. Aggregration, blowup, and collapse: the abc's of taxis in reinforced random walks. *Siam. J. Appl. Math.*, 57:1044–1081, 1997.

[513] H. G. Othmer, S. R. Dunbar, and W. Alt. Models of dispersal in biological systems. *J. Math. Biol.*, 26:263–298, 1988.

[514] M. Owen, T. Alarcón, P. Maini, and H. Byrne. Angiogenesis and vascular remodeling in normal and cancerous tissues. *J. Math. Biol.*, 58:689–721, 2009.

[515] M. R. Owen, H. M. Byrne, and C. E. Lewis. Mathematical modelling of the use of macrophages as vehicles for drug delivery to hypoxic tumour sites. *J. Theor. Biol.*, 226(4):377–91, 2004.

[516] T. Padera, B. Stoll, J. Tooredman, D. Capen, E. di Tomaso, and R. Jain. Cancer cells compress intratumour vessels. *Nature*, 427:695, 2004.

[517] D. Page, T. Anderson, and G. Sakamoto. *Diagnostic Histopathology of the Breast*. Churchill Livingstone, New York, 1987.

[518] D. L. Page, W. D. Dupont, L. W. Rogers, and M. Landenberger. Intraductal carcinoma of the breast: follow-up after biopsy only. *Cancer*, 49(4):751–8, 1982.

[519] S. Paget. The distribution of secondary growths in cancer of the breast. *Lancet*, 133(3421):571–573, 1889.

[520] S. Paku. First step of tumor-related angiogenesis. *Lab. Invest.*, 65:334–346, 1991.

[521] D. Palmieri, C. E. Horak, J.-H. Lee, D. O. Halverson, and P. S. Steeg. Translational approaches using metastasis suppressor genes. *J. Bioenerg. Biomembr.*, 38(3-4):151–161, 2006.

[522] E. Palsson and H. Othmer. A model for individual and collective cell movement in dictyostelium discoideum. *Proc. Nat. Acad. Sci. USA*, 97:10338–10453, 2000.

[523] S. Pamuk. Qualitative analysis of a mathematical model for capillary formation in tumor angiogenesis. *Math. Models Meth. Appl. Sci.*, 13:19–33, 2003.

[524] P. Panorchan, M. S. Thompson, K. J. Davis, Y. Tseng, K. Konstantopoulos, and D. Wirtz. Single-molecule analysis of cadherin-mediated cell-cell adhesion. *J. Cell Sci.*, 119:66–74, 2006.

[525] W. Pao, T. Y. Wang, G. J. Riely, et al. KRAS mutations and primary resistance of lung adenocarcinomas to gefitinib or erlotinib. *PLoS Med.*, 2:e17, 2005.

[526] S. Parnuk. A mathematical model for capillary formation and development in tumor angiogenesis: A review. *Chemotherapy*, 52:35–37, 2006.

[527] S. Patan, S. Tanda, S. Roberge, R. Jones, R. Jain, and L. Munn. Vascular morphogenesis and remodeling in a human tumor xenograft: blood vessel formation and growth after ovariectomy and tumor implantation. *Circ. Research*, 89:732–739, 2001.

[528] N. Patani, B. Cutuli, and K. Mokbel. Current management of DCIS: a review. *Breast Cancer Res. Treat.*, 111(1):1–10, 2008.

[529] A. Patel, E. Gawlinski, S. Lemieux, and R. Gatenby. A cellular automaton model of early tumor growth and invasion: The effects of native tissue vascularity and increased anaerobic tumor metabolism. *J. Theor. Biol.*, 213:315–331, 2001.

[530] N. Paweletz and M. Knierim. Tumor-related angiogenesis. *Crit. Rev. Oncol. Hematol.*, 9:197–242, 1989.

[531] S. Peirce. Computational and mathematical modeling of angiogenesis. *Microcirculation*, 15(8):739–751, 2008.

[532] S. Pennacchietti, P. Michieli, M. Galluzzo, S. Giordano, and P. Comoglio. Hypoxia promotes invasive growth by transcriptional activation of the met protooncogene. *Cancer Cell*, 3:347–361, 2003.

[533] C. Peskin. The immersed boundary method. *Acta Numer.*, 11:479–517, 2002.

[534] C. S. Peskin. Flow patterns around heart valves: A numerical method. *J. Comput. Phys.*, 10(2):252–71, 1972.

[535] J. Peterson, G. Carey, D. Knezevic, and B. Murray. Adaptive finite element methodology for tumour angiogenesis modelling. *Int. J. Num. Meth. Eng.*, 69:1212–1238, 2007.

[536] G. Pettet, C. Please, M. Tindall, and D. McElwain. The migration of cells in multicell tumor spheroids. *Bull. Math. Biol.*, 63:231–257, 2001.

[537] M. Plank and B. Sleeman. A reinforced random walk model of tumour angiogenesis and anti-angiogenic strategies. *Math. Med. Biol.*, 20:135–181, 2003.

[538] M. Plank and B. Sleeman. Lattice and non-lattice models of tumour angiogenesis. *Bull. Math. Biol.*, 66:1785–1819, 2004.

[539] C. Please, G. Pettet, and D. McElwain. A new approach to modeling the formation of necrotic regions in tumors. *Appl. Math. Lett.*, 11:89–94, 1998.

[540] C. Please, G. Pettet, and D. McElwain. Avascular tumour dynamics and necrosis. *Math. Models Appl. Sci.*, 9:569–579, 1999.

[541] N. Poplawski, U. Agero, J. Gens, M. Swat, J. Glazier, and A. Anderson. Front instabilities and invasiveness of simulated avascular tumors. *Bull. Math. Biol.*, 71:1189–1227, 2009.

[542] L. Postovit, M. Adams, G. Lash, J. Heaton, and C. Graham. Oxygen-mediated regulation of tumor cell invasiveness. involvement of a nitric oxide signaling pathway. *J. Biol. Chem.*, 277:35730–35737, 2002.

[543] J. Pouysségur, F. Dayan, and N. Mazure. Hypoxia signalling in cancer and approaches to enforce tumour regression. *Nature*, 441:437–443, 2006.

[544] F. Prall. Tumour budding in colorectal carcinoma. *Histopathology*, 50:151–162, 2007.

[545] M. Preusser, H. Heinzl, E. Gelpi, K. Schonegger, C. Haberler, P. Birner, C. Marosi, M. hegi, T. Gorlia, and J. Hainfellner. Histopathologic assessment of hot-spot microvessel density and vascular patterns in glioblastoma: Poor observer agreement limits clinical utility as prognostic factors: a translational research project of the european organization for research and treatment of cancer brain tumor group. *Cancer*, 107:162–170, 2006.

[546] L. Preziosi. *Cancer Modelling and Simulation*. Chapman and Hall/CRC, London, 2003.

[547] L. Preziosi and S. Astanin. Modelling the formation of capillaries. In A. Quarteroni, L. Formaggia, and A. Veneziani, editors, *Complex Systems in Biomedicine*. Springer, Milan, 2006.

[548] L. Preziosi and A. Tosin. Multiphase modeling of tumor growth and extracellular matrix interaction: Mathematical tools and applications. *J. Math. Biol.*, 58:625–656, 2009.

[549] A. Pries, B. Reglin, and T. Secomb. Structural adaptation and stability of microvascular networks: functional roles of adaptive responses. *Am. J. Physiol. Heart Circ. Physiol.*, 281:H1015–H1025, 2001.

[550] A. Pries, B. Reglin, and T. Secomb. Structural adaptation of vascular networks: the role of pressure response. *Hypertension*, 38:1476–1479, 2001.

[551] A. Pries and T. Secomb. Control of blood vessel structure: insights from theoretical models. *Am. J. Physiol. Heart Circ. Physiol.*, 288:1010–1015, 2005.

[552] A. Pries and T. Secomb. Modeling structural adaptation of microcirculation. *Microcirculation*, 15(8):753–64, 2008.

[553] A. Pries, T. Secomb, and P. Gaehtgens. Structural adaptation and stability of microvascular networks: theory and simulations. *Am. J. Physiol. Heart Cir. Physiol.*, 275:H349–H360, 1998.

[554] W. C. Prozialeck, P. C. Lamar, and D. M. Appelt. Differential expression of E-cadherin, N-cadherin and beta-catenin in proximal and distal segments of the rat nephron. *BMC Physiol.*, 4(10), 2004.

[555] V. Quaranta, K. Rejniak, P. Gerlee, and A. Anderson. Invasion emerges from cancer cell adaptation to competitive microenvironments: Quantitative predictions from multiscale mathematical models. *Sem. Cancer Biol.*, 18(5):338–48, 2008.

[556] V. Quaranta, A. Weaver, P. Cummings, and A. Anderson. Mathematical modeling of cancer: The future of prognosis and treatment. *Clinica Chimica Acta*, 357:173–179, 2005.

[557] C. M. Quick, W. L. Young, E. F. Leonard, S. Joshi, E. Gao, and T. Hashimoto. Model of structural and functional adaptation of small conductance vessels to arterial hypotension. *Am. J. Physiol. Heart Circ. Physiol.*, 279(4):H1645–H1653, 2000.

[558] K. C. Quon and A. Berns. Haplo-insufficiency? Let me count the ways. *Genes Dev.*, 15(22):2917–21, 2001.

[559] A. Ramanathan, C. Wang, and S. Schreiber. Perturbational profiling of a cell-line model of tumorigenesis by using metabolic measurements. *PNAS*, 102:5992–5997, 2005.

[560] I. Ramis-Conde, M. Chaplain, and A. Anderson. Mathematical modelling of cancer cell invasion of tissue. *Math. Comp. Model.*, 47:533–545, 2008.

[561] I. Ramis-Conde, D. Drasdo, A. Anderson, and M. Chaplain. Modeling the influence of the e-cadherin-beta-catenin pathway in cancer cell invasion: A multiscale approach. *Biophys. J.*, 95:155–165, 2008.

[562] A. Rätz, A. Ribalta, and A. Voigt. Surface evolution of elastically stressed films under deposition by a diffuse interface model. *J. Comput. Phys.*, 214:187–208, 2006.

[563] K. Rejniak. A single-cell approach in modeling the dynamics of tumor microregions. *Math. Biosci. Eng.*, 2:643–655, 2005.

[564] K. Rejniak. An immersed boundary framework for modeling the growth of individual cells: An application to the early tumour development. *J.Theor. Biol.*, 247:186–204, 2007.

[565] K. Rejniak and A. Anderson. A computational study of the development of epithelial acini: 1. sufficient conditions for the formation of a hollow structure. *Bull. Math. Biol.*, 70:677–712, 2008.

[566] K. Rejniak and A. Anderson. A computational study of the development of epithelial acini: Ii. necessary conditions for structure and lumen stability. *Bull. Math. Biol.*, 70:1450–1479, 2008.

[567] K. Rejniak and R. Dillon. A single cell-based model of the ductal tumor microarchitecture. *Comp. Math. Meth. Med.*, 8(1):51–69, 2007.

[568] K. Rennstam and I. Hedenfalk. High-throughput genomic technology in research and clinical management of breast cancer. molecular signatures of progression from benign epithelium to metastatic breast cancer. *Breast Canc. Res.*, 8(4):213ff, 2006.

[569] B. Ribba, T. Alarcón, K. Marron, P. Maini, and Z. Agur. The use of hybrid cellular automaton models for improving cancer therapy. In B. C. P.M.A. Sloot and A. Hoekstra, editors, *ACRI, LNCS*, pages 444–453. Springer, Berlin, 2004.

[570] B. Ribba, O. Saut, T. Colin, D. Bresch, E. Grenier, and J. P. Boissel. A multiscale mathematical model of avascular tumor growth to investigate the therapeutic benefit of anti-invasive agents. *J. Theor. Biol.*, 243(4):532–41, 2006.

[571] A. Ridley, M. Schwartz, K. Burridge, R. Firtel, M. Ginsberg, G. Borisy, J. Parsons, and A. Horwitz. Cell migration: Integrating signals from front to back. *Science*, 302:1704–1709, 2003.

[572] E. Robinson, K. Zazzali, S. Corbett, and R. Foty. α5b1 integrin mediates strong tissue cohesion. *J. Cell. Sci.*, 116:377–386, 2003.

[573] E. Rofstad and E. Halsør. Hypoxia-associated spontaneous pulmonary metastasis in human melanoma xenographs: involvement of microvascular hotspots induced in hypoxic foci by interleukin. *Br. J. Cancer*, 86:301–308, 2002.

[574] E. Rofstad, H. Rasmussen, K. Galappathi, B. Mathiesen, K. Nilsen, and B. Graff. Hypoxia promotes lymph node metastasis in human melanoma xenografts by upregulating the urokinase-type plasminogen activator receptor. *Cancer Res.*, 62:1847–1853, 2002.

[575] J. Rohzin, M. Sameni, G. Ziegler, and B. Sloane. Pericellular ph affects distribution and secretion of cathepsin b in malignant cells. *Cancer Res.*, 54:6517–6625, 1994.

[576] T. Roose, S. J. Chapman, and P. Maini. Mathematical models of avascular tumor growth. *SIAM Review*, 49:179–208, 2007.

[577] T. Roose, P. Netti, L. Munn, Y. Boucher, and R. Jain. Solid stress generated by spheroid growth using a linear poroelastic model. *Microvascular Res.*, 66:204–212, 2003.

[578] B. Rubenstein and L. Kaufman. The role of extracellular matrix in glioma invasion: A cellular potts model approach. *Biophys. J.*, 95:5661–5680, 2008.

[579] J. Rubenstein, J. Kim, T. Ozawa, K. Zhang, M. Westphal, D. Deen, and M. Shuman. Anti-vegf antibody treatment of glioblastoma prolongs survival but results in increased vascular cooption. *Neoplasia*, 2:306–314, 2000.

[580] K. Rygaard and M. Spang-Thomsen. Quantitation and gompertzian analysis of tumor growth. *Breast Cancer Res. Treat.*, 46:303–312, 1997.

[581] Y. Saad and M. Schultz. Gmres: A generalized minimal residual algorithm for solving nonsymmetric linear systems. *SIAM J. Sci. Stat. Comput.*, 7:856–869, 1986.

[582] E. Sahai. Mechanisms of cancer cell invasion. *Curr. Opin. Genet. Dev.*, 15:87–96, 2005.

[583] T. Sairanen, R. Szepesi, M.-L. Karjalainen-Lindsberg, J. Saksi, A. Paetau, and P. J. Lindsberg. Neuronal caspase-3 and PARP-1 correlate differentially with apoptosis and necrosis in ischemic human stroke. *Acta Neuropathologica*, 118(4):541–52, 2009.

[584] G. Sakamoto. Infiltrating carcinoma: major histological types. In D. Page and T. Anderson, editors, *Diagnostic Histopathology of the Breast*. Churchill-Livingstone, London, 1987.

[585] M. E. Sanders, P. A. Schuyler, W. D. Dupont, and D. L. Page. The natural history of low-grade ductal carcinoma in situ of the breast in women treated by biopsy only

revealed over 30 years of long-term follow-up. *Cancer*, 103(12):2481–4, 2005.

[586] S. Sanga, M. E. Edgerton, P. Macklin, and V. Cristini. From receptor dynamics to directed cell motion: A predictive multiscale model of cell motility in complex microenvironments. in press, 2009.

[587] S. Sanga, H. Frieboes, X. Zheng, R. Gatenby, E. Bearer, and V. Cristini. Predictive oncology: a review of multidisciplinary, multiscale in silico modeling linking phenotype, morphology and growth. *NeuroImage*, 37:S120–S134, 2007.

[588] S. Sanga, J. Sinek, H. Frieboes, M. Ferrari, J. Fruehauf, and V. Cristini. Mathematical modeling of cancer progression and response to chemotherapy. *Expert Rev. Anticancer Ther.*, 6:1361–1376, 2006.

[589] B. Sansone, P. D. Santo, M. Magnano, and M. Scalerandi. Effects of anatomical constraints on tumor growth. *Phys. Rev. E*, 64:21903, 2002.

[590] B. Sansone, M. Scalerandi, and C. Condat. Emergence of taxis and synergy in angiogenesis. *Phys. Rev. Lett.*, 87:128102, 2001.

[591] M. Santini, G. Rainaldi, and P. Indovina. Apoptosis, cell adhesion and the extracellular matrix in three-dimensional growth of multicellular tumor spheroids. *Crit. Rev. Oncol. Hematol.*, 36:75–87, 2000.

[592] M. Sarntinoranont, F. Rooney, and M. Ferrari. Interstitial stress and fluid pressure within a growing tumor. *Ann. Biomed. Eng.*, 31:327–335, 2003.

[593] J. Satulovsky, R. Lui, and Y. L. Wang. Exploring the control circuit of cell migration by mathematical modeling. *Biophys. J.*, 94(9):3671–83, 2008.

[594] N. Savill and P. Hogeweg. Modeling morphogenesis: From single cells to crawling slugs. *J. Theor. Biol.*, 184:229–235, 1997.

[595] J. L. Scarlett, P. W. Sheard, G. Hughes, E. C. Ledgerwood, H.-K. Ku, and M. P. Murphy. Changes in mitochondrial membrane potential during staurosporine-induced apoptosis in Jurkat cells. *FEBS Letters*, 475(3):267–72, 2000.

[596] J. Schlessinger. Ligand-induced, receptor-mediated dimerization and activation of EGF receptor. *Cell*, 110(6):669–72, 2002.

[597] K. Schmeichel, V. Weaver, and M. Bissel. Structural cues from the tissue microenvironment are essential determinants of the human mammary epithelial cell phenotype. *J. Mammary Gland Biol. Neoplasia*, 3:201–213, 1998.

[598] L. S. Schulman and P. E. Seiden. Statistical mechanics of a dynamical system based on conway's game of life. *J. Stat. Phys.*, 19(3):293–314, 1978.

[599] E. Seftor, P. Meltzer, D. Kirshmann, J. Pe'er, A. Maniotis, J. Trent, R. Folberg, and M. Hendrix. Molecular determinants of human uveal melanoma invasion and metastasis. *Clin. Exp. Metastasis*, 19:233–246, 2002.

[600] M. J. Seidensticker and J. Behrens. Biochemical interactions in the wnt pathway. *Biochim. Biophys. Acta*, 1495:168–82, 2000.

[601] B. Selam, U. A. Kayisli, J. A. Garcia-Velasco, and A. Arici. Extracellular matrix-dependent regulation of FAS ligand expression in human endometrial stromal cells. *Biol. Reprod.*, 66(1):1–5, 2002.

[602] G. L. Semenza. HIF-1, O_2, and the 3 PHDs: How animal cells signal hypoxia to the nucleus. *Cell*, 107(1):1–3, 2001.

[603] G. Serini, D. Ambrosi, E. Giraudo, A. Gamba, L. Preziosi, and F. Bussolino. Modeling the early stages of vascular network assembly. *EMBO J.*, 22:1771–1779, 2003.

[604] S. Setayeshgar, C. Gear, H. Othmer, and I. Kevrekidis. Application of coarse integration to bacterial chemotaxis. *SIAM Multiscale Model. Sim.*, 4:307–327, 2005.

[605] J. A. Sethian. *Level Set Methods and Fast Marching Methods*. Cambridge University Press, New York, NY, 1999.

[606] J. A. Sethian and P. Smereka. Level set methods for fluid interfaces. *Ann. Rev. of Fluid Mech.*, 35(1):341–372, 2003.

[607] M. Shannon and B. Rubinsky. The effect of tumor growth on the stress distribution in tissue. *Adv. Biol. Heat Mass Transfer*, 231:35–38, 1992.

[608] N. Sharifi, B. T. Kawasaki, E. M. Hurt, and W. L. Farrar. Stem Cells in Prostate Cancer: Resolving the Castrate-Resistant Conundrum and Implications for Hormonal Therapy. *Cancer Biol. Ther.*, 5(8):910–906, 2006.

[609] C. J. Sherr. Cancer Cell Cycles. *Science*, 274(5293):1672–1677, 1996.

[610] J. Sherratt. Traveling wave solutions of a mathematical model for tumor encapsulation. *SIAM J. Appl. Math.*, 60:392–407, 1999.

[611] J. Sherratt and M. Chaplain. A new mathematical model for avascular tumour growth. *J. Math. Biol.*, 43:291–312, 2001.

[612] A. N. Shiryaev. *Probability*. Springer, New York, NY, 2nd edition, 1995.

[613] B. I. Shraiman. Mechanical feedback as a possible regulator of tissue growth. *Proc. Natl. Acad. Sci. USA*, 102(9):3318–23, 2005.

[614] C.-W. Shu and S. Osher. Efficient implementation of essentially non-oscillatory shock-capturing schemes. *J. Comput. Phys.*, 77:439–471, 1988.

[615] C.-W. Shu and S. Osher. Efficient implementation of essentially non-oscillatory shock capturing schemes, II. *J. Comput. Phys.*, 83:32–78, 1989.

[616] D. Shweiki, A. Itin, D. Soffer, and E. Keshet. Vascular endothelial growth factor induced by hypoxia may mediate hypoxia-initiated angiogenesis. *Nature*, 359:843–845, 1992.

[617] A. Sierra. Metastases and their microenvironments: linking pathogenesis and therapy. *Drug Resist. Updates*, 8:247–257, 2005.

[618] S. A. Silver and F. A. Tavassoli. Ductal carcinoma in situ with microinvasion. *Breast J.*, 4(5):344–8, 1998.

[619] M. J. Silverstein. Predicting residual disease and local recurrence in patients with ductal carcinoma in situ. *J. Natl. Cancer Inst.*, 89(18):1330–1, 1997.

[620] M. J. Silverstein. Recent advances: diagnosis and treatment of early breast cancer. *BMJ*, 314(7096):1736ff, 1997.

[621] M. J. Silverstein. Ductal carcinoma in situ of the breast. *Annu. Rev. Med.*, 51:17–32, 2000.

[622] P. T. Simpson, J. S. Reis-Filho, T. Gale, and S. R. Lakhani. Molecular evolution of breast cancer. *J. Pathol.*, 205(2):248–54, 2005.

[623] J. Sinek, H. Frieboes, X. Zheng, and V. Cristini. Two-dimensional chemotherapy simulations demonstrate fundamental transport and tumor response limitations involving nanoparticles. *Biomedical Microdevices*, 6:297–309, 2004.

[624] J. Sinek, S. Sanga, X. Zheng, H. Frieboes, M. Ferrari, and V. Cristini. Predicting drug pharmacokinetics and effect in vascularized tumors using computer simulation. *J. Math. Biol.*, 58:485–510, 2009.

[625] S. Skinner. Microvascular architecture of experimental colon tumors in the rat. *Cancer Res.*, 50:2411–2417, 1990.

[626] V. I. F. Slettenaar and J. L. Wilson. The chemokine network: A target in cancer biology? *Adv. Drug Deliv. Rev.*, 58(8):962–974, 2006.

[627] K. Smallbone, R. Gatenby, R. Gillies, P. Maini, and D. Gavaghan. Metabolic changes during carcinogenesis: Potential impact on invasiveness. *J. Theor. Biol.*, 244:703–713,

2007.
[628] K. Smallbone, R. Gatenby, and P. Maini. Mathematical modelling of tumour acidity. *J. Theor. Biol.*, 255:106–112, 2008.
[629] K. Smallbone, D. Gavaghan, R. Gatenby, and P. Maini. The role of acidity in solid tumor growth and invasion. *J. Theor. Biol.*, 235:476–484, 2005.
[630] K. Smallbone, D. Gavaghan, P. Maini, and J. M. Brady. Quiescence as a mechanism for cyclical hypoxia and acidosis. *J. Math. Biol.*, 55:767–779, 2007.
[631] S. A. A. Sohaib and R. H. Reznek. MR imaging in ovarian cancer. *Canc. Img.*, 7(Special Issue A):S119–29, 2007.
[632] V. Spencer, R. Xu, and M. Bissell. Extracellular matrix, nuclear and chromatin structure, and gene expression in normal tissues and malignant tumors: a work in progress. *Adv. Cancer Res.*, 97:275–294, 2007.
[633] T. A. Springer. Adhesion receptors of the immune system. *Nature*, 346(6283):425–34, 1990.
[634] P. Steeg. Angiogenesis inhibitors: motivators of metastasis? *Nature Med.*, 9:822–823, 2003.
[635] A. Stein, T. Demuth, D. Mobley, M. Berens, and L. Sander. A mathematical model of glioblastoma tumor spheroid invasion in a three-dimensional in vitro experiment. *Biophys. J.*, 92:356–365, 2007.
[636] M. S. Steinberg and M. Takeichi. Experimental specification of cell sorting, tissue spreading, and specific spatial patterning by quantitative differences in cadherin expression. *Proc. Natl. Acad. Sci. USA*, 91:206–9, 1994.
[637] A. Stephanou, S. McDougall, A. Anderson, and M. Chaplain. Mathematical modelling of flow in 2d and 3d vascular networks: Applications to anti-angiogenic and chemotherapeutic drug strategies. *Math. Comput. Model.*, 41:1137–1156, 2005.
[638] A. Stephanou, S. McDougall, A. Anderson, and M. Chaplain. Mathematical modelling of the influence of blood rheological properties upon adaptative tumour-induced angiogenesis. *Math. Comput. Model.*, 44:96–123, 2006.
[639] J. Stewart, P. Broadbridge, and J. Goard. Symmetry analysis and numerical modelling of invasion by malignant tumour tissue. *Nonlinear Dyn.*, 28:175–193, 2002.
[640] C. Stokes and D. Lauffenburger. Analysis of the roles of microvessel endothelial cell random motility and chemotaxis in angiogenesis. *J. Theor. Biol.*, 152:377–403, 1991.
[641] P. C. Stomper and F. R. Margolin. Ductal carcinoma in situ: the mammographer's perspective. *Am. J. Roentgenology*, 162:585–91, 1994.
[642] E. Stott, N. Britton, J. Glazier, and M. Zajac. Simulation of benign avascular tumour growth using the potts model. *Math. Comput. Model.*, 30:183–198, 1999.
[643] D. Stupack and D. Cheresh. Get a ligand, get a life: Integrins, signaling and cell survival. *J. Cell. Sci.*, 115:3729–3738, 2002.
[644] C. Sun and L. Munn. Lattice-boltzmann simulation of blood flow in digitized vessel networks. *Comp. and Math. Appl.*, 55:1594–1600, 2008.
[645] S. Sun, M. Wheeler, M. Obeyesekere, and C. P. Jr. A deterministic model of growth factor-induced angiogenesis. *Bull. Math. Biol.*, 67:313–337, 2005.
[646] S. Sun, M. Wheeler, M. Obeyesekere, and C. P. Jr. Multiscale angiogenesis modeling using mixed finite element methods. *Multiscale Model. Simul.*, 4:1137–1167, 2005.
[647] X.-F. Sun and H. Zhang. Clinicopathological significance of stromal variables: angiogenesis, lymphangiogenesis, inflammatory infiltration, MMP and PINCH in colorectal carcinomas. *Mol. Cancer*, 5:43, 2006.

[648] K. Sundfor, H. Lyng, and E. Rofstad. Tumour hypoxia and vascular density as predictors of metastasis in squamous cell carcinoma of the uterine cervix. *Br. J. Cancer*, 78:822–827, 1998.

[649] M. Sussman, P. Smereka, and S. Osher. A level set approach for computing solutions to incompressible two-phase flow. *J. Comput. Phys.*, 114(1):146–159, 1994.

[650] R. Sutherland. Cell and environment interactions in tumor microregions: the multicell spheroid model. *Science*, 240:177–184, 1988.

[651] R. Sutherland, J. Carlsson, R. Durand, and J. Yuhas. Spheroids in cancer research. *Cancer Res.*, 41:2980–2994, 1981.

[652] K. Swanson, C. Bridge, J. Murray, and E. A. Jr. Virtual and real brain tumors: Using mathematical modeling to quantify glioma growth and invasion. *J. Neuro. Sci.*, 216:1–10, 2003.

[653] L. A. Taber. An optimization principle for vascular radius including the effects of smooth muscle tone. *Biophys. J.*, 74(1):109–114, 1998.

[654] P. J. Tannis, O. E. Nieweg, R. A. Valdés Olmos, and B. B. R. Kroon. Anatomy and physiology of lymphatic drainage of the breast from the perspective of sentinel node biopsy. *J. Am. Coll. Surg.*, 192(3):399–409, 2001.

[655] Y. Tao and M. Chen. An elliptic-hyperbolic free boundary problem modelling cancer therapy. *Nonlinearity*, 19:419–440, 2006.

[656] Y. Tao, N. Yoshida, and Q. Guo. Nonlinear analysis of a model of vascular tumour growth and treatment. *Nonlinearity*, 17:867–895, 2004.

[657] M. J. Terol, M. Tormo, J. A. Martinez-Climent, I. Marugan, I. Benet, A. Ferrandez, A. Teruel, R. Ferrer, and J. Garcia-Conde. Soluble intercellular adhesion molecule-1 (s-ICAM-1/s-CD54) in diffuse large B-cell lymphoma: association with clinical characteristics and outcome. *Ann. Oncol.*, 14(3):467–74, 2003.

[658] R. Thomlinson and L. Gray. The histological structure of some human lung cancers and the possible implications of radiotherapy. *Br. J. Cancer*, 9:539–549, 1955.

[659] B. Thorne, A. Bailey, and S. Peirce. Combining experiments with multi-cell agent-based modeling to study biological tissue patterning. *Briefings in Bioinformatics*, 8:245–257, 2007.

[660] M. Tindall, C. Please, and M. Peddie. Modelling the formation of necrotic regions in avascular tumours. *Math. Biosci.*, 211:34–55, 2008.

[661] S. Tong and F. Yuan. Numerical simulations of angiogenesis in the cornea. *Microvasc. Res.*, 61:14–27, 2001.

[662] A. Tosin. Multiphase modeling and qualitative analysis of the growth of tumor cords. *Networks Heterogen. Media*, 3:43–84, 2008.

[663] A. Tosin, D. Ambrosi, and L. Preziosi. Mechanics and chemotaxis in the morphogenesis of vascular networks. *Bull. Math. Biol.*, 68:1819–1836, 2006.

[664] P. Tracqui. Biophysical models of tumor growth. *Rep. Prog. Phys.*, 72:056701, 2009.

[665] U. Trottenberg, C. Oosterlee, and A. Schüller. *Multigrid*. Academic Press, New York, 2005.

[666] C. Truesdell and R. Toupin. Classical field theories. In S. Flugge, editor, *Handbuch der Physik, Vol III/I*. Springer-Verlag, Berlin, 1960.

[667] S. Turner and J. Sherratt. Intercellular adhesion and cancer invasion: A discrete simulation using the extended potts model. *J. Theor. Biol.*, 216:85–100, 2002.

[668] B. Tysnes and R. Mahesparan. Biological mechanisms of glioma invasion and potential therapeutic targets. *J. Neurooncol.*, 53:129–147, 2001.

[669] P. Vajkoczy, M. Farhadi, A. Gaumann, R. Heidenreich, R. Erber, A. Wunder, J.C., M. M. Tonn, and G. Breier. Microtumor growth initiates angiogenic sprouting with simultaneous expression of vegf, vegf receptor-2, and angiopoietin-2. *J. Clin. Invest.*, 109:777–785, 2002.

[670] L. van Kempen, D. Ruiter, G. van Muijen, and L. Coussens. The tumor microenvironment: a critical determinant of neoplastic evolution. *Eur. J. Cell. Biol.*, 82:539–548, 2003.

[671] I. van Leeuwen, C. Edwards, M. Ilyas, and H. Byrne. Towards a multiscale model of colorectal cancer. *World Gastroenterol.*, 13:1399–1407, 2007.

[672] V. V. Vasko and M. Saji. Molecular mechanisms involved in differentiated thyroid cancer invasion and metastasis. *Curr. Opin. Oncol.*, 19(1):11–17, 2007.

[673] P. Vaupel, H. Haugland, T. Nicklee, A. Morrison, and D. Hedley. Hypoxia-inducible factor-1 alpha is an intrinsic marker for hypoxia in cervical cancer xenografts. *Cancer Res.*, 61:7394–7398, 2001.

[674] R. Vernon, J. Angello, M. Iruela-Arispe, and T. Lane. Reorganization of basement membrane matrices by cellular traction promotes the formation of cellular networks in vitro. *Lab. Invest.*, 66:536–547, 1992.

[675] E. Villa-Cuesta, E. Gonz/'alez-P/'erez, and J. Modolell. Apposition of *iroguois* expressing and non-expressing cells leads to cell sorting and fold formation in *Drosphila* imaginal wing disc. *BMC Devel. Biol.*, 7(106), 2007.

[676] B. Vollmayr-Lee and A. Rutenberg. Stresses in growing soft tissues. *Acta Biomaterialia*, 2:493–504, 2006.

[677] J. von Neumann. *Theory of Self-Replicating Automata*. University of Illinois Press, 1966. Edited by Arthur W. Burks.

[678] C. Walker and G. Webb. Global existence of classical solutions for a haptotaxis model. *SIAM J. Math. Anal.*, 38(5):1694–1713, 2007.

[679] T. Walles, M. Weimer, K. Linke, J. Michaelis, and H. Mertsching. The potential of bioartificial tissues in oncology research and treatment. *Onkologie*, 30:388–394, 2007.

[680] R. Wang, L. Jinming, K. Lyte, N. K. Yashpal, F. Fellows, and C. G. Goodyer. Role for $\beta 1$ integrin and its associated $\alpha 3$, $\alpha 5$, and $\alpha 6$ subunits in development of the human fetal pancreas. *Diabetes*, 54:2080–9, 2005.

[681] Z. Wang, L. Zhang, J. Sagotsky, and T. Deisboeck. Simulating non-small cell lung cancer with a multiscale agent-based model. *Theor. Biol. Med. Model.*, 4:50, 2007.

[682] J. Ward and J. King. Mathematical modelling of avascular tumour growth. *IMA J. Math. Appl. Medicine Biol.*, 14:36–69, 1997.

[683] J. Ward and J. King. Mathematical modelling of avascular-tumour growth ii: modelling growth saturation. *Math. Med. Biol.*, 16:171–211, 1999.

[684] J. Ward and J. King. Modelling the effect of cell shedding on avasacular tumour growth. *J. Theor. Med.*, 2:155–174, 2000.

[685] J. Ward and J. King. Mathematical modelling of drug transport in tumour multicell spheroids and monolayer cultures. *Math. Biosci.*, 181:177–207, 2003.

[686] R. Wcislo and W. Dzwinel. Particle based model of tumor progression stimulated by the process of angiogenesis. In J. Adam and N. Bellomo, editors, *Computational Science - ICCS 2008*, pages 177–186. Springer, Heidelberg, 2008.

[687] A. M. Weaver. Invadopodia: specialized cell structures for cancer invasion. *Clin. Exp. Metastasis*, 23(2):97–105, 2006.

[688] C. Wei, M. Larsen, M. P. Hoffman, and K. M. Yamada. Self-organization and branching morphogenesis of primary salivary epithelial cells. *Tissue Eng.*, 13(4):721–35, 2007.

[689] O. D. Weiner, W. A. Marganski, L. F. Wu, S. J. Altschuler, and M. W. Kirschner. An actin-based wave generator organizes cell motility. *PLoS Biol*, 5(9):e221, 08 2007.

[690] S. R. Wellings, H. M. Jensen, and R. G. Marcum. An atlas of subgross pathology of the human breast with special reference to possible precancerous lesions. *J. Natl. Cancer Inst.*, 55(2):231–73, 1975.

[691] A. Wells, B. Harms, A. Iwabu, L. Koo, K. Smith, L. Griffith, et al. Motility signaled from the EGF receptor and related systems. *Meth. Mol. Biol.*, 327:159–77, 2006.

[692] A. Wells, J. Kassis, J. Solava, T. Turner, and D. A. Lauffenburger. Growth factor-induced cell motility in tumor invasion. *Acta Oncol.*, 41(2):124–30, 2002.

[693] M. Welter, K. Bartha, and H. Rieger. Emergent vascular network inhomogeneities and resulting blood flow patterns in a growing tumor. *J. Theor. Biol.*, 250:257–80, 2008.

[694] M. Welter, K. Bartha, and H. Rieger. Hot spot formation in tumor vasculature during tumor growth in an arterio-venous-network environment. arXiv.org ¿ q-bio ¿ arXiv:0801.0654v2, 2008.

[695] N. Wentzensen, S. Vinokurova, and M. von Knebel Doeberitz. Systematic review of genomic integration sites of human papillomavirus genomes in epithelial dysplasia and invasive cancer of the female lower genital tract. *Canc. Res.*, 64(11):3878–84, 2004.

[696] K. Wiesenfeld and F. Moss. Stochastic resonance and the benefits of noise: from ice ages to crayfish and squids. *Nature*, 373:33, 1995.

[697] H. S. Wiley, S. Y. Shvartsman, and D. A. Lauffenburger. Computational modeling of the EGF-receptor system: a paradigm for systems biology. *Trends Cell. Biol.*, 13(1):43–50, 2003.

[698] S. Wise, J. Kim, and J. Lowengrub. Solving the regularized, strongly anisotropic Cahn-Hilliard equation by an adaptive nonlinear multigrid method. *J. Comput. Phys.*, 226:414–446, 2007.

[699] S. Wise, J. Lowengrub, and V. Cristini. An adaptive algorithm for simulating solid tumor growth using mixture models. in prep.

[700] S. Wise, J. Lowengrub, H. Frieboes, and V. Cristini. Three-dimensional multispecies nonlinear tumor growth– i. model and numerical method. *J. Theor. Biol.*, 253:524–543, 2008.

[701] E. K. Wolf, A. C. Smidt, and A. E. Laumann. Topical sodium thiosulfate therapy for leg ulcers with dystrophic calcification. *Arch. Dermatol.*, 144(12):1560–2, 2008.

[702] K. Wolf and P. Friedl. Molecular mechanisms of cancer cell invasion and plasticity. *Br. J. Dermatology*, 154:11–15, 2006.

[703] K. Wolf, R. Müller, S. Borgmann, E.-B. Bröcker, and P. Friedl. Amoeboid shape change and contact guidance: T-lymphocyte crawling through fibrillar collagen is independent of matrix remodeling by MMPs and other proteases. *Blood*, 102(9):3262–9, 2003.

[704] J. Wu and S. Cui. Asymptotic behavior of solutions of a free boundary problem modeling the growth of tumors with stokes equations. *Discr. Contin. Dyn. Sys.*, 24(2):625–51, 2009.

[705] J. Wu, F. Zhou, and S. Cui. Simulation of microcirculation in solid tumors. *IEEE/ICME Int. Conf. on Complex Med. Eng.*, pages 1555–1563, 2007.

[706] M. Wurzel, C. Schaller, M. Simon, and A. Deutsch. Cancer cell invasion of brain tissue: guided by a prepattern? *J. Theor. Medicine*, 6:21–31, 2005.

[707] Y. Xiong, P. Rangamani, B. Dubin-Thaler, M. Sheetz, and R. Iyengar. A three-dimensional stochastic spatio-temporal model of cell spreading. *Nat. Proc.*, 2007. Available from Nature Proceedings: http://10.1038/npre.2007.62.2.

[708] R. Xu, V. Spencer, and M. Bissell. Extracellular matrix-regulated gene expression requires cooperation of swi/snf and transcription factors. *J. Biol. Chem.*, 282:14992–14999, 2007.

[709] S. Xu. Hopf bifurcation of a free boundary problem modeling tumor growth with two time delays. *Chaos Solitons Fractals*, 41(5):2491–4, 2009.

[710] Y. Xu and R. Gilbert. Some inverse problems raised from a mathematical model of ductal carcinoma in situ. *Math. Comp. Model.*, 49(3-4):814–28, 2009.

[711] H. Yamaguchi, J. Wyckoff, and J. Condeelis. Cell migration in tumors. *Curr. Op. Cell Biol.*, 17:559–564, 2005.

[712] K. Yamauchi, M. Yang, P. Jiang, M. Xu, N. Yamamoto, H. Tsuchiya, K. Tomita, A. R. Moossa, M. Bouvet, and R. M. Hoffman. Development of real-time subcellular dynamic multicolor imaging of cancer-cell trafficking in live mice with a variable-magnification whole-mouse imaging system. *Canc. Res.*, 66:4028–4214, 2006.

[713] S. Young and R. Hill. Effects of reoxygenation of cells from hypoxic regions of solid tumors: anticancer drug sensitivity and metastatic potential. *J. Natl. Cancer Inst.*, 82:338–339, 1990.

[714] S. Young, R. Marshall, and R. Hill. Hypoxia induces dna overreplication and enhances metastatic potential of murine tumor cells. *Proc. Natl. Acad. Sci. USA*, 85:9533–9537, 1988.

[715] J. Yu, J. Rak, B. Coomber, D. Hicklin, and R. Kerbel. Effect of p53 status on tumor response to antiangiogenic therapy. *Science*, 295:1526–1528, 2002.

[716] A. Zagorska and J. Dulak. HIF-1: the knowns and unknowns of hypoxia sensing. *Acta Biochimica Polonica*, 51(3):563–585, 2004.

[717] D. Zagzag, A. R., M. Greco, H. Yee, J. Holash, S. Wiegand, S. Zabski, G. Yancopoulos, and M. Grumet. Vascular apoptosis and involution in gliomas precede neovascularization: a novel concept for glioma growth and angiogenesis. *Lab. Invest.*, 80:837–849, 2000.

[718] M. Zajac, G. Jones, and J. Glazier. Model of convergent extension in animal morphogenesis. *Phys. Rev. Lett.*, 85:2022–2025, 2000.

[719] M. H. Zaman, R. D. Kamm, P. Matsudaira, and D. A. Lauffenburger. Computational model for cell migration in three-dimensional matrices. *Biophys. J.*, 89(2):1389–97, 2005.

[720] A. Zetterberg, O. Larsson, and K. G. Wilman. What is the restriction point? *Curr. Opin. Cell Biol.*, 7(6):835–842, 1995.

[721] L. Zhang, C. Athale, and T. Deisboeck. Development of a three-dimensional multiscale agent-based tumor model: simulating gene-protein interaction profiles, cell phenotypes and multicellular patterns in brain cancer. *J. Theor. Biol.*, 244:96–107, 2007.

[722] L. Zhang, C. Strouthos, Z. Wang, and T. Deisboeck. Simulating brain tumor heterogeneity with a multiscale agent-based model: Linking molecular signatures, phenotypes and expansion rate. *Math. Comp. Model.*, 49:307–319, 2009.

[723] L. Zhang, Z. Wang, J. Sagotsky, and T. Deisboeck. Multiscale agent-based cancer modeling. *J. Math. Biol.*, 58(4-5):545–59, 2009.

[724] G. Zhao, J. Wu, S. Xu, M. Collins, Q. Long, C. Koenig, Y. Jiang, J. Wang, and A. Padhani. Numerical simulation of blood flow and interstitial fluid pressure in solid

tumor microcirculation based on tumor-induced angiogenesis. *Mech. Sinica*, 23:477–483, 2007.

[725] X. Zheng, S. Wise, and V. Cristini. Nonlinear simulation of tumor necrosis, neovascularization and tissue invasion via an adaptive finite-element/level-set method. *Bull. Math. Biol.*, 67:211–259, 2005.

[726] F. Zhou and S. Cui. Bifurcation for a free boundary problem modeling the growth of multi-layer tumors. *Nonlinear Analysis Theory Meth. Appl.*, 68:2128–2145, 2008.

[727] F. Zhou, J. Escher, and S. Cui. Well-posedness and stability of a free boundary problem modeling the growth of multi-layer tumors. *J. Diff. Eq.*, 244:2909–2933, 2008.

[728] D. Zipori. The mesenchyme in cancer therapy as a target tumor component, effector cell modality and cytokine expression vehicle. *Cancer Metastasis Rev.*, 25(3):459–467, 2006.